

First and Second order Coherence Studies of Optical Vortices

A THESIS

submitted for the Award of Ph. D. degree of

MOHANLAL SUKHADIA UNIVERSITY

in the

Faculty of Science

by

Ashok Kumar



Under the Supervision of

Dr. R. P. Singh

Scientist-F

Theoretical Physics Division

Physical Research Laboratory, Ahmedabad, India.

DEPARTMENT OF PHYSICS

MOHANLAL SUKHADIA UNIVERSITY

UDAIPUR

2011

CERTIFICATE

I feel great pleasure in certifying the thesis entitled “**First and Second order Coherence Studies of Optical Vortices**” by Mr. Ashok Kumar under my guidance. He has completed the following requirements as per Ph.D. regulations of the University

- (a) Course work as per the university rules.
- (b) Residential requirements of the university.
- (c) Presented his work in the departmental committee.
- (d) Published/accepted minimum of two research papers in referred research journals,

I am satisfied with the analysis of data, interpretation of results and conclusions drawn.

I recommend the submission of the thesis.

Date:
June 29, 2011

Dr. R. P. Singh
(Supervisor)
Scientist-F
Physical Research Laboratory
Ahmedabad, India.

Countersigned by
Head of the Department

DECLARATION

*I Ashok Kumar, S/O Shri Dharmanand, resident of C-102, PRL residences, Navrangpura, Ahmedabad - 380009, hereby declare that the research work incorporated in the present thesis entitled “**First and Second order Coherence Studies of Optical Vortices**” is my own work and is original. This work (in part or in full) has not been submitted to any university or institute for the award of a Degree or a Diploma. I have properly acknowledged the material collected from secondary sources wherever required. I solely own the responsibility for the originality of the entire content.*

Date:

June 29, 2011

Ashok Kumar

(Author)

**To my
Parents
(Eeja & Pitaji)**

Acknowledgments

The last five years in PRL have been very much enjoyable, memorable and learning period for me. The credit goes to many individuals and they really deserve to be acknowledged. Of course the first and the foremost name comes as Dr. R. P. Singh, my supervisor, who has given me the opportunity to work under his guidance. I am very much thankful and indebted to him for his valuable guidance and constant encouragement. His ever friendly attitude encouraged me to discuss many things with him, sometimes even very small problems. I learned a lot of things during long discussions with him. There was full freedom to implement all new ideas in the laboratory. It is his humble nature and caring attitude which have always inspired me to do the best in the laboratory.

I am very grateful to Prof. J. Banerji for his involvement in my research work. His excellent teaching skill and “no compromise with quality of the results” made a big impression on me. His suggestions and critical comments from time to time helped me to improve my manuscripts. I am very thankful to Prof. P. K. Panigrahi for his encouragement and bringing excitement in science since my early stage of research. I am indebted to Mr. V. K. Jaiswal for his care and teaching the basic experimental techniques in the lab.

I sincerely thank Prof. R. E. Amritkar, Prof. R. Ramesh, Prof. S. A. Haider, Dr. Varun Sheel, Dr. R. Rangarajan, Dr. Dilip Angom, Dr. Jitesh Bhatt and Dr. H. Mishra for teaching various new techniques during the course work. I am very grateful to Prof. U. C. Joshi and Dr. Bhas Bapat for their suggestions, critical comments and encouragement during my progress evaluation in early stage of the research.

I would like to thank Prof. J. N. Goswami, the Director, Prof. Anjan Joshipura, the Dean, Prof. Utpal Sarkar & Prof. A. K. Singhvi, former Deans, Dr. Bhushit Vaishnav, Head, Academic Services and Mr. Y. M. Trivedi, the Registrar, Physical Research Laboratory for providing me the necessary facilities to carry out my thesis work. I am also thankful to the chairman and the members of academic committee for their critical evaluation.

My lab mates and friends deserve special thanks. Starting from Jitendra Bhatt, thank you very much for motivating me to join PRL. The times we spent together in the lab, in various conferences and visits are memorable. The discussions with you were really fruitful and exciting. Pravin, it has been very nice to work with you. During my critical period of PhD, the support I got from you is incredible and the various useful discussions we had in the lab were very useful. Shashi, thank you very much for helping me in various computational related problems, your excellent computational skill helped me a lot starting from Ubuntu installation to thesis writing in LaTeX. Thanks to Aadhi and Gangi for carefully reading of my thesis and manuscripts.

I am grateful to Dr. Goutam Samanta for his encouragement and bringing confidence in myself. Also, I would like to thank you for learning me various technical issues in Optics Laboratory.

I would like to express my gratitude to Prof. S. D. Rindani, Prof. V. K. B. Kota, Prof. S. Mohanty, Dr. Srubabati Goswami, Dr. Namit Mahajan, Dr. B. K. Sahoo, Dr. Navinder Singh and Dr. Partha Konar for their cooperation and encouragement.

I am greatly indebted to Prof. P. Janardhan for carefully reading my manuscripts and suggestions for the improvement of English writing. I sincerely thank Prof. Harishchandra, Prof. K. S. Baliyan, Prof. N. M. Ashok, Dr. Ramachandran and Dr. K. P. Subramanian for their encouragement.

I also thank all staff members of library, computer center, workshop, glass blowing, dispensary, canteen and administration for rendering their help and cooperation at all stages. Special thanks to Nishtha madam, Uma madam and Ghanshyam bhai for their cooperation.

I was very nervous while joining PRL for various reasons, however I found it the best place I have had ever been, thanks to my jovial batchmates- Amzad, Anand, Arvind, Bhaswar, Naveen, Pankaj, Priyam, Rabiul, Rohit, Sandeep, Soumya, Sreekanth, Suman, Suratna, Vimal, Vineet and Vivek for their wonderful company. Initial C-19 days with Sreeku are memorable. The volleyball matches in hostel quadrangle were very refreshing and enjoyable.

It would be hard to finish my Ph.D. without the support and nice company of my seniors cum friends like Subimal da, Tarun Jhaji, Morthekai, Santosh bhai, Sanat da, Shreyash, Santosh Bhaiyya, Kushwahaji, Ritesh, Akhilesh bhaiji, Rohit bhai, Salman, Ramkrishna, Alok, Sumanta, Gyana, Kirpa, Bhavik, Vishal, Lokesh, Harindar, Manan, Brajesh, Naveen Gandhi, Rahman, timmy, Sumita, Suchita and S. K. Sharmaji.

I would further extend my gratitudes to my friends Patra, Ketan, Arvind Saxena, Neeraj, Ashish, Arvind Rajpuruhit, Subrata, Tapas, Jayati, Moumita, Srinivas, Prasant, Abhishek, Siddharth, Satinder, Sunil, Chitrabhanu, Mala, Kabitri, Zeen, Purnendu da, Anjishnu, Praveen Srivastava, Fazlul and Tanushree for their cooperation.

I am deeply indebted to my School teachers Mr. N. C. Gahtoriji and Mr. B. D. Bhattji for their excellent teaching and encouragement.

Special thanks go to my longtime friends outside PRL, Kapil and Ravi for their support and company.

Lastly I thank my near and dear ones for making me what and where I am. It is a fortune to have a younger brother like Sanju, he has always been with me in all the up and down of my personal and professional life. Words can not explain my affection. Pramod da is specially acknowledged for support and encouragement. I sincerely thank to my elder brothers and bhabhis for being very caring. My sisters and jijajis have always been encouraging for me. Cute telephonic chats with my nephews and niece, Munnu, Anki and Gunnu, are always refreshing for me. Special thanks to Priya (Pushpa) for being with me in very crucial time of my life, your unconditional love, support and encouragement have always motivated me to move towards my goal. My parents (Eeja and Pitaji) deserve the last word; where would I be without them.

Abstract

Optical vortices, manifestation of phase singularities, are light beams with helical wavefronts. This dissertation concerns with the study of the first and the second order coherences of optical vortices.

We have used computer generated holography technique for the generation of optical vortices. An algorithm has been developed to make a vortex of variable core size and demonstrated experimentally. Interferometric techniques have been described to characterize the optical vortices.

It has been observed that the diffraction of an optical vortex through an iris diaphragm produces ball bearing sort of structures of darkness and brightness. The singularity of the vortex beam is found to be persistent even after diffraction through the aperture. The position of the singularity in the diffracted beam depends on the relative positions of vortex center and the center of iris diaphragm. These results may have implications to sub-diffraction imaging. A further study of diffraction through a two dimensional sinusoidal grating produces four copies of vortex with the same topological charge.

The stability and the propagation dynamics of high topological charge optical vortices have also been discussed. We introduce an asymmetry in the core of a high charge optical vortex by using a spatial light modulator. The splitting of a high charge optical vortex core into unit charge vortices has been found to depend on the extent of introduced asymmetry. The trajectories of the split unit charged vortices and their separation have been recorded as a function of change in the asymmetry of the core.

We have examined the spatial coherence characteristics of the one dimensional projection of optical vortices. The obtained spatial coherence function is found to be the characteristic of the order of the vortex. The knowledge of the spatial coherence is used to extract the information entropy and the Wigner distribution function as well.

We have studied intensity correlation function for optical vortices passing through a rotating ground glass (RGG) plate and compared them with that of the TEM_{00} mode of a He-Ne laser beam passing through the same RGG plate. It has been observed that the intensity correlation curves for the scattered optical vortices decrease much faster than the corresponding curve for a TEM_{00} mode of the He-Ne laser. We attribute this to the complex phase structure of the optical vortices.

Keywords: Singular optics, Optical vortex, Coherence, Diffraction, Stability of high charge vortex, Computer generated holography.

Contents

Abstract	iii
List of Figures	viii
1 Introduction	1
1.1 Singular Optics and Optical Vortices	4
1.2 First Order Coherence	8
1.3 Second Order Coherence	10
2 Generation and Characterization of Optical Vortices	17
2.1 Generation of Optical Vortices	18
2.1.1 Computer Generated Holography	18
2.1.1.1 Computer Generated Holograms	18
2.1.1.2 Spatial Light Modulator	21
2.1.2 Astigmatic Mode Converter	26
2.1.3 Spiral Phase Plate	26
2.2 Characterization of Optical Vortices	27
2.2.1 Topological Charge	28
2.2.2 Orbital Angular Momentum	30
2.2.3 Propagation	31
3 Diffraction Characteristics of Optical Vortices	34
3.1 Diffraction of Optical Vortex through an Iris Aperture	35

Contents

3.1.1	Experiment	35
3.1.2	Simulation	38
3.1.3	Diffraction of an Optical Vortex	40
3.1.4	Diffraction of a Gaussian Beam	42
3.2	Diffraction of Optical Vortices through a Two Dimensional Sinu- soidal Grating	43
3.2.1	Experiment	44
3.2.2	Theoretical Analysis	46
3.2.3	Copies of Optical Vortices	51
3.2.4	Conclusions	54
4	Stability and Propagation Dynamics of High Charge Optical Vor- tices	55
4.1	Introduction	56
4.2	Experiment	57
4.3	Theoretical Background	60
4.4	Effect of Asymmetry to High-Charge Optical Vortices	61
4.4.1	Splitting of a Second Order Optical Vortex	61
4.4.2	Trajectories of Split Vortices	63
4.4.3	Splitting of Higher Order Optical Vortices	66
4.5	Conclusion	69
5	Spatial Coherence Properties of Optical Vortices	70
5.1	Introduction	71
5.2	Theoretical Analysis	72
5.3	Experiment	73
5.4	Two Point Correlation Function of Optical Vortices	75
5.4.1	One Dimensional Projection of Two Point Correlation Function	76
5.4.2	Degree of Coherence	77
5.4.3	Information Entropy	78

Contents

5.4.4	Wigner Distribution Function	79
5.5	Conclusion	80
6	Intensity Correlation Properties of Optical Vortices	81
6.1	Introduction	82
6.2	Experiment	83
6.3	Intensity Correlation Function for Optical Vortices and TEM ₀₀ Mode of He-Ne Laser	85
6.4	Scattering of Optical Vortices through Rotating Ground Glass Plate	86
6.5	Theoretical Analysis	89
6.6	Summary	93
7	Summary and Scope for Future Work	94
	Bibliography	99
	List of Publications	110

List of Figures

1.1	Comparison of the intensity profiles, wavefronts, phase profiles and interference patterns of a Gaussian beam and optical vortices of topological charge ± 1	6
1.2	Comparison of the intensity profiles, wavefronts, phase profiles and interference patterns of optical vortices of topological charge ± 2	7
1.3	Schematic of the Mach-Zehnder Interferometer	9
1.4	Laboratory setup of the Hanbury-Brown and Twiss experiment	13
1.5	Plot showing the intensity correlation results of the Hanbury-Brown Twiss experiments	14
2.1	Computer generated holograms with different transmission functions (sinusoidal, binary and blazed) for the generation of optical vortex of order 1	20
2.2	Schematic of the generation of optical vortex from a Computer Generated Hologram	21
2.3	Schematic of the generation of optical vortex from a spatial light modulator	22
2.4	Images of an optical vortex with different resolutions of the CGH	24
2.5	Plot showing the variation of normalized diameter of an optical vortex core with resolution of the CGH	25
2.6	Schematic of the Mach-zehnder interferometer for the characterization of optical vortices	28

List of Figures

2.7	Interference fringes obtained through the Mach-Zehnder interferometer for beams with topological charges 0, 1 and -1	30
2.8	Shape of an optical vortex after passing through a cylindrical lens at different distances	32
2.9	Shape of an optical vortex without cylindrical lens at different distances	33
3.1	Experimental setup for the generation of optical vortices, their diffraction with iris diaphragm and characterization through interferometry	36
3.2	Images of an optical vortex of topological charge 1 passed through an iris diaphragm of variable radii and their interference patterns with a reference beam	41
3.3	Images of a Gaussian laser beam passed through an iris diaphragm of variable radii and their interference patterns with a reference beam	42
3.4	Experimental setup for generating copies of optical vortices and finding their topological charges	44
3.5	Experimental and theoretical intensity profiles of the original vortex and its copies for topological charges 1, 2 and 3	52
3.6	Experimental and theoretical interferograms corresponding to the copies of the vortices	53
4.1	Schematic of the experimental setup for the generation of asymmetrical vortices	58
4.2	Images of a second order vortex and the characteristic interferogram	61
4.3	Experimental results of the splitting of a second order optical vortex on increasing the asymmetry	62
4.4	Simulated results of the splitting of a second order optical vortex on increasing the asymmetry	63

List of Figures

4.5	Trajectories of the unit charge vortices after splitting from a doubly charge vortex with increasing asymmetry	64
4.6	Symmetric and asymmetric vortices of order 2 at $z=0$	65
4.7	Plot showing the increase of the distance between split vortices with increasing asymmetry	66
4.8	Experimental results of the splitting of third and fourth order optical vortex with increasing asymmetry and their interferograms with a reference beam	67
4.9	Simulated results of the splitting of third and fourth order optical vortex with increasing asymmetry and their interferograms with a reference beam	68
5.1	Experimental setup of a shearing Sagnac interferometer for obtaining the two-point correlation function of optical vortices	74
5.2	Two-point correlation function for a Gaussian beam and an optical vortex of order 1	75
5.3	Plots showing the 1D projection of two-point correlation function of a Gaussian beam and optical vortices of order 1, 2 and 3	76
5.4	Plot of the degree of coherence of 1D projections of a Gaussian beam and optical vortices of orders 1, 2 and 3	77
5.5	Plot of the information entropy of 1D projections of a Gaussian beam and optical vortices of orders 1, 2 and 3	78
5.6	Theoretical plot of Wigner distribution functions of the 1D projections of a Gaussian beam and optical vortices of order 1, 2 and 3	79
5.7	Experimental plot of Wigner distribution functions of the 1D projections of a Gaussian beam and optical vortices of order 1, 2 and 3	80
6.1	Schematic of the experimental setup to study the intensity correlation function	83

List of Figures

6.2	Intensity correlation curves for a Gaussian beam and optical vortices of first and third order	85
6.3	Experimental results for the normalized intensity correlation function of the scattered TEM_{00} mode and scattered optical vortices of order 1, 4, and 7 and correlation time; speed of the RGG plate is 645.1 ± 0.8 mm/sec	87
6.4	Experimental results for the normalized intensity correlation function of the scattered TEM_{00} mode and scattered optical vortices of order 1, 4, and 7 and correlation time; speed of the RGG plate is 879.4 ± 0.4 mm/sec	88
6.5	Schematic of the focusing of laser/vortices towards the plane of rotating ground glass and the geometry of rotating ground glass . . .	90
6.6	Plot showing analytical results for (a) $ g^{(1)}(\tau) ^2$ at the speed of RGG plate 879.4 mm/sec and (b) correlation time obtained from $ g^{(1)}(\tau) ^2$	92

Chapter 1

Introduction

The concept of phase in optics is important because it gives a visual perception of wave propagation and transformation along its path. The phase in a beam of light is characterized by the wavefront that is a surface of equal phase, which can have regular shapes like planer, spherical, cylindrical and even helical. The correlation in the phases of two wavefronts led to the interference fringes in the celebrated Young's double slit experiment [1] and supported the wave theory of light. These interference fringes were the bright and the dark patches. Instead of bright and dark patches, Thomas Young could have seen the points of darkness, if he would have further extended his experiment to three or more slits. It is observed that the interference pattern of three or more waves consists the points of darkness in destructive interference. At these points, the intensity of the wave is zero and the phase is undefined (singular); being phase singular points, the optical energy circulates around them. Such singular points are common in optical fields and are known by various names like nodal points, phase singularities, wave dislocations and optical vortices [2-5].

One hundred and fifty years ago, the Scottish Physicist James Clerk Maxwell [6, 7] unified the three apparently separate phenomena i.e. electricity, magnetism and light through the four differential equations. They are now known as Maxwell's equations and elegantly describe several scientific laws very concisely. Using

Maxwell's equations, one can derive second order partial differential equations for electric and magnetic fields those govern the propagation of electromagnetic fields. Only the electric field is responsible for optical effects, therefore we would discuss the solutions of the second order partial differential equations with electric field. When the direction of the polarization is fixed, the electric field vector may be replaced by the scalar electric field strength. In this case, the original vector wave equation reduces to scalar wave equation and in free space it has the form

$$(\nabla^2 + k^2)\chi(x, y, z) = 0 \quad (1.1)$$

where $k = 2\pi/\lambda$ and λ is the wavelength. This equation is known as the Helmholtz equation and it is the most general equation of the propagation of electromagnetic fields. If the space dependent field $\chi(x, y, z)$ is propagating in the z-direction, it can be written as $\chi(x, y, z) = u(x, y, z)\exp(ikz)$. In case of lasers, the z-dependence of the wave amplitude $u(x, y, z)$ is very slow compared to the transverse variation in the width of the beam i.e. the following inequalities can be used in the scalar wave equation [8]

$$\left| \frac{\partial^2 u}{\partial z^2} \right| \ll k \left| \frac{\partial u}{\partial z} \right|, \left| \frac{\partial^2 u}{\partial x^2} \right|, \left| \frac{\partial^2 u}{\partial y^2} \right| \quad (1.2)$$

On using these inequalities, the scalar wave equation reduces to

$$i \frac{\partial u}{\partial z} = -\frac{1}{2k} \left(\frac{\partial^2}{\partial x^2} + \frac{\partial^2}{\partial y^2} \right) u \quad (1.3)$$

This is the paraxial wave equation for the wave propagation. Output fields from the most of practical lasers are described by the solution of the paraxial wave equation. The most common solution is given in terms of the Hermite-Gaussian (HG) polynomials. In rectangular coordinates, these solutions can be separated into products of identical solutions in the x and y directions, i.e. $u_{nm}^{HG}(x, y, z) = u_n(x, z)u_m(y, z)$, where $u_n(x, z)$ and $u_m(y, z)$ have the same mathematical form, n and m are positive integers. The most general form of the HG mode functions can

be written as [9]

$$\begin{aligned}
 u_{nm}^{HG}(x, y) &= \frac{C_{nm}^{HG}}{w(z)} \exp\left[-ik \frac{(x^2 + y^2)z}{2(z^2 + z_R^2)}\right] \exp\left(-\frac{x^2 + y^2}{w^2(z)}\right) \\
 &\times \exp[-(n + m + 1)\psi(z)] H_n\left(\frac{\sqrt{2x}}{w(z)}\right) H_m\left(\frac{\sqrt{2y}}{w(z)}\right)
 \end{aligned} \tag{1.4}$$

where $w^2(z) = \frac{2(z^2 + z_R^2)}{kz_R}$, $\psi(z) = \arctan(\frac{z}{z_R})$, C_{nm}^{HG} is a normalization constant, $H_n(x)$ is the Hermite polynomial of order n , k is the wave number, z_R is the Rayleigh range, $(n + m + 1)\psi(z)$ is the Guoy phase, $R(z)$ the radius of curvature and $w(z)$ is the radius at which the Gaussian term falls to $1/e$ of its on-axis value.

In addition to these HG modes which have rectangular symmetry, the solutions of paraxial wave equation could also be expressed in terms of cylindrically symmetric Laguerre-Gaussian (LG) functions. The field amplitude of the LG modes is given as [9]

$$\begin{aligned}
 u_{lp}^{LG}(x, y) &= \frac{C_{lp}^{LG}}{w(z)} \left(\frac{r\sqrt{2}}{w(z)}\right)^l \exp\left[-\frac{r^2}{w^2(z)}\right] L_p^l\left(\frac{2r^2}{w^2(z)}\right) \\
 &\times \exp\left[-\frac{ikr^2z}{2(z^2 + z_R^2)}\right] \exp(-il\phi) \exp[i(2p + l + 1)\psi(z)]
 \end{aligned} \tag{1.5}$$

where C_{lp}^{LG} is the normalization constant, $L_p^l(x)$ is the generalized Laguerre polynomial, $l = m - n$ and $p = \min(n, m)$. These LG modes have an azimuthal phase dependence term $\exp(-il\phi)$ which makes the wavefront helical and in turn gives an orbital angular momentum to these beams. The LG modes with a particular mode indices ($p = 0$ and $l = \text{integer}$) are called optical vortices of order l . Since the HG and LG modes form a complete basis sets therefore each of these can be expressed in terms of the other.

It is clear from the above discussion that solutions of the paraxial wave equation which is derived from the Maxwell's equations can contain azimuthal phase terms. These phase terms are responsible for the existence of the singularities.

It should be noted that the Laguerre- Gaussian modes are not the only solution

of paraxial wave equation that contain the azimuthal phase dependence, there are other class of solutions also, like Mathieu [10], Bessel [11], Bessel-Gaussian [12], Ince-Gaussian [13], Circular [14], Hypergeometric [15], Hypergeometric-Gaussian type-I and type-II beams [16, 17] that contain the azimuthal phase dependence.

This thesis deals with the coherence properties of optical vortices. It includes interference, diffraction and intensity correlation of electromagnetic waves which are some of the observable facts and owe their explanation to the coherence.

1.1 Singular Optics and Optical Vortices

In the beginning of 1970s, it was observed that in the ultrasonic pulses reflected from a rough surface, the scattered wave trains carried dislocations in their wavefront (surface of constant phase) which were similar to the dislocations in imperfect crystals [2, 18]. This discovery originated from the understanding of the radio echoes from the bottom of the Antarctic ice sheet. The spatial fine structure of the radio echoes was studied for the precise determination of the position of hidden objects. The laboratory analogue of this experiment was done with ultrasound instead of radio waves due to the obvious reason of low frequency of ultrasound. The low frequency of ultrasounds enabled to the detailed study of phase structure of the echoes and led to the discovery of dislocations in the wavefront. In detailed theoretical model of Nye and Berry [2], it was proposed that these dislocations may be edge, screw or mixed edge-screw. It has also been proposed that these dislocations can be curved, collide and rebound, annihilate each other or be created as loops or pairs. The phase of waves remains indeterminate on the points along the dislocation line. Such phase indeterminate points of the wave fields are called phase singularities. The earliest known scientific description of phase singularity was made in the 1830s by Whewell as described by Berry [19]. Dirac [20] in 1931 was the next who talked about the quantized singularities in electromagnetic fields. Nowadays, singularities are identified differently in different systems like in acous-

tics, they are threads of silence [2]; in optics, they are caustics-the infinite intensity points [18], optical vortices-the points of phase singularity [3], and polarization singularities [21]; in superfluids and superconductors, they are quantized vortices [22]. The wide interests of singularities in electromagnetic fields have motivated to start a new branch in optics known as singular optics [5, 23].

Although there exist different types of singularities, we will focus only on the phase singularities of the electromagnetic fields. At the point of a phase singularity, phase is undefined. This can be understood by considering the simplest complex function $x + iy$ whose phase can be given as $\arctan(y/x)$. At the point $x = y = 0$, amplitude of the wave becomes zero and phase is not defined, hence it is a phase singular point, or the function is said to have a phase singularity at this point.

Waves those possess phase singularity and rotational flow around the singular points are called vortices. Vortices can be found in nature at different scales from water whirlpools, atmospheric tornadoes to quantized vortices in superfluids and Bose Einstein condensate. However, we are interested in studying the properties of optical vortices. They are recognized as beams having zero intensity (darkness) at their center. The phase of an optical vortex varies in a cork screw manner along the direction of propagation. Unlike the well known plane, spherical and cylindrical wave fronts, an optical vortex has helical wavefront. As discussed in LG beams, the phase in such a wavefront depends on the azimuthal angle like $\exp(il\theta)$. The factor l is called the order of the vortex or its topological charge, which determines how many times the phase should change by 2π on one complete rotation around the center of the vortex [24]. It is positive for clockwise sense of rotation of the phase and negative for the counter-clockwise (Fig. [1.1]). As a result of the helical wavefront, an optical vortex contains orbital angular momentum [25]. If a vortex beam is circularly polarized it will have both the spin angular momentum and the orbital angular momentum.

In Fig. [1.1], we have shown a comparison of different properties of a plane Gaussian beam and optical vortices of positive and negative unit charges. In case

of oppositely charged vortices the intensity profiles are similar, however other

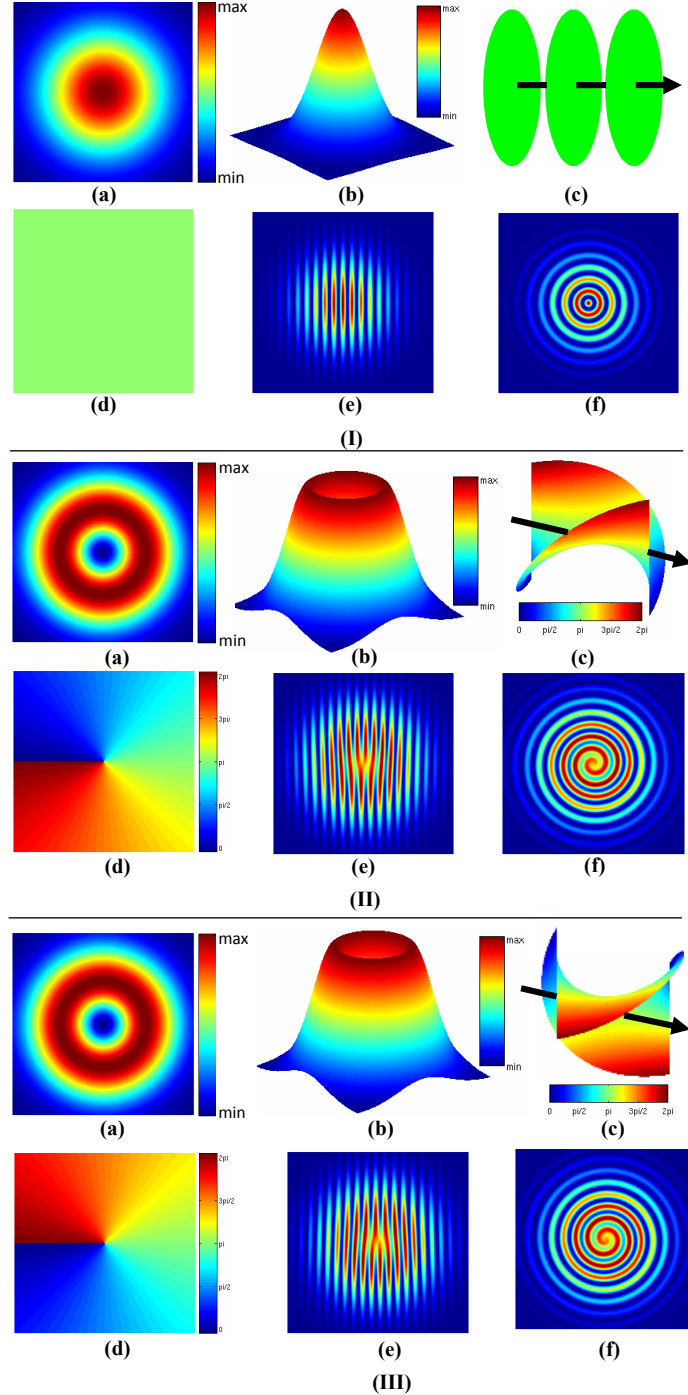


Figure 1.1: Comparison of (a,b) 2D and 3D intensity profile (c) wavefront (d) phase profile and (e,f) interference pattern with a plane reference beam and spherical beam of (I) a plane Gaussian beam (II,III) optical vortex of charge +1 and -1

properties are different. In Fig. [1.2] we show all of these properties for optical vortices of charge $+2$ and -2 .

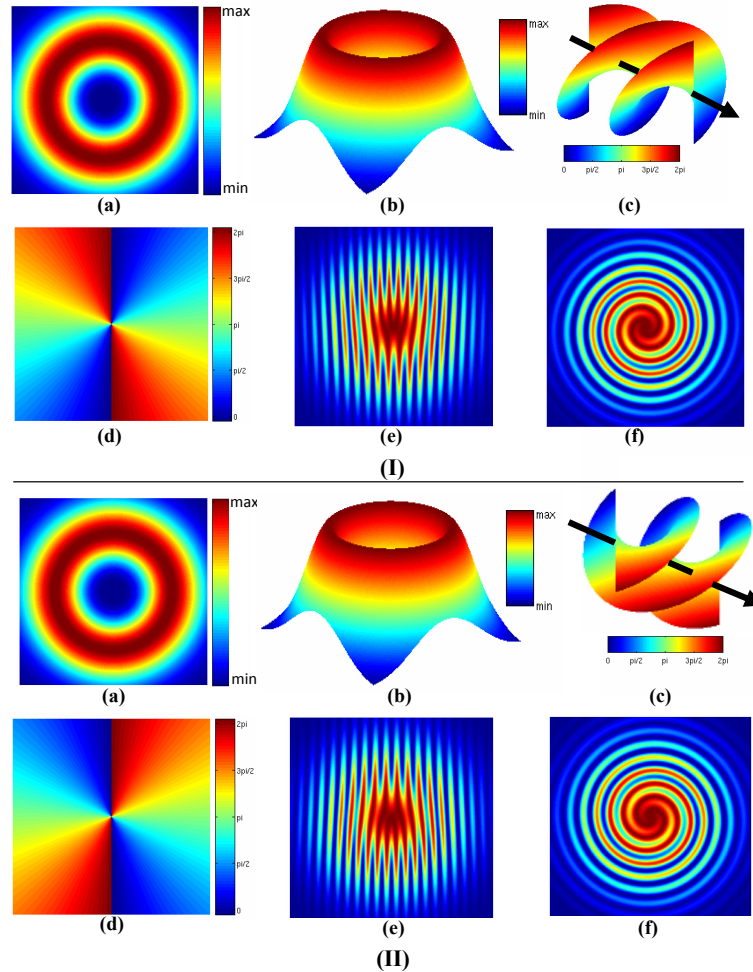


Figure 1.2: Comparison of (a-b) 2D and 3D intensity profile (c) wavefront (d) phase profile and (e-f) interference pattern with a plane reference beam and spherical beam of (I-II) optical vortex of charge $+2$ and -2

Optical vortices could be seen in scattering of laser light through rough surfaces [26], however, they can also be generated in a controlled manner [27]. In the speckle patterns formed by scattering of laser beams, one can see many dark spots which are actually optical vortices of order 1. These are formed by the interference of many scattered waves [28]. In isotropic random fields the probability of creating

positive and negative-charge vortex is the same, so the sum of all the vortex charges remains zero.

1.2 First Order Coherence

Interference is a key aspect for demonstrating the wave nature of light. The famous Young's double-slit experiment shows the interference phenomena and has supported the wave nature of light. The concept of coherence comes from this landmark double slit experiment of Thomas Young [1]. Since then the coherence properties of electromagnetic fields have been a source of interest to many fundamental and applied issues in science and technology. The simplest manifestation of coherence in the oscillations of electromagnetic fields is provided by the interference fringes. Traditionally, the degree of coherence in optics is defined as a measure of the degree of correlation in the electromagnetic field at two spatial or temporal coordinates [29]. If the coherence is measured at two spatial points at a fixed time then it is said to be a spatial coherence, and the maximum distance between the two points where the considerable correlation of the field is observed, is called the coherence distance. The total area in which fields between any two points could be correlated is called coherence area. On the other hand, if the correlation of the field is measured at a fixed point for different time intervals then it is said to be temporal coherence. The time for which the correlation between the fields exist is called the coherence time and the coherence time multiplied by the speed of light is known as the coherence length.

All the properties which deal with the correlation of fields can be listed under the first order coherence [29]. The diffraction pattern is one of the consequences of the first order coherence. According to Huygens theory, the diffraction from an aperture is the superposition of many secondary wavelets and forms a characteristic pattern. We have studied the vortex diffraction through different apertures. The spatial phase distribution of a beam also plays a crucial role in its propagation

and governs the stability of the propagating beam. The distribution of composite vortices in a beam can be studied through the interference. We have used the interferometric technique to detect the splitting of higher order optical vortices with introduced asymmetry.

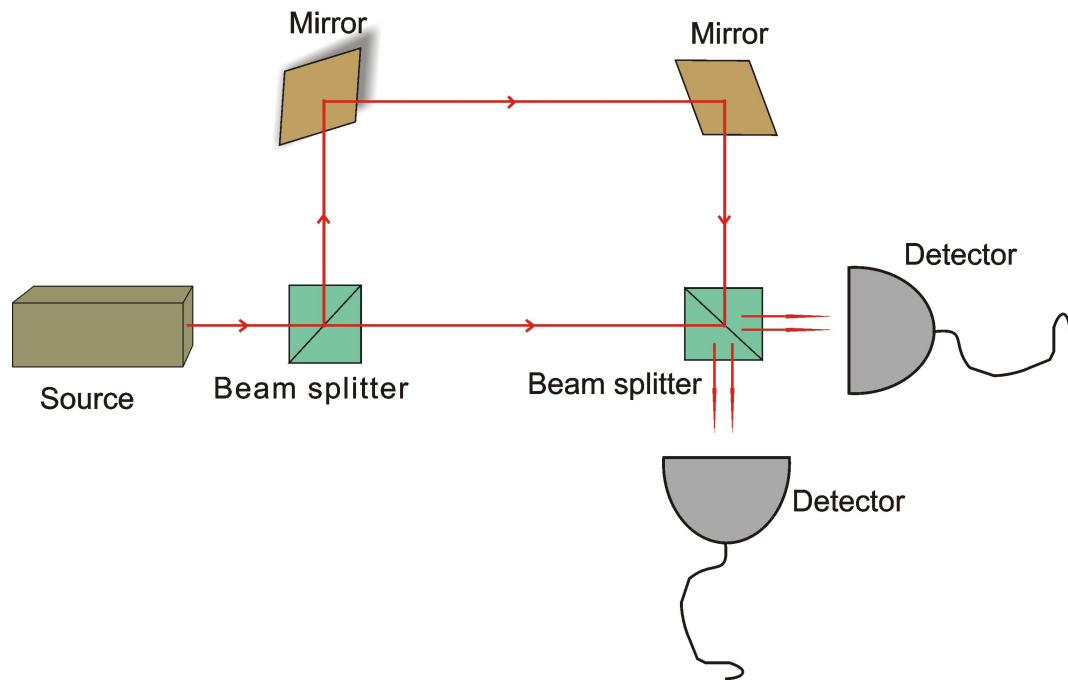


Figure 1.3: *Mach-Zehnder Interferometer to study the first order coherence.*

Mach-Zehnder interferometer shown in Fig. [1.3] is one of the simplest arrangements that could be used to study the first order coherence of the electromagnetic fields. It is an arrangement of two mirrors and two beam splitters. The light beam from the source is divided by a beam splitter into two beams and with the help of two mirrors the desired additional path is introduced in one of the beams. Finally these two beams are combined at the second beam splitter and results into the interference fringes that can be recorded by either of the two detectors. The visibility of these fringes is a measure of the first order coherence.

1.3 Second Order Coherence

In astronomy, the Michelson stellar interferometer is the most common method to determine the angular size of the visible stars. This interferometer measures the fringe visibility to find the size of stars and deals with the first order coherence. In the 1950s, two astronomers Robert Hanbury Brown and Richard Q. Twiss (HBT) thought of doing intensity interferometric experiments. They performed a series of experiments to show whether there exists any correlation between the intensities coming from stars. As a result, they found the existence of correlation between the intensities. If the two points where the correlation in intensities are to be measured lie within the coherence area of the source, a good correlation is observed. In this way they developed a new interferometric technique called intensity interferometry [30] which was a breakthrough in astronomy as well as in the fundamental coherence theory of electromagnetic fields. Until this experiment, it was known that the coherence could be defined only by the interference fringes and the degree of coherence was found to depend on the field variables. However, after the HBT experiments, the coherence could not only be restricted to the correlation between the fields but can also be measured by the correlation between the intensities. Since intensities depend quadratically on the field variables therefore these experiments have led to study of higher order correlations in fields. The intensity is defined as the modulus square of the field, therefore, coherence measured in HBT experiments can be named as the second order coherence. The results of HBT experiments heralded the birth of modern quantum optics [31].

The intensity correlation is studied under various names like the intensity correlation spectroscopy (ICS), the intensity fluctuation spectroscopy (IFS), the photon correlation spectroscopy (PCS), the quasi elastic light scattering (QELS) and the dynamic light scattering (DLS) [32].

After this brief introduction we would like to elaborate on interesting historical progress of the second order coherence phenomena. As pointed out in earlier dis-

cussion, the concept of second order coherence came from the radio astronomy [33]. It was known since a long ago that the Michelson stellar interferometer could be used to determine the size of astronomical objects. This technique relies on the visibility of interference fringes, therefore, it is very much sensitive to the atmospheric turbulence and other fluctuations. Also, if somebody wants to do the radio astronomy with this interferometer it would not be possible to get encouraging results because of the large wavelength of radio waves. The required stability in the interferometer could not be maintained over such long distances and the resolving power of the instrument was the main problem in measuring the angular diameter of the distant stars. In Michelson stellar interferometer, the resolving power depends primarily on the ratio of the wavelength to the base line. For achieving a good resolution in interference fringes either wavelength should be very small or the base line should be large. To measure the angular size of the two brightest radio stars Cygnus and Cassiopeia with much accuracy, it was estimated a need of interferometer with 10-50 Km baseline [33]. However, with such a large baseline it was very difficult task to maintain the adequate stability of the phase. To overcome these difficulties Robert Hanbury Brown and colleagues in 1952 [33] suggested a new technique for determining the size of radio stars. In their new setup, radio waves were collected by two aerials and passed through the two separate square law detectors and the to low band pass filters. Finally, the individual intensities from the two detectors and a correlation between them was measured. It was essential that all the low frequency components preserve the phase of the two low frequency signals. In practice this process was considerably simpler than preserving the relative phase of the radio frequency signals in conventional interferometer. Therefore this new type of interferometer was easier to use and became popular.

The simplest expression of the cross correlation coefficient (ρ) is calculated by assuming a rectangular source with uniform surface intensity and is given as

$$\rho = \frac{\sin^2(\pi\alpha b/\lambda)}{(\pi\alpha b/\lambda)^2} \quad (1.6)$$

where b is the base line length, λ is the wavelength of the light and α is the angular width of the source. Therefore, by knowing the value of the cross correlation coefficient and the base line length, the angular diameter of the star can be evaluated. This expression is equivalent to the fringe visibility in a Michelson stellar interferometer. To find the shape of stars, base lines of different lengths and different orientations are used.

In the theoretical formulation of the new type of interferometer, the different points of the radio star are considered to emit electromagnetic radiation of slightly different frequencies in different directions. At a particular detection point the superposition of the many frequencies forms the beats and the detector detects the intensity variation of the beats [30]. In this arrangement, it is noteworthy that although the use of the two independent receivers destroy all information about the absolute phase in either aerial of any single radio frequency component, information about the angular size of the source is preserved by the relative phases of the corresponding beat-frequencies in the detectors output.

Soon after the successful experiment on radio sources, Brown and Twiss used intensity interferometer for the visible (optical) sources. It was expected that the time of arrival of photons at two photo cathodes should be correlated when the incident light beam upon two mirrors are coherent, but it was not tested until the HBT experiment. However, it is by no means certain that the correlation would be preserved in the photo detection process. To demonstrate these facts, HBT [34] performed a laboratory experiment (setup shown in Fig.[1.4]) with Hg arc lamp ($\lambda = 435.8$ nm). The light from the Hg arc lamp was divided by a half silvered mirror (beam splitter) and detected by two photomultiplier tubes (PMTs). One of the PMT was mounted on a horizontal slide which could be traversed normal to the incident light. The outputs of the two PMTs were amplified and sent to the correlator. First data set was recorded by keeping two PMTs as the mirror image of each other (cathodes of the PMTs superimposed) and the next set of data was recorded with displacing one of the PMTs. As a result, maximum corre-

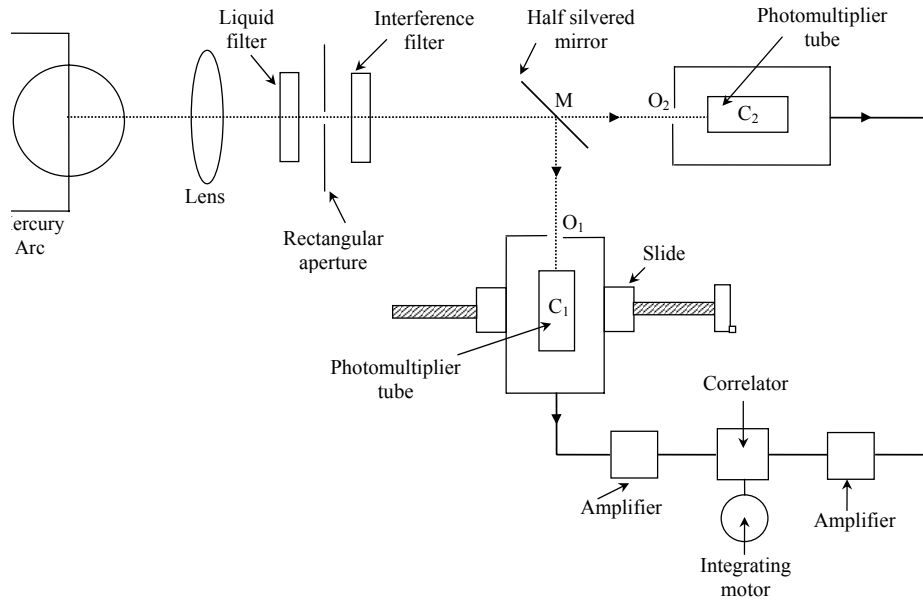


Figure 1.4: *Laboratory setup of the Hanbury-Brown and Twiss experiment (not to scale). (Redrawn following Hanbury Brown et al.) [34].*

lation was observed when both the cathodes were superimposed. It decreased with the displacement of the PMT and became minimum (ideally zero) when the two cathodes were separated by twice of their aperture size (Fig.[1.5]) [35]. Thus the experiment answered the question that the photons in two coherent beams of light were correlated and this correlation was preserved in the process of the photoelectric emission. Theoretical formulation of these experimental results was made by assuming that the probability of emission of a photoelectron is proportional to the square of the amplitude of the incident light. The classical electromagnetic wave theory was employed to calculate the correlation between the fluctuations in the currents from the two cathodes. The experimental results were in a fair agreement with the theoretical results. Soon after the successful laboratory experiment of the HBT, some controversy surrounded the HBT results [36].

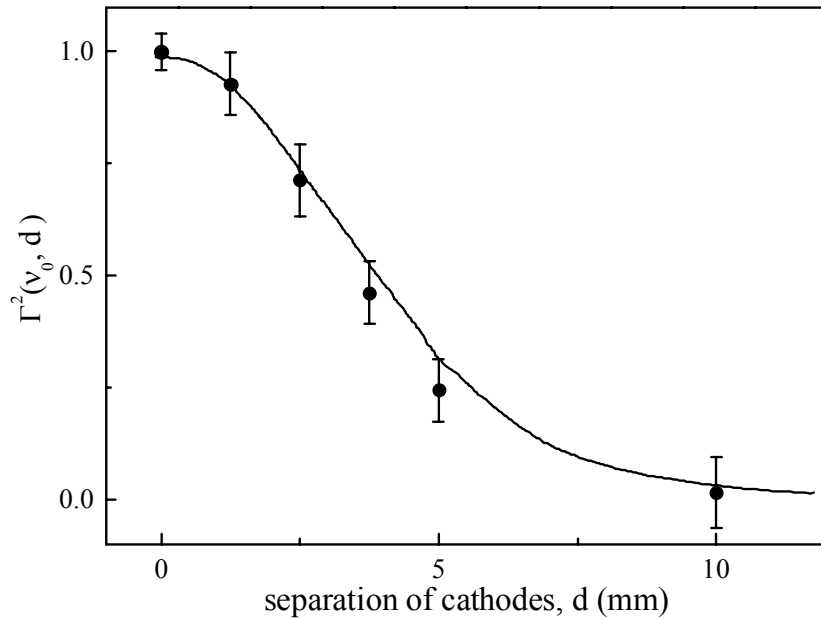


Figure 1.5: *The experimental and theoretical values for the normalized correlation factor $\Gamma^2(\nu_0, d)$ for different values of separation of the photocathodes. The full line represents the theoretical while dots show experimental values. (Redrawn following Hanbury Brown et al.) [35].*

A few papers appeared showing no change in the results of HBT type experiments with coincidence techniques, for coherent and incoherent light. Furthermore, these authors suggested that the results obtained by HBT were due, not to a true correlation between the arrival times of quanta, but to some other cause such as an intensity fluctuation in the light source.

In reply to all these controversies, it was stated by Purcell [37] and HBT [38] that there was no real disagreement between the results of these two experiments but the experiments which raised the controversy were too insensitive to detect the effect. A new experiment was performed [39] and instead of the correlator, a coincidence technique was used to detect the behavior of the light quanta from the coherent beams of light. The results of the experiments were found consistent with the previously reported HBT experiment. In addition, the experiments

which created controversy were also repeated under the conditions which permit the detection of the effect and obtained positive results. Thus, it was confirmed again that the arrival times of photons at different points were correlated when these were illuminated by a coherent beam of light. Soon after the laboratory experiment, HBT tested this new type of interferometer for calculating the size of a star (Sirius) and found good agreement in the experimentally observed and theoretically calculated results [40].

The explanation of the detection processes for the radio waves and the optical waves through a consistent theory was a difficult task. The measurement of the correlation in intensity fluctuations is straightforward for the radio waves, however the detection of the optical waves rely on the fast photoelectric detectors. In the spectral regions of radio waves, the electromagnetic field drives the oscillatory motion of electrons in an antenna and the subsequent detection of intensity fluctuations is done by well known electronic devices. However, the situation is quite different with the detection of optical waves. Optical frequencies oscillate too rapidly to directly measure and process the electric field electronically. Instead optical photons are (usually) detected by absorbing the photon's energy, thus only revealing the magnitude, and not the electric field's phase. Such detectors are, however, highly non-classical devices, making use of photoelectric effect. Therefore, it was a genuine issue that whether the expression for the intensity correlation function based on the classical wave theory of radio waves would also hold for optical detection or not. This issue was resolved and results pointed to the validity of the classical formula even under the optical detection [41]. The justification involved the beautiful physics of the wave-particle duality of light.

The original HBT experiment was done with a thermal light source and a bunching effect (tendency of photons to clump) was observed for this source. However, after the invention of laser, the same experiment was repeated with a laser beam that gave a flat correlation curve (no bunching effect) [42]. The HBT results are even more surprising when the experiment is done with a single photon source, for

such sources minimum correlation is observed for zero path delay between the two arms in HBT experiment (anti bunching) [43]. These results are purely quantum mechanical and beyond the scope of this thesis.

We have performed the HBT type experiments with optical vortices- beams carrying an additional degree of freedom i. e. orbital angular momentum. Results are compared with the that of the Gaussian laser beam.

Chapter 2

Generation and Characterization of Optical Vortices

In the laser speckle one can see many dark points/spots which are randomly distributed optical vortices, however, in this form they could not be useful for further applications. Therefore, it is necessary to generate optical vortices in a controlled manner. The prime task for the generation of optical vortex is to make a suitable diffractive optical element (DOE). Although the DOE for the generation of optical vortices can be fabricated by the lithography techniques, but these are relatively expensive and labor intensive. Thanks to the computer generated holography technique that has made life much simpler, its inexpensiveness and versatility of the generation of the desired DOE has been widely acclaimed. For some specific applications, other methods like spiral phase plate and astigmatic mode converters are also used for the generation of optical vortices. We would elaborate on the computer generated holography technique and also highlight some of the other methods in the first section of this chapter.

Optical vortices have helical wavefront that defines the topological charge and gives orbital angular momentum to such beams. To characterize vortices for their charge, interferometric method would be discussed in the second part of the chapter.

2.1 Generation of Optical Vortices

2.1.1 Computer Generated Holography

In this section we would discuss computer generated holograms and spatial light modulators. These are technically two different methods working on the principle of computer generated holography.

2.1.1.1 Computer Generated Holograms

This is the simplest method to generate an optical vortex. Computer generated hologram (CGH) is basically an interference pattern of an object beam with a reference beam obtained through a computer [44–46]. When the object beam is an optical vortex and the reference beam is a plane Gaussian beam then the interference pattern looks a fork like pattern. The reduced size of this pattern is either cast on a holographic sheet [44] or printed by a high dpi laser printer on a transparency sheet. On passing a laser beam through the branch point of generated fork pattern we get a diffraction pattern consisting of various orders of optical vortex. The intensity of these vortices decreases as the order increases. The dark area at the center of the cross section of the beam increases with the increase in the order of the vortex.

Before describing the experimental part, we would discuss the mathematical formulation for the generation of the CGH. The electric field of an optical vortex of order m can be given as

$$E = E_0(x + iy)^m e^{-(x^2+y^2)/w^2} e^{-ik(x^2+y^2)/2R} e^{-i(kz+\phi)} \quad (2.1)$$

where w is the spot size, R is the radius of the curvature and ϕ is the Guoy phase shift. In cylindrical coordinate system this equation reduces to

$$E = E_0 r^m e^{\pm im\theta} e^{-r^2/w^2} e^{-ikr^2/2R} e^{-i(kz+\phi)} \quad (2.2)$$

Consider a plane reference beam

$$E_r = E_{r0}e^{-i(k_x x + k_z z)} \quad (2.3)$$

The intensity distribution of the interference of a first order vortex (say at beam waist, $R \rightarrow \infty$) and the reference beam at $z = 0$ can be given as

$$I = |E_{r0}e^{-ik_x x} + E_0 r e^{\pm i\theta} e^{-r^2/w^2}|^2 \quad (2.4)$$

Assuming E_{r0} , E_0 and w as unity and ignoring all the amplitude variations in Eq. (2.4), we get the spatially varying transmission function as

$$T = 2[1 + \cos(k_x x + m\theta)] \quad (2.5)$$

When this pattern is illuminated by a Gaussian beam propagating along the axis then the field just after the hologram becomes

$$E_T = T A_0 e^{-r^2/\sigma^2} \quad (2.6)$$

here A_0 is the amplitude and σ is the beam size. On using Eq. (2.5) we get

$$E_T = 2A_0 e^{-r^2/\sigma^2} + A_0 e^{-r^2/\sigma^2} e^{i(k_x x + m\theta)} + A_0 e^{-r^2/\sigma^2} e^{-i(k_x x + m\theta)} \quad (2.7)$$

This output field contains one zero order diffraction pattern along the axis and two first order diffracted beams with vortices of opposite charge on either side of the zeroth order. The amplitude transmission function of Eq. (2.5) is a fork like grating with sinusoidal optical density variation (Fig. [2.1a]). This is called an amplitude hologram because it modulates the amplitude of the incident beam. The white portion (transparent part) of this hologram allows the light beam to transmit while the black portion (opaque part) absorbs the light. Therefore, the

light diffracted through such hologram acquires the prescribed phase-front defined by the transmission function.

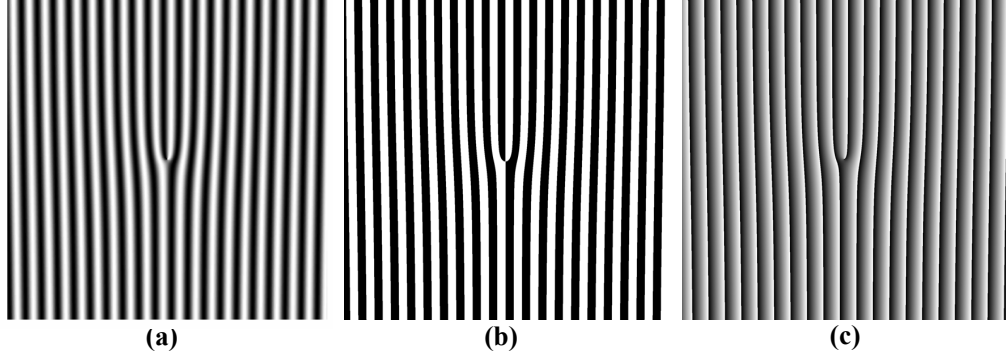


Figure 2.1: *Computer generated holograms with different transmission functions for the generation of optical vortex of order 1, (a) Sinusoidal (b) Binary (c) Blazed.*

Apart from sinusoidal transmission function, holograms with other types of transmission functions can also be generated, e.g. for binary hologram, the transmission function becomes

$$T_{binary} = \text{sign}[2(1 + \cos(k_x x + m\theta))] \quad (2.8)$$

where $\text{sign}[x] = x/|x|$. Binary holograms (Fig. [2.1b]) are much easier to print than the sinusoidal variation of optical density given in Eq. (2.5) and also their diffraction efficiency is better than the sinusoidal transmission grating.

Blazed gratings are also used to generate optical vortex with good diffraction efficiency in the first diffracted order. The transmission function for such a grating is

$$T_{blazed} = \frac{1}{2\pi} \text{Mod}(k_x x + m\theta, 2\pi) \quad (2.9)$$

where $\text{Mod}(\alpha, \beta)$ is the remainder on division of α by β . A blazed grating for the formation of an optical vortex of order 1 is shown in Fig. [2.1c].

Amplitude holograms absorb most of the input power therefore their diffraction efficiency is poor. To overcome this limitation and to maximize the power of optical

vortices phase holograms are used. These holograms ideally do not absorb any power and modulate the phase of incident light according to the stored interference pattern.

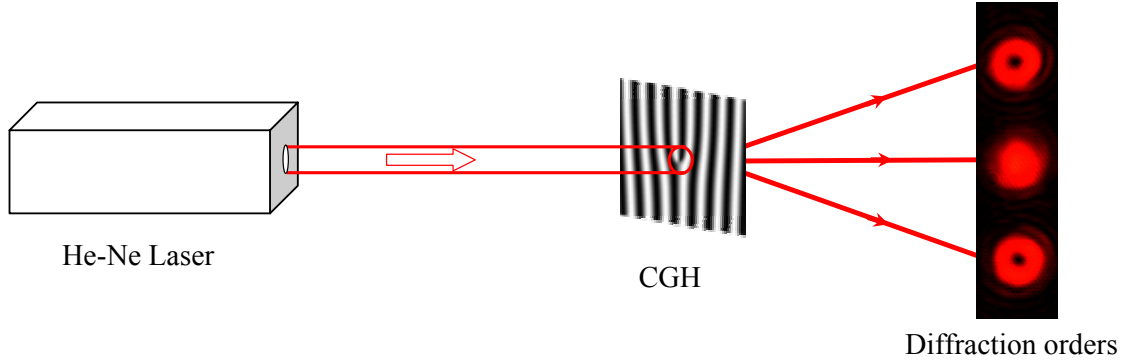


Figure 2.2: *Generation of optical vortex from the CGH and a He-Ne laser.*

In Fig. [2.2], we have shown a simple setup for the generation of optical vortices through a CGH with sinusoidal transmission function. The central order diffraction is a Gaussian beam while first order diffracted beams carry vortices of unit opposite charges.

2.1.1.2 Spatial Light Modulator

Spatial light modulator (SLM) is a device that can modulate light spatially in amplitude and phase [47]. The principle of SLM is based on the properties of liquid crystals. It consists of liquid crystals' cells in which the arrangement of liquid crystal molecules can be altered by applying electric field. SLMs can be electrically addressed or optically addressed. However, in our experiments we have used electrically addressed SLM (Holoeye LC-R 2500). The calculated fork like pattern is transferred into the SLM through a computer. The graphics card for the SLM which is installed in a computer, generates video signal corresponding to the input fork like pattern. This signal is transmitted to the SLM. The electric field of the signal align molecules of the liquid crystals to form a fork type pattern. If

a laser beam is incident on the SLM it results into optical vortices as diffracted orders in reflection or transmission. The SLM we have used is of reflective type. In Fig. [2.3], we have shown a pictorial diagram for working of the SLM used for our experiments.

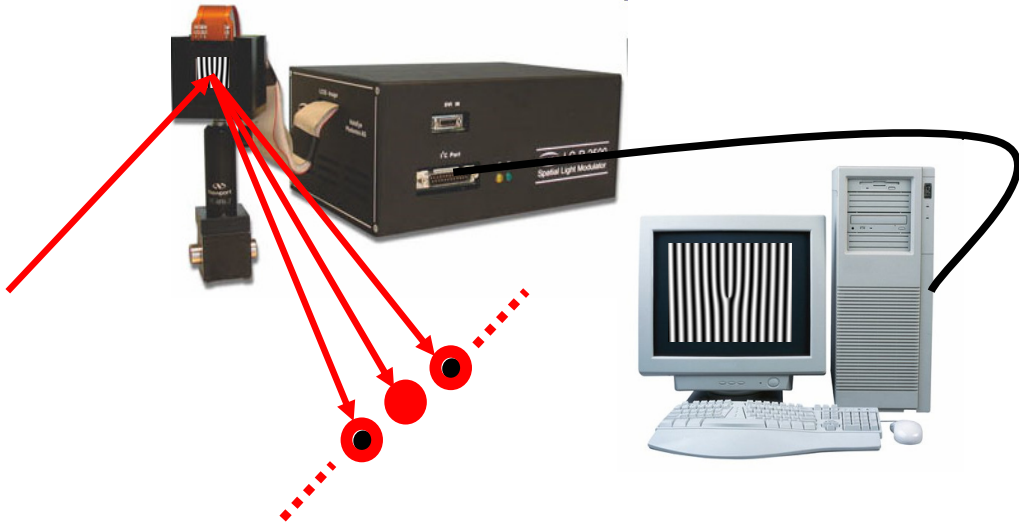


Figure 2.3: *Generation of optical vortex from the SLM and a He-Ne laser.*

SLMs are used to generate optical vortex beams in a prompt and efficient manner. We can generate an array of optical vortices using SLMs [48], which are used for trapping of microscopic particles. The main advantage of SLM over CGH lies in its flexibility and control in real time. One can make any diffractive optical element and refresh it to generate optical vortex of any order when required.

We have studied the effect of resolution of the CGH onto the core size of optical vortices [49]. The CGH with different resolution are transferred to the SLM and corresponding images of vortices are recorded. If we holographically store the interference of a perfect vortex beam with a plane reference beam and reproduce it with the same reference beam, we would get the vortex beam itself with zero intensity at the center, where it has phase singularity. Ideally, the complete darkness (zero intensity) should be only at the center. Practically, we get a dark

region around the center and the holographic image is not having enough resolution to store the detailed information about the rapid variation of the phase near the center of the vortex. To store an interference pattern of a vortex beam and a plane beam of wavelength 632.8 nm, both making angles $\pi/6$ and $-\pi/6$ with the axis, the hologram should be able to record around 16,000 values within 1 cm [50]. But neither a laser printer nor a spatial light modulator is having such an accuracy. It is this inefficiency of casting the hologram, which causes expansion of the dark region from an ideally single point to a larger region. Therefore, as the quality of hologram improves, the quality of image should also improve, which in the case of a vortex, causes a compression of the phase singularity region. We have tried to prove this fact by studying the intensity profile of the vortex of order 1 while changing the resolution of the computer generated holograms.

We supplied holograms to the SLM (Holoeye, LC-R 2500) via a computer monitor interface. The SLM, which works in reflection mode, produces the same diffracting effect as that produced by a grating on a holographic sheet. The resolution of the our SLM is 1024×768 that matches with the interfacing computer monitor. An intensity stabilized He-Ne laser (Spectra-Physics, 117A), wavelength 632.8 nm and power 1 mW is used as the source. The incident laser beam creates a diffraction pattern with vortices whose topological charge increases with diffraction order. The zero order is Gaussian, and the vortices have opposite helicity on either side of this central order. Thus it reproduces the vortex - our object beam. The images are captured using a CCD camera (Point Grey, Flea2 20S4) and the horizontal line intensity profile is analyzed.

We took different images by changing the resolution of the diffracting optical element on the SLM. However, on increasing the resolution of the grating element beyond the resolution of the SLM, the quality of the vortex remains unchanged. Therefore in experiments, the maximum possible resolution of the diffracting element is limited to the maximum resolution 1024×768 of the SLM while in the case of simulation this restriction was imposed by the limited memory of the system.

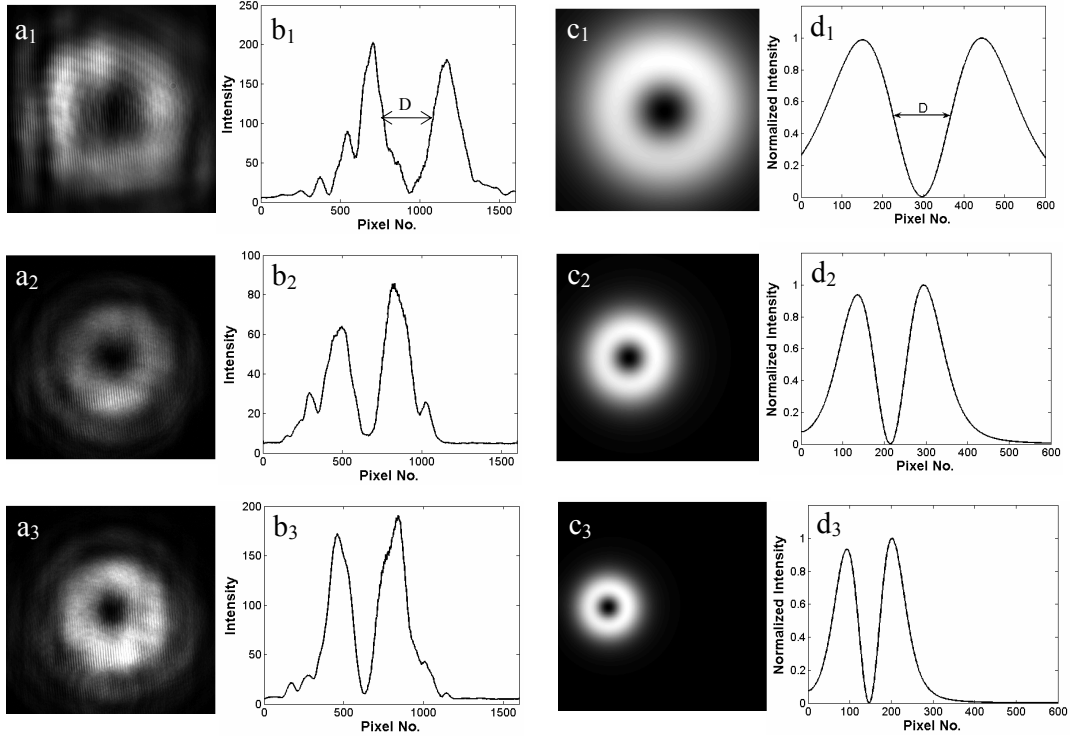


Figure 2.4: *Experimental (a_{is}, b_{is}) and simulated (c_{is}, d_{is}) images of optical vortices ($m=1$) and their horizontal line intensity profiles at different resolutions: ($a_1 - d_1$) 250; ($a_2 - d_2$) 500; and ($a_3 - d_3$) 800.*

The quality of the image is enhanced by increasing the number of data points used to store a fixed computer generated hologram, that is, by increasing the resolution. In Fig. [2.4] we have shown the experimental (two left side columns) as well as the simulated images (two right side columns) of optical vortex of order 1 and their intensity profiles along a horizontal line passing through the center of the vortex. As expected, the diameter of the hole was found to be decreasing with increasing resolution.

We have plotted the normalized diameter (D) of the core (the distance between two diametrically opposite points inside a vortex core where the intensity falls to half of its maximum value) with the resolution of computed diffracting element for simulated as well as experimentally obtained vortices in Fig. [2.5]. The nature of

both experimental and simulated results matches to a great extent. However, as expected, increasing the resolution of the CGH beyond the total number of pixels of the SLM does not make any difference to the diameter of the experimentally obtained vortex. This can be seen through the flat portion of the experimental curve. On the other hand, for simulation there is not any practical limitation for the higher resolution except the memory of the computer used.

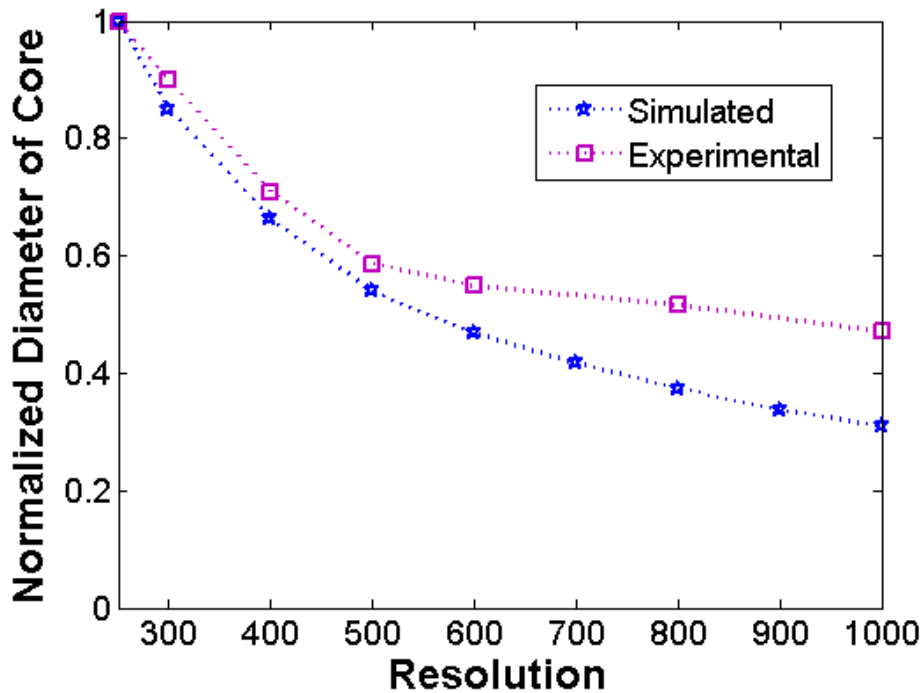


Figure 2.5: *Plot showing the variation of normalized diameter of an optical vortex core with resolution of the CGH transferred to the SLM*

Our results suggest that when vortex beams are produced using computer generated holography, the vortex diameter can be controlled by simply varying the resolution of the hologram i.e. by changing the number of data points used to make the hologram.

2.1.2 Astigmatic Mode Converter

The paraxial Laguerre-Gaussian (LG) beams have an azimuthal phase dependence $\exp(il\phi)$ which causes the orbital angular momentum in these beams. The LG modes as well as the well known Hermite-Gaussian (HG) modes of the lasers form a complete basis set, therefore any of the fields can be written as a superposition of the other. The principle of astigmatic mode converter is based on the conversion of HG mode into LG mode by using a suitable combination of two cylindrical lenses [9, 51]. This conversion exploits properties of the Guoy phase shift which is a phase shift acquired by a Gaussian beam along the direction of propagation during its propagation. At a distance z from the beam waist ($z = 0$) it is defined as $\phi(z) = \tan^{-1}(z/z_R)$, where z_R is the Rayleigh range. The astigmatic mode converter converts a HG mode of arbitrary order into the same order of Laguerre-Gaussian mode and vice-versa. Therefore, using this method one cannot convert the common HG_{00} or TEM_{00} Gaussian beam of the laser to an optical vortex.

2.1.3 Spiral Phase Plate

The spiral phase plate is also a type of mode converter that can generate LG mode from HG beam by introducing a spiral phase to the HG beam [52]. It is a transparent disc whose thickness varies circumferally but is uniform radially. These are constructed from a piece of transparent dielectric materials. When a light beam passes through such plates then it suffers different path delays around the center of the disc. Light beams passing through the thicker part suffer longer optical path and hence greater phase shift. On the whole, due to spiraling thickness it generates spiral phase distribution of the optical vortex.

The traditional spiral phase plate is useful only for one wavelength of light and produces one topological charge. However, the adjustable spiral phase plates [53] can be used with multiple wavelengths and can produce a range of topological charges. Such kind of plates are created by making a crack in a parallel sided

transparent plexiglass, the crack starts from one edge and terminates near the center. Now the plate is mounted in a rigid frame and keeping one tab fixed the other tab is twisted. If a laser beam falls perpendicular to one tab then it will not remain perpendicular to other tab. This modifies the phase of incident light in such a way that a laser beam directed at the end of crack will produce an optical vortex. Thus by changing the twist we can change the order of vortex.

2.2 Characterization of Optical Vortices

The presence of darkness in the intensity profile of any beam does not imply helical wavefront (optical vortex) for the beam, one requires to find out a phase variation around the darkness to confirm the existence of optical vortices in a given beam. Therefore, to identify the helical wavefront or the Laguerre-Gaussian mode, interferometric techniques are used. We know that the interference fringes resulting from the superposition of the two beams with plane wavefronts are straight lines whose spacing depends on the intersection angle and the wavelength of light. However, when we interfere a beam having helical wavefront with a beam having plane wavefront, we get a complicated fringe pattern. The resulting fringe pattern looks like a fork or spiral that depends on the shape and relative orientations of the interfering wavefronts. The number of prongs in the resulting fork pattern decides the order of the vortex. In general, for l^{th} order vortex, we get a fork pattern with $l + 1$ prongs. Interestingly, when we pass a laser beam through a hologram having $l + 1$ prongs in its fork, we get l^{th} order vortex as first diffracted order. However, some find easier to interfere an optical vortex with its own mirror image rather than a plane wave, the resulting interference pattern consists of $2l$ dark spokes (for l^{th} order vortex) [54]. In Fig. [2.6], we show a Mach-Zehnder interferometric setup to characterize an optical vortex. In one arm of the interferometer we have kept a CGH to form vortices and here, we have selected a first order vortex. We let it interfere with a reference Gaussian beam at the beam splitter BS2 and the

interferograms are recorded through a CCD camera.

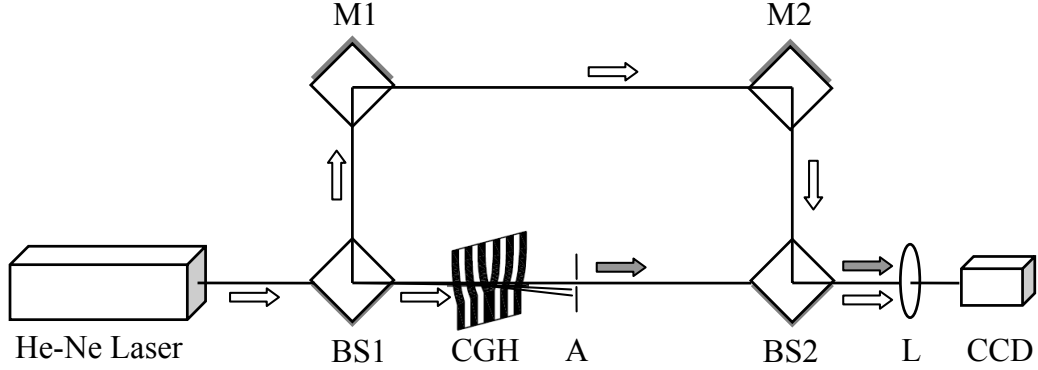


Figure 2.6: *Mach-Zehnder interferometric setup for the characterization of optical vortices. BS1, BS2 beam splitters; M1, M2 mirrors; CGH computer generated hologram; A aperture; L lens; CCD charge coupled device camera.*

In general, for the characterization of an optical vortex, we look for its following physical properties.

2.2.1 Topological Charge

The order of optical vortex is characterized by its topological charge. Topological charge is defined as the number of twists in wavefront per unit wavelength of the light, higher the topological charge more the twisting of wavefront [55]. For an optical vortex of topological charge l , the circulation of the argument of the field $E(x, y)$ along a closed contour containing $x = y = 0$ is defined as

$$\oint \nabla \cdot \text{arg}[E(x, y)] dL = 2l\pi \quad (2.10)$$

The topological charge of a vortex is a direct measure of the orbital angular momentum content, therefore, a great deal of attention has been paid for its determination. Common methods for the determination of topological charge of an

optical vortex include interferometry [56] and diffraction [57, 58]. The interference of an optical vortex with a reference wave produces either spiral fringe pattern or the radial/fork like fringes [59, 60] depending on the relative wavefront curvatures of the two interfering beams. On interfering a vortex beam with a coherent co-propagating divergent spherical beam, one gets the spiral interference fringes exhibiting l fringes starting from the center. The sense of the circulation of the interference fringes is determined by the sign of the topological charge and relative curvatures of the two interfering waves [59]. With equal radii of curvatures, the interference fringes do not bend and look like a star with number of arms equal to the modulus of the topological charge. Topological charge of an optical vortex can also be determined by using off-axis interferograms [59]. When a reference wave has positive projection of a wave vector with polar axis and the topological charge is positive, a fork like pattern directed upward appears and this orientation would be downward for the negative topological charge. The magnitude of the topological charge is equal to the number of prongs in fork minus one i.e. for the topological charge l we would get a fork with $l + 1$ prongs.

In Fig. [2.7], we have shown the interference fringes obtained through the Mach-Zehnder interferometer shown in Fig. [2.6] for beams with topological charges 0, 1 and -1. In first row, the interference fringes obtained by interfering a vortex beam with a tilted plane reference beam has been shown. As discussed, it can be seen that the interference fringes are straight lines for a plane Gaussian beam ($l=0$) and these are fork like patterns with upward and downward orientations for positive and negative topological charges respectively. In second row, interference fringes are recorded for co-propagating plane reference wave and object beam with topological charges 0, 1 and -1. The resulted interferograms verify our earlier assertion.

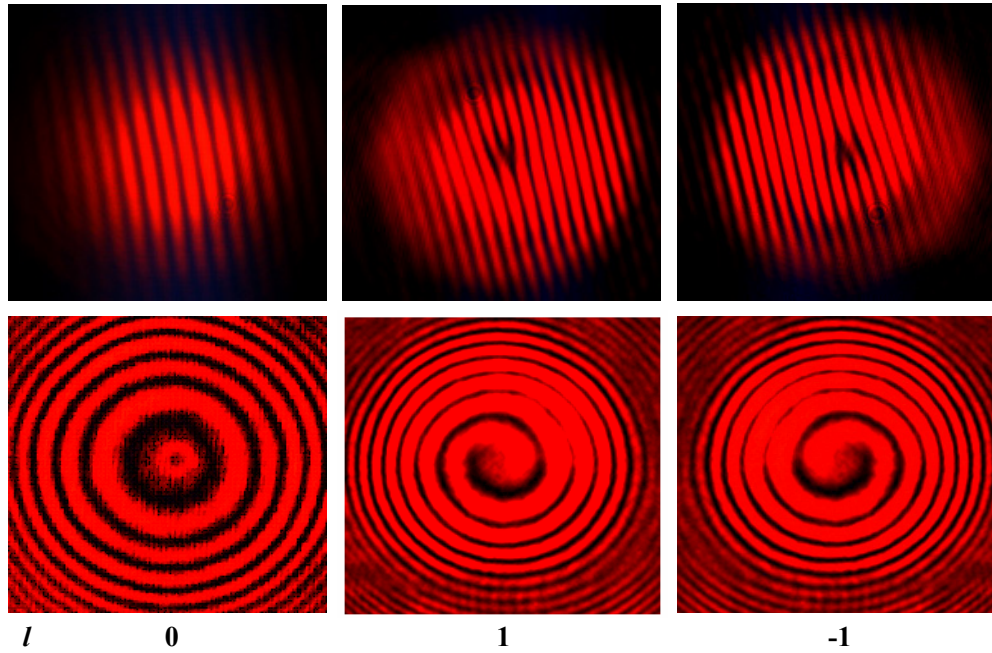


Figure 2.7: *Interference fringes obtained through the Mach-Zehnder interferometer for beams with topological charges 0, 1 and -1.*

It has been found that the topological charge of a noncanonical vortex, for example a vortex passed through a cylindrical lens reverses its sign on propagation [56, 61]. The coaxial and the non coaxial superposition of optical vortices create different topological charge content in the resultant beam [62]. Topological charges are found to be very robust with respect to the perturbation. On adding a small coherent background to such beams they do not destroy, however, they shift to the new positions that could be found out by equating the total wave amplitude to zero [24]; the higher topological charges break up into same number of unit charges [63].

2.2.2 Orbital Angular Momentum

Unlike usual Gaussian beams from the lasers, optical vortices have an orbital angular momentum (OAM). The spin angular momentum of light or photon is always

intrinsic but the orbital angular momentum of the photon may be either intrinsic or extrinsic [64, 65]. The OAM of a light beam depends on the inclination of wavefront [66]. The spin angular momentum of light is always $\sigma\hbar$ where degree of polarization $\sigma = \pm 1$ for right and left handed circularly polarized light respectively and it is zero for linearly polarized light. Unlike spin angular momentum, the OAM depends on the choice of aperture or calculation axis. The OAM is $l\hbar$ per photon only when the aperture or calculation axis coincides with the axis of original beam.

Allen et al. [25] proposed the measurement of OAM of the LG beam by measuring the torque applied to an optical system by the transfer of OAM. Consequently the direct transfer of OAM to absorptive particles from a laser beam with phase singularity (optical vortex) was observed [67]. They trapped an absorptive particle by an optical vortex and observed the rotation of particles in the trap. To confirm that this rotation is only due to the OAM associated with the helical wavefront they took the linearly polarized light having zero spin angular momentum. They also observed that on inverting the sign of optical vortex, the direction of rotation of particles also gets inverted. Presently, experimental techniques are available which can measure orbital angular momentum of single photon [68] along with spin angular momentum and total angular momentum [69] of the photon.

The transfer of OAM by a fractional optical vortex has also been observed [70]. It was observed that the rotational speed of particles decreases with increase of the radial opening of optical vortex even though the fractional charge has increased. Unlike the integer order optical vortices, fractional optical vortices have radial opening which resists or even stops the rotation of particles.

2.2.3 Propagation

The propagation dynamics of a single charge vortex or the multiple charges sitting in the same host beam is very peculiar either in free space or any optical system.

The propagation of an optical vortex embedded in a host beam depends upon the shape and evolution of the host beam [71–73]. A canonical vortex, a vortex for which lines of zero crossing of the field form a right angle, sitting in a rotationally symmetric beam can propagate without change of its shape and location in free space [74]. However, for a non-canonical vortex for which lines of zero crossing of the field don't form a right angle [75], the trajectories are not straight lines. For such a vortex, the topological charge also changes its sign even for free space propagation [56, 61]. Propagation of non-canonical vortices can be controlled by the non-canonical parameter associated with these vortices.

To produce a noncanonical vortex, one can put a cylindrical lens in the path of canonical vortex. Singh et al. [75] placed a positive cylindrical lens in the path of the vortex beam. The shape of the resulting noncanonical vortex at two different distances from the cylindrical lens is shown in Fig. [2.8]. It is clear from the the images that the shape of noncanonical vortex changes on propagation, initially it is aligned along the horizontal axis, however, on propagation it tends to align in vertical direction.

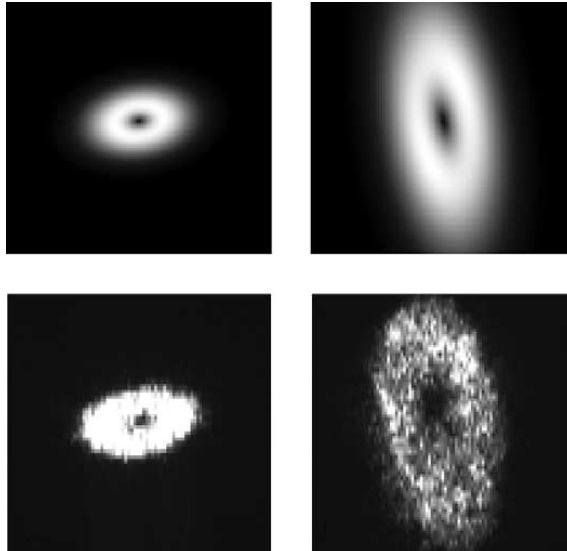


Figure 2.8: *Shape of the vortex after passing through the cylindrical lens of focal length 7 cm at distances 2.5 cm (left) and 22.5 cm (right) from the lens: theoretical (top), experimental (bottom) with no image processing.*

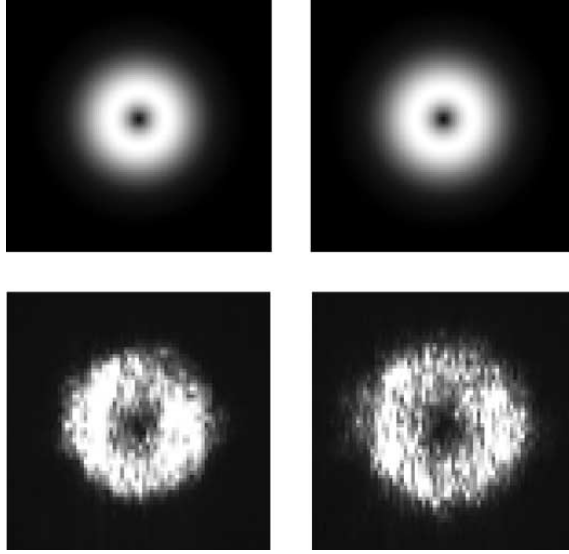


Figure 2.9: *Shape of the vortex without cylindrical lens at same distances as in Fig. [2.8]*

The interferometric investigation has also been done [56] and it was found that the topological charge inverts its sign after such propagation. Images of the canonical vortex are also recorded at the same distances just by removing cylindrical lens. Fig. [2.9] shows experimental and theoretical images for a canonical vortex. It could be seen that the shape of a canonical vortex does not change on the propagation. It has also been tested that the sign of topological charge remains invariant on propagation. A good agreement has been seen in the experimental and the theoretical images.

Chapter 3

Diffraction Characteristics of Optical Vortices

Although the phenomenon of diffraction is a very old concept in classical physics, nevertheless, it plays a role of utmost importance in many branches of physics and engineering that deal with the propagation of wave. It is widely observed phenomenon in nature and has always motivated scientists to make new discoveries. The Fresnel and Fraunhofer diffraction of light through the circular aperture are well known with Airy pattern being one of the most ubiquitous diffraction patterns in optics. In this chapter, our motivation is to explore the diffraction of optical vortices through the different apertures and gratings. In first section we would study the diffraction effects produced by an iris diaphragm and in second section the diffraction through a sinusoidal grating would be discussed. In addition, we also suggest the possible applications of our findings.

3.1 Diffraction of Optical Vortex through an Iris Aperture

The diffraction of an optical vortex through an iris diaphragm which is a close approximation to a circular aperture has been investigated. The results are compared with those obtained from the diffraction of a Gaussian beam through the same aperture. In our findings, diffractions of an optical vortex and a Gaussian beam produce ball bearing sort of structure of darkness and brightness. The singularity of the vortex beam is found to be persistent even after the diffraction through the aperture. The presence of singularity at the center of diffraction pattern of an optical vortex has been confirmed by interferometry. There is a good agreement between the experimental and the numerical results. We propose that these results may find various applications in optical trapping experiments.

An iris aperture is an extensively used device in most of the optics experiments and microscopy. The important thing to notice is that although the iris diaphragm is a close approximation to a circular aperture, however, in contrary to smooth bright and dark rings produced by circular aperture diffraction [76], we have observed fascinating structure of darkness and brightness. Our results could be used to make array of optical traps by just exploiting the diffraction properties of an iris diaphragm. It shows that one can produce the desired number of traps only by changing the number of leaves in the diaphragm.

3.1.1 Experiment

The setup used for the experiments is given in Fig. [3.1]. An intensity stabilized He-Ne laser (Spectra-Physics, 117A), wavelength 632.8 nm, and power 1 mW is used as a source of light. The light beam coming from the laser is divided into two parts by a beam splitter (BS1). The transmitted part goes towards the Spatial Light Modulator (Holoeye, LC-R 2500) and the reflected one is sent towards the

lens L1 and mirror M. The Spatial Light Modulator SLM is a liquid crystal based device and can modulate light spatially in amplitude and phase, so it acts as a dynamic diffractive optical element. The holographic image or the computer generated interferogram with the fork pattern is introduced to the SLM via the computer interface PC1. The light diffracted from the SLM contains the optical vortices of different orders whose topological charge increases with diffraction order. The zero order is Gaussian, and the vortices on either side of this central order have opposite helicity.

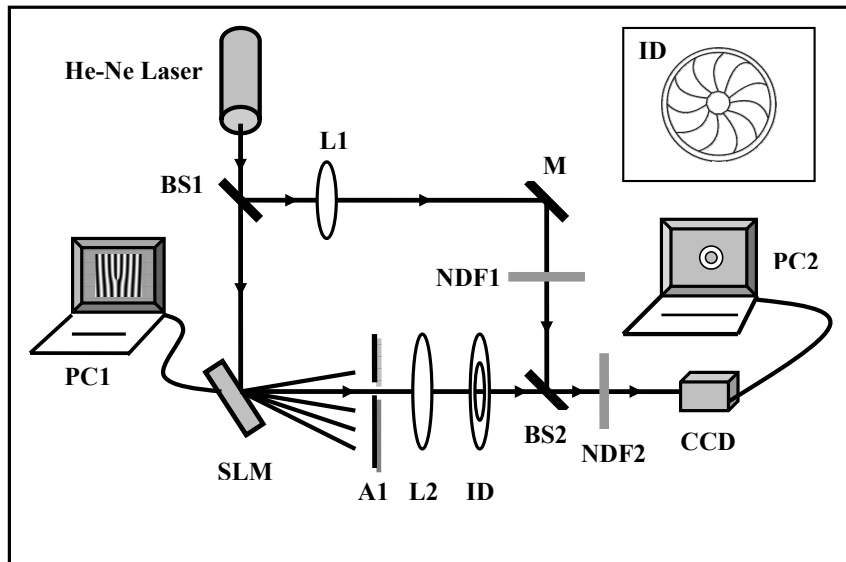


Figure 3.1: *Experimental setup for the generation of optical vortices, their diffraction and characterization through interferometry (Inset shows the structure of iris diaphragm that encloses a polygon with eleven arms). BS1, BS2, beam splitters; L1, L2, lenses; SLM, spatial light modulator; PC1, PC2, computers; A1, aperture; ID, iris diaphragm; M, mirror; NDF1, NDF2, neutral density filters; CCD, charge coupled device camera.*

To check whether a given beam with darkness at its center is really a vortex, we use the interferometric method (the Mach-Zehnder interferometer shown in Fig. [3.1]). If the interference of the beam with a reference beam produces a spiral or fork pattern then it proves the presence of the vortex. The interference pattern

will be of the form of spiral or a fork that depends on the shape and relative orientations of the interfering wavefronts [59, 60].

In our experimental setup, aperture A1 is used to stop all the diffracted orders except the required vortex. The selected vortex is then expanded by using a lens L2 of focal length 12 cm. Thereafter it is passed through the iris diaphragm (ID-Melles Griot) which is the key element of this experiment and also shown in inset of the Fig. [3.1]. This ID has 11 leaves and hence the aperture formed by this ID has a shape of regular hendecagon. The reflected beam from BS1 (reference beam) is expanded by a lens L1 of focal length 7 cm and then again reflected by mirror M. This reflected part is combined with optical vortex at the beam splitter BS2. To record the experimental images, we first blocked the reference beam and then the image of the vortex limited by the ID of a particular size is captured using a CCD camera (Media-Cybernetics) and recorded in a computer PC2. Afterwards, we let the reference beam mix with ID limited vortex and allow them to interfere. The CCD camera is kept at a distance of 430 mm from the ID. To equalize the intensity of both interfering beams we have put a neutral density filter NDF1 in the path of reference beam. The interference fringes are then captured and recorded in PC2. Another neutral density filter NDF2, kept in front of CCD camera is used to avoid the saturation of the camera. After recording the intensity patterns for the vortex limited by aperture of different sizes and corresponding interference fringes, we have replaced SLM by a plane mirror and repeated the experiment with a Gaussian beam with different radii of the ID.

We have made all the observations in the near field zone (Fresnel zone). By moving the observation plane (CCD Camera) away from the aperture, we observed that the central fringe in diffraction of the Gaussian beam regularly alters as bright and dark which proves that our observations are in Fresnel Zone. Also, we calculated the Fresnel number $F = R^2/z\lambda$ at the observation plane ($z = 430$ mm). The values of F for three radii 0.68 mm, 0.71 mm and 0.88 mm of our aperture come out as 1.699, 1.853 and 2.846 respectively. All of these F numbers are greater than

1 that is again a justification for Fresnel diffraction.

To ascertain the size of opening of the iris diaphragm (ID) i.e. the radius of aperture, we use the diffraction method. In the diffraction of a circular aperture, the radius of the central maxima (y) is given as $y = D\lambda/2R$ where D is the distance of screen from the aperture, λ is the wavelength of the light used and R is the radius of the aperture. The uncertainties in the measurements of the radius of the central maxima and the distance of the observation give a total uncertainty of 0.03 mm in the radius of the ID.

3.1.2 Simulation

The results of our experiments could be modeled simply by using the scalar diffraction theory [50]. Let us consider our observation plane at (x, y) and the aperture (iris diaphragm) plane at (ξ, η) . The resultant field at the observation plane can be calculated using Huygens-Fresnel principle. In the limiting case, when the distance z of the observation plane is too large in comparison to the size of diffracting object, the resulting expression for the field at (x, y) becomes

$$U(x, y) = \frac{\exp(ikz)}{i\lambda z} \int_{-\infty}^{\infty} \int_{-\infty}^{\infty} MU(\xi, \eta) \exp\left[i\frac{k}{2z} \left\{ (x - \xi)^2 + (y - \eta)^2 \right\}\right] d\xi d\eta \quad (3.1)$$

Here $U(\xi, \eta)$ is the incident field at the aperture plane. M is the aperture function of the iris diaphragm which is a regular hendecagon (Inset in Fig. [3.1]) and it is constructed numerically.

The mechanism for the numerical construction of aperture function is as follows: We find the coordinates of the vertices of hendecagon using parametric equation of a circle, $x = r\cos\theta$, $y = r\sin\theta$ where r is the radius of the aperture and θ is the polar angle. The angle θ is divided into 11 equal intervals to find the coordinates for the vertices of the hendecagon. After finding the coordinates for all the 11 vertices of hendecagon, we take any two consecutive vertices, say, (x_1, y_1) and (x_2, y_2) . A

line, $(y - y_2)(x_1 - x_2) - (x - x_2)(y_1 - y_2) = 0$, is constructed by joining these two points. Now we define a function $f(x, y) = (y - y_2)(x_1 - x_2) - (x - x_2)(y_1 - y_2)$ which has very interesting properties, i.e. $f(x, y) = 0$, for all points lying on the line, $f(x, y) < 0$ for all points lying on the left side of line and $f(x, y) > 0$ for all points lying on the right side (we go in an anticlockwise direction from the point (x_1, y_1) to (x_2, y_2)). We check the condition $f(x, y) \leq 0$ for all the pair of vertices, the points for which it is true lie to the left of all the 11 arms and form the aperture.

When the aperture is illuminated by an optical vortex then the field $U(\xi, \eta)$ can be given as

$$U(\xi, \eta) = (\xi + i\eta)^l \exp\left(-\frac{\xi^2 + \eta^2}{\sigma^2}\right) \exp\left\{i\frac{k}{2f}(\xi^2 + \eta^2)\right\} \quad (3.2)$$

where l is the topological charge of the vortex, σ is the beam radius, $k = 2\pi/\lambda$ is the magnitude of wave vector, λ is the wavelength of light and f is the focal length of the lens used.

Therefore, the diffracted field for a vortex of charge $l = 1$, say $U_V(x, y)$, becomes

$$U_V(x, y) = \frac{1}{\lambda z} \int_{-\infty}^{\infty} \int_{-\infty}^{\infty} M \exp\left(-\frac{\xi^2 + \eta^2}{\sigma^2}\right) [(\xi \sin\beta + \eta \cos\beta) - j(\xi \cos\beta - \eta \sin\beta)] d\xi d\eta \quad (3.3)$$

where β is a function of (ξ, η, x, y) which is expressed as

$$\beta(\xi, \eta, x, y) = \frac{k}{2f}(\xi^2 + \eta^2) + \frac{k}{2z}\{(x - \xi)^2 + (y - \eta)^2\} + kz. \quad (3.4)$$

When the aperture is illuminated by a Gaussian beam then the field at the aperture plane can be obtained just by removing the complex part $(\xi + i\eta)^l$ in Eq. [3.2]. Thereafter, the diffracted field for the Gaussian beam, say $U_G(x, y)$, can be calculated by following the same steps that yields

$$U_G(x, y) = \frac{1}{i\lambda z} \int_{-\infty}^{\infty} \int_{-\infty}^{\infty} M \exp\left(-\frac{\xi^2 + \eta^2}{\sigma^2}\right) [\cos\beta + i\sin\beta] d\xi d\eta \quad (3.5)$$

To get the resultant intensity distribution for diffracted optical vortex and Gaussian beam, we have numerically solved Eqs. [3.3] and [3.5] separately and evaluated the absolute square of each of them.

3.1.3 Diffraction of an Optical Vortex

The diffraction of an optical vortex through an iris diaphragm have been studied experimentally as well as numerically. It has been found that the singularity of the optical vortex retains its presence even after the diffraction through the iris diaphragm. The position of the singularity in the diffracted beam depends on the relative positions of vortex center and the center of iris diaphragm. When both of the centers coincide, the position of singularity remains unchanged after the diffraction, however, if it is not so, the singularity position shifts from the center. To measure and adjust the relative positions of the center of the vortex and the center of the ID we make use of our experimental observations. When the vortex center is not aligned with the center of the aperture then on reducing the size of the aperture, the dark core of the vortex in the recorded images do not appear at the center of circularly symmetric bright background. We align the aperture in such a way that on reducing the aperture size to its smallest value, the dark spot of the vortex remains at the center of circularly symmetric bright background. In a separate, but parallel to our experiment, Brunet et. al. [77] have exploited the shift of a vortex center with aperture for the subwavelength imaging.

We observe very interesting ball bearing sort of structures of darkness and brightness in the diffraction of the vortex through the iris diaphragm. These structures look similar to the vortices; however using interferometry we have confirmed that these are not the vortices. In Fig. [3.2], we have shown the experimental (first

column) and simulated (second column) images of an optical vortex of topological charge ($l = 1$) passed through the ID of three different radii (R). It has been observed that as the size of aperture decreases the ball bearing structure of darkness becomes pronounced and for an optimum value of aperture size these structures become quite prominent. The corresponding interferograms for these images with a reference beam have been shown in third and fourth column of Fig. [3.2]. It is very clear from the interference fringes that the singularity or the vortex is present only at the center of the beam and even after the diffraction through the very small size of the aperture the singularity does not get disturbed. The single arm of the spiral starting from the center proves that the singularity is present only at the center of the diffracted vortex beam. The experimental results are consistent with simulated results.

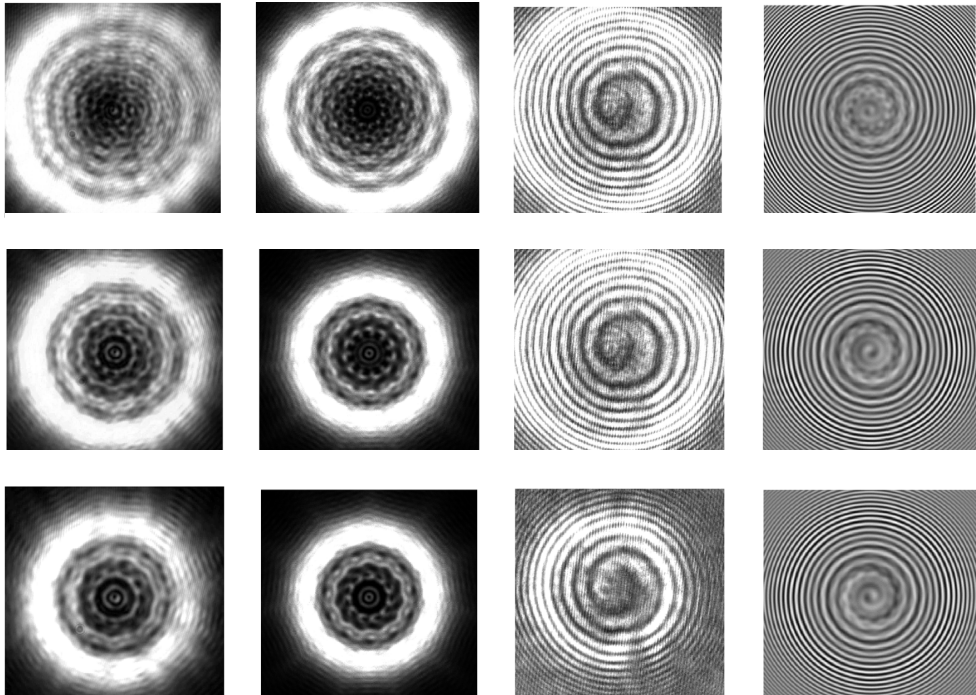


Figure 3.2: *Experimental (first column) and simulated (second column) images of an optical vortex of topological charge $l = 1$ passed through an iris diaphragm of variable radii R and their interference patterns (third column experimental and fourth column simulated) with a reference beam: R varies as- first row, $R = 0.88$ mm; second row, $R = 0.71$ mm; third row, $R = 0.68$ mm.*

3.1.4 Diffraction of a Gaussian Beam

Like vortex diffraction, we also observe the ball bearing sort of structures of darkness and brightness in the diffraction of a Gaussian beam through the iris diaphragm. However, unlike the vortex diffraction where the center of diffracted beam is always dark, in the case of a Gaussian beam ($l = 0$) the center of the diffracted beam may be dark or bright (Fig. [3.3]). The interference fringes do not show any signature of the singularity in the diffracted Gaussian beam. Therefore, we can conclude that the spots of darkness visible in the intensity profile of the diffracted beam are not the optical vortices. The experimental results of Gaussian beam diffraction and their interferograms (first and third column) are also consistent with the simulated results (second and fourth column).

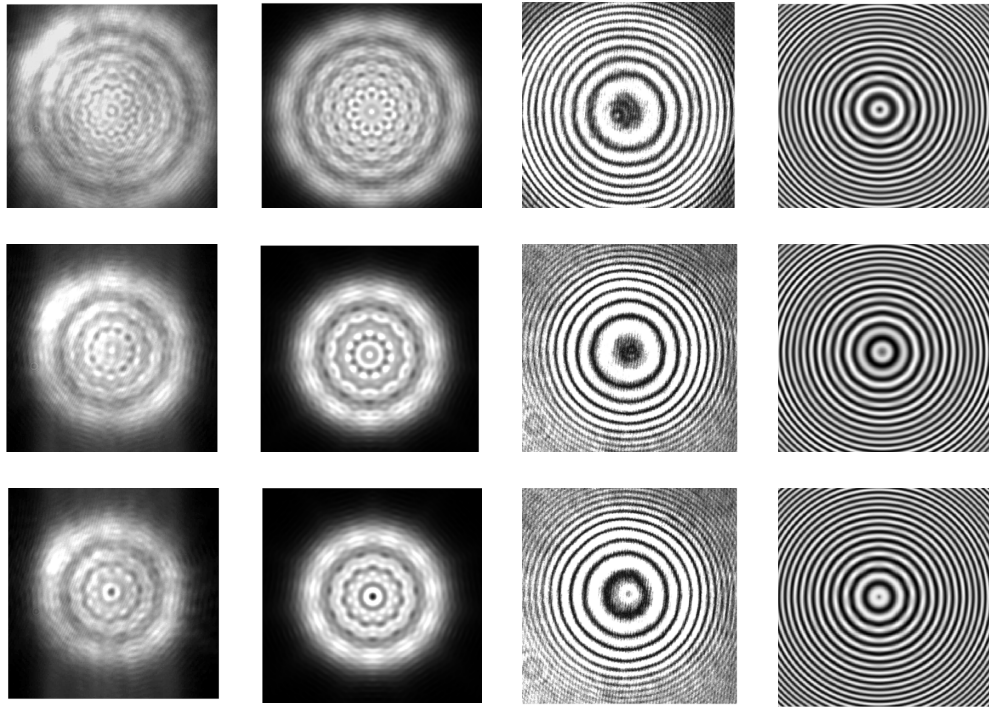


Figure 3.3: *Experimental (first column) and simulated (second column) images of a Gaussian beam ($l = 0$) passed through an iris diaphragm of variable radii R and their interference patterns (third column experimental and fourth column simulated) with a reference beam: R varies as- first row, $R = 0.88$ mm; second row, $R = 0.71$ mm; third row, $R = 0.68$ mm.*

It is quite clear from the experimental and simulated diffraction patterns of iris diaphragm that the numbers of dark or bright spots in the diffraction rings are equal to the number of the leaves of ID. Therefore by clever choice of the ID we can have full control over the number of these bright and dark spots. The ball bearing sort of structures may be useful in optical trapping experiments. These structures may be utilized as a multiple trap. In the diffraction patterns formed by an optical vortex we get singularity at the center, this means that the dark spot at the center is a vortex while the rest of the dark spots are the usual zero intensity points. If we trap an absorptive particle at the center of such beam it will gain the orbital angular momentum of light and will start rotating. Meanwhile, if we use these ball bearing structures as the trap center for other particles then it would be very interesting to observe the effect of the central rotating particle on the neighboring stationary trapped particles. By increasing the topological charge or the order of the vortex we can increase the rotation speed. We can change the sense of rotation also by just changing the sign of the topological charge. We anticipate that it would give a new insight on the distribution of orbital angular momentum in a system of micro particles.

3.2 Diffraction of Optical Vortices through a Two Dimensional Sinusoidal Grating

We demonstrate a technique for making copies of optical vortices. It has been shown that by using suitable diffractive optical elements, several copies of optical vortices could be created with the same topological charge. We have devised such diffractive optical element (two dimensional sinusoidal grating) using a spatial light modulator which could be used to make copies of the vortices without inverting the charge. The nature of the topological charge was investigated with the interferometric technique. The experimental results are verified with the theoretical

can generate many identical topological charges from a single charge is introduced to the SLM via the same computer PC1. Note that to economize the resources, we are displaying two different diffractive optical elements at two portions of the same SLM. The SLM generates many copies of optical vortices after diffraction through the 2D sinusoidal grating.

This grating produces four copies of optical vortices in each diffraction order. However the intensity of these copies decreases with increasing diffraction order. Therefore, we have selected only the first order diffraction pattern along with the central beam using iris aperture A2. The selected copies of optical vortices are imaged by using a lens L2 of focal length 20 cm onto a color camera CCD (shown through the dashed line in Fig. [3.4]).

To investigate the topological charges of generated vortices, we perform an interference experiment. The generated beam that carries different vortices propagates towards the beam splitter BS2 with the help of mirror M4 and combines with the reference beam coming from BS1. Since the size of the beam carrying copies of the vortex becomes large, a lens L1 (focal length 5 cm) is used to expand the reference beam as well. A lens L2' (focal length 20 cm) is used to image the resultant interference pattern at the monochrome camera CCD' interfaced with the computer PC2'. We could have recorded the images of the copies of vortices at this position. However, to make the copies clean and free from the noise introduced by the additional optics used in the interferometric setup, we preferred to record them earlier at the camera CCD.

The recorded intensity of the copies of vortex beam appears much less than that of the central vortex beam. For a better contrast between the vortex copies and the central vortex beam, we note that the polarization of the different copies of optical vortex is different from the central vortex beam. Therefore, we use polarizers P and P' in the path of the beam and rotate them until maximum contrast is obtained.

In the interference patterns, the number of fringes radiating from the center is equal to the modulus of the topological charge, and the direction of the spiraling

is determined by the sign of the topological charge and the relative curvature of the wavefront.

3.2.2 Theoretical Analysis

The propagation of a field through a paraxial optical segment is described by the Huygens-Fresnel diffraction integral containing the ABCD matrix elements for that segment. All these integrals have been evaluated exactly.

The electric field amplitude of an optical vortex of order l propagating along the z -direction, at the plane (u, v) just after the SLM, is given as (we have ignored the overall phase factor due to the optical path length throughout the analysis)

$$E_1(u, v) = E_0(u + iv)^l \exp [-(u^2 + v^2)/w_1^2], \quad (3.6a)$$

$$\frac{1}{w_1^2} = \frac{1}{w^2} + \frac{ik}{2R}. \quad (3.6b)$$

Here, $w = w_0\sqrt{1 + (z_1/z_0)^2}$ is the radius of the Gaussian beam containing the vortex, $w_0 = 0.3$ mm is the beam waist at the laser exit, $z_1 = AB + BC + CD = 78$ cm is the distance between the laser and the SLM, $z_0 = \pi w_0^2/\lambda$, $R = z_1 + z_0^2/z_1$ and $k = 2\pi/\lambda$ is the magnitude of the wave vector of He-Ne laser light with wavelength $\lambda = 632.8$ nm.

The vortex is redirected to a different location in the SLM after a free-space propagation by a distance $z_2 = DE + EF + FG = 126$ cm. The field $E_2(x, y)$ at the SLM is given by

$$E_2(x, y) = \frac{ik}{2\pi B_0} \int \int du dv E_1(u, v) \times \exp \left[-\frac{ik}{2B_0} \{A_0(u^2 + v^2) - 2(xu + yv) + D_0(x^2 + y^2)\} \right] \quad (3.7)$$

where, $A_0 = D_0 = 1$ and $B_0 = z_2$. Substituting the expression for $E_1(u, v)$, one

can write $E_2(x, y)$ as

$$E_2(x, y) = \frac{ikE_0}{2\pi z_2} \exp \left[-\frac{ik}{2z_2} (x^2 + y^2) \right] I(X, Y) \quad (3.8)$$

where

$$I(X, Y) = \int \int du dv (u + iv)^l \exp \left[-(u^2 + v^2)/w_2^2 + i(uX + vY) \right], \quad (3.9a)$$

with

$$\frac{1}{w_2^2} = \frac{1}{w_1^2} + \frac{ik}{2z_2} \quad \text{and} \quad \begin{pmatrix} X \\ Y \end{pmatrix} = \frac{k}{z_2} \begin{pmatrix} x \\ y \end{pmatrix}. \quad (3.9b)$$

Note that

$$-i \left(\frac{\partial}{\partial X} + i \frac{\partial}{\partial Y} \right) \exp[i(uX + vY)] = (u + iv) \exp[i(uX + vY)]. \quad (3.10)$$

Thus, $I(X, Y)$ can be re-written as

$$I(X, Y) = (-i)^l \left(\frac{\partial}{\partial X} + i \frac{\partial}{\partial Y} \right)^l \mathcal{I}(X, Y) \quad (3.11)$$

where

$$\mathcal{I}(X, Y) = \int \int du dv \exp \left[-(u^2 + v^2)/w_2^2 + i(uX + vY) \right]. \quad (3.12)$$

Using the formula $\int_{-\infty}^{\infty} dx \exp[-ax^2 - 2bx] = \sqrt{\pi/a} \exp[b^2/a]$ [79], we obtain

$$\mathcal{I}(X, Y) = \pi w_2^2 \exp(-w_2^2 \rho \rho^* / 4), \quad \text{where } \rho = X + iY. \quad (3.13)$$

We evaluate $I(X, Y)$ by noting that

$$\frac{\partial}{\partial X} + i \frac{\partial}{\partial Y} \equiv 2 \frac{\partial}{\partial \rho^*} \quad (3.14a)$$

and

$$\left(\frac{\partial}{\partial \rho^*}\right)^l \exp(-w_2^2 \rho \rho^*/4) = (-w_2^2 \rho/4)^l \exp(-w_2^2 \rho \rho^*/4) \quad (3.14b)$$

Thus,

$$I(X, Y) = \pi w_2^2 (i w_2^2 \rho/2)^l \exp(-w_2^2 \rho \rho^*/4) \quad (3.15)$$

Substituting the above expression in Eq. [3.8] and simplifying, we get

$$E_2(x, y) = E_0 \left(\frac{i k w_2^2}{2 z_2}\right)^{l+1} (x + i y)^l \exp[-(x^2 + y^2)/w_3^2], \quad (3.16a)$$

where

$$w_3^2 = w_1^2 - 2i z_2/k. \quad (3.16b)$$

At the SLM, the vortex reflects off a sinusoidal grating which provides a phase factor $\exp(i \sin \alpha x \sin \alpha y)$ to the propagating vortex $E_2(x, y)$. After reflection, the beam traverses a free-space distance $z_3 = GH + HJ = 75$ cm, passes through a lens L2 of focal length $f_1 = 20$ cm and reaches the CCD placed at a distance $z_4 = JK + KL = 16$ cm from the lens. The field at the CCD has the expression

$$E_3(x, y) = \frac{i k}{2\pi B_1} \int \int du dv E_2(u, v) \exp(i \sin \alpha x \sin \alpha y) \\ \times \exp\left[-\frac{i k}{2 B_1} \{A_1(u^2 + v^2) - 2(xu + yv) + D_1(x^2 + y^2)\}\right] \quad (3.17)$$

where, $A_1 = 1 - z_4/f_1$, $B_1 = z_3 + z_4 - z_3 z_4/f_1$ and $D_1 = 1 - z_3/f_1$. Substituting for $E_2(u, v)$, using the Bessel function expansion

$$\exp[ix \cos \phi] = \sum_n i^n J_n(x) \exp[-in\phi]$$

and simplifying the resulting expression, we get

$$E_3(x, y) = \left(\frac{ikE_0}{2\pi B_1} \right) \left(\frac{ikw_2^2}{2z_2} \right)^{l+1} \exp \left[- \left(\frac{ikD_1}{2B_1} \right) (x^2 + y^2) \right] \\ \times \sum_{n, n'} i^n (-i)^{n'} J_n(1/2) J_{n'}(1/2) K_{nn'}(x, y) \quad (3.18)$$

where

$$K_{nn'}(x, y) = \int \int du dv (u + iv)^l \exp \left[-(u^2 + v^2)/w_4^2 + i(uX_{nn'} + vY_{nn'}) \right]. \quad (3.19a)$$

Here,

$$\frac{1}{w_4^2} = \frac{1}{w_3^2} + i \frac{kA_1}{2B_1}, \quad (3.19b)$$

and

$$X_{nn'} = kx/B_1 + \alpha(n' - n), \quad Y_{nn'} = ky/B_1 + \alpha(n' + n). \quad (3.19c)$$

Using an identity of the form [3.14a], we write

$$K_{nn'}(x, y) = (-i)^l \left(\frac{\partial}{\partial X_{nn'}} + i \frac{\partial}{\partial Y_{nn'}} \right)^l \mathcal{K}_{nn'}(x, y) \quad (3.20)$$

where

$$\mathcal{K}_{nn'}(x, y) = \int \int du dv \exp \left[-(u^2 + v^2)/w_4^2 + i(uX_{nn'} + vY_{nn'}) \right] \\ = \pi w_4^2 \exp \left[-w_4^2 \rho_{nn'} \rho_{nn'}^* / 4 \right] \quad (3.21a)$$

with

$$\rho_{nn'} = X_{nn'} + iY_{nn'}. \quad (3.21b)$$

Since

$$\frac{\partial}{\partial X_{nn'}} + i \frac{\partial}{\partial Y_{nn'}} \equiv 2 \frac{\partial}{\partial \rho_{nn'}^*}, \quad (3.22)$$

the differentiation in Eq. [3.20] can be easily performed. Substituting in Eq. [3.18]

and simplifying, we obtain

$$\begin{aligned}
 E_3(x, y) &= \left(\frac{kE_0}{B_1} \right) \left[\frac{-kw_2^2 w_4^2}{4z_2} \right]^{l+1} \exp \left[- \left(\frac{ikD_1}{2B_1} \right) (x^2 + y^2) \right] \sum_{n, n'} f_{n, n'}(x, y), \\
 f_{n, n'} &= i^n (-i)^{n'} J_n(1/2) J_{n'}(1/2) \rho_{nn'}^l \exp \left[-w_4^2 \rho_{nn'} \rho_{nn'}^* / 4 \right]. \tag{3.23}
 \end{aligned}$$

The term with $n = n' = 0$ corresponds to the vortex with zero order diffraction whereas terms corresponding to first order diffraction will have either $n = 0, n' = \pm 1$ or $n' = 0, n = \pm 1$. As copies with diffraction orders higher than one are cropped, we restrict the values of n and n' to -1, 0 and 1 only. Furthermore, the term with zero order diffraction has been pre-multiplied by a factor 0.25 to model the role of the polarizer in the reduction of its intensity. Thus $E_3(x, y)$ reduces to

$$\begin{aligned}
 E_3(x, y) &= \left(\frac{kE_0}{B_1} \right) \left[\frac{-kw_2^2 w_4^2}{4z_2} \right]^{l+1} \exp \left[- \left(\frac{ikD_1}{2B_1} \right) (x^2 + y^2) \right] \\
 &\times (0.25 f_{0,0} + f_{0,1} + f_{0,-1} + f_{1,0} + f_{-1,0}) \tag{3.24}
 \end{aligned}$$

To measure the fringe pattern, the vortex from the SLM is sent to a different CCD. The beam traverses a free-space distance $z_5 = GH + HI + IJ' = 145$ cm, passes through a lens of focal length $f_2 = 20$ cm and reaches the CCD placed at a distance $z_6 = J'K' + K'L' = 13$ cm from the lens. Replacing z_3, z_4 and f_1 in Eq. [3.17] by z_5, z_6 and f_2 respectively, we immediately obtain the field $E_4(x, y)$ at the camera CCD':

$$\begin{aligned}
 E_4(x, y) &= \left(\frac{kE_0}{B_2} \right) \left[\frac{-kw_2^2 w_5^2}{4z_2} \right]^{l+1} \exp \left[- \left(\frac{ikD_2}{2B_2} \right) (x^2 + y^2) \right] \\
 &\times (0.25 \hat{f}_{0,0} + \hat{f}_{0,1} + \hat{f}_{0,-1} + \hat{f}_{1,0} + \hat{f}_{-1,0}) \tag{3.25a}
 \end{aligned}$$

where

$$\hat{f}_{n, n'} = i^n (-i)^{n'} J_n(1/2) J_{n'}(1/2) \hat{\rho}_{nn'}^l \exp \left[-w_5^2 \hat{\rho}_{nn'} \hat{\rho}_{nn'}^* / 4 \right], \tag{3.25b}$$

$$A_2 = 1 - z_6/f_2, B_2 = z_5 + z_6 - z_5 z_6/f_2, D_2 = 1 - z_5/f_2,$$

$$\frac{1}{w_5^2} = \frac{1}{w_3^2} + i \frac{kA_2}{2B_2} \quad (3.25c)$$

and

$$\hat{\rho}_{nn'} = \rho_{nn'} \Big|_{B_1 \rightarrow B_2}. \quad (3.25d)$$

This beam is made to interfere with the laser beam which reaches CCD' after passing respectively through a free-space distance $d_1 = AB + BC + CM = 55$ cm, a lens of focal length $f_3 = 5$ cm, a free-space distance $d_2 = MI + IJ' = 104$ cm, a lens of focal length $f_4 = 20$ cm, and finally, a free-space distance $d_3 = J'K' + K'L' = 13$ cm. The Gaussian beam at the laser exit is given by $E_0 \exp[-(x^2 + y^2)/w_0^2]$. At CCD', this beam evolves into $E_5(x, y)$ which has the form

$$E_5(x, y) = \left(\frac{ikE_0}{2\pi B_3} \right) \int \int du dv \exp[-(u^2 + v^2)/w_0^2] \\ \times \exp \left[-\frac{ik}{2B_3} \{ A_3(u^2 + v^2) - 2(xu + yv) + D_3(x^2 + y^2) \} \right] \quad (3.26a)$$

where,

$$\begin{aligned} A_3 &= (1 - d_2/f_3)(1 - d_3/f_4) - d_3/f_3 \\ B_3 &= d_1(1 - d_3/f_4) + (1 - d_1/f_3)(d_2 + d_3 - d_2 d_3/f_4) \\ D_3 &= -d_1/f_4 + (1 - d_1/f_3)(1 - d_2/f_4) \end{aligned} \quad (3.26b)$$

3.2.3 Copies of Optical Vortices

In Fig. [3.5], we have shown the experimental and theoretical intensity profiles of copies of the optical vortex for different topological charges.

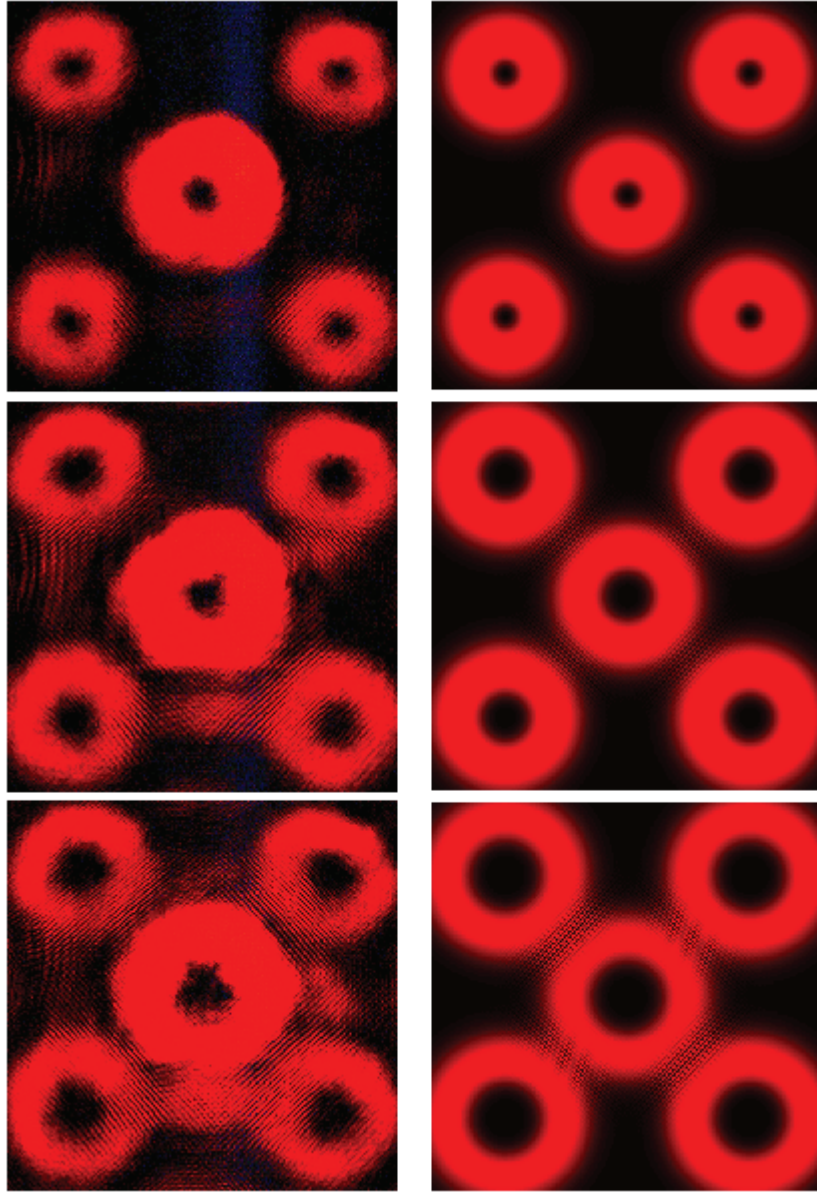


Figure 3.5: *Experimental (left column) and theoretical (right column) intensity profiles of the original vortex and its copies for topological charges 1 (top row), 2 (middle row) and 3 (bottom row).*

The theoretical intensity plot is based on the absolute square of $E_3(x, y)$ as given by Eq. (19). The vortex at the center of each image is of zero order diffraction and is identical to the original vortex beam. The copies of the vortex are situated at the four corners of each image. Fig. [3.6] show both experimentally and theoretically

obtained interference fringes of vortices with a reference beam.

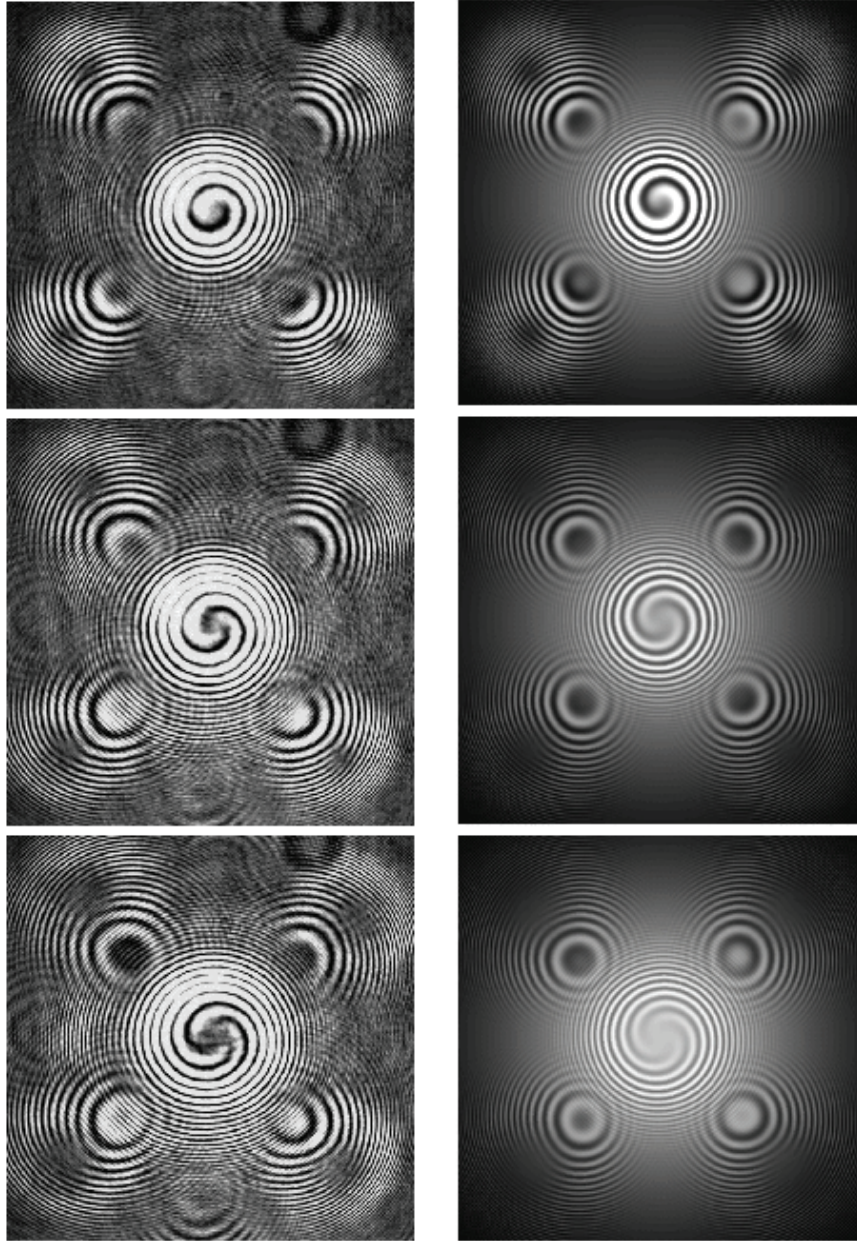


Figure 3.6: *Experimental (left column) and theoretical (right column) interferograms corresponding to the results of Fig. [3.5]. The topological charges are as in Fig. [3.5].*

The theoretical plot is based on $|E_4(x, y) + E_5(x, y)|^2$. It is evident from the fringes that the direction of the branching and the number of branches in a fork

are the same for all the vortex copies of a fixed topological charge. This shows that all the formed copies have the same topological charge.

As shown in Figs. [3.5] and [3.6], the experimental results for intensity and fringe patterns are in excellent agreement with the corresponding theoretical predictions.

3.2.4 Conclusions

In the first section of this chapter, we have studied the diffraction of a single charge optical vortex through the iris diaphragm. It has been observed that the phase singularity of a vortex beam is very robust and it doesn't destroy even after diffraction through the ID. In addition, the beautiful dark and bright ring lattice structures could be obtained just by exploiting the diffraction through the ID.

In the second section of the chapter, diffraction of optical vortices through a 2D sinusoidal grating has been studied. It has been shown that such diffraction produces four identical copies of an optical vortex. Therefore, we suggest a very simple yet efficient method for the generation of copies of optical vortices. One could argue that the copies of optical vortices can also be generated by using a beam splitter. However, the problem with a beam splitter is that an optical vortex inverts its charge on reflection. Therefore the transmitted and the reflected vortex beams from a beam splitter carry opposite topological charges and thus they would not be identical. Our findings may be useful in the field of optical manipulation and optical communication. The identical copies of optical vortex could be used as a vortex lattice where the behavior of different objects trapped in identical vortex traps may be studied. Furthermore, the same technique of producing copies of the vortex could be utilized to make copies of the down converted orbital angular momentum (OAM) states for quantum information and computation since these OAM states are spatial modes which are detected through holograms only.

Chapter 4

Stability and Propagation

Dynamics of High Charge Optical Vortices

We introduce an asymmetry in the core of a high charge optical vortex by using an appropriate computer generated hologram. The splitting of a high charge optical vortex core into unit charge vortices has been found to depend on the extent of the asymmetry. For a second order vortex, the trajectories of the split unit charged vortices and their separation have been recorded as a function of change in the asymmetry of the core. We also study the effect of core asymmetry to the third and fourth order vortices. We find a good agreement between the experimentally obtained and numerically calculated results.

4.1 Introduction

An optical vortex is characterized by a unique phase profile and it is only this phase profile that makes optical vortices very special and very important in optics. Fundamentally, the phase profile of a vortex governs the propagation dynamics of a single vortex or multiple vortices sitting in the same host beam. Also the stability of high charge vortices could be determined by investigating the phase profiles of the vortices.

The stability and the propagation dynamics of a vortex core may be of relevance to the field of optical communication using such beams. Therefore, a great deal of attention has been given to the dynamics and propagation properties of optical vortices in free space and in nonlinear media [56, 74, 80–82]. Ginzburg and Pitaevskii [83] pointed out that a vortex with higher charge (say l , where $l > 1$) in a superfluid is energetically unfavorable compared to l vortices of unit charge. Hence, a vortex with higher charge always has a tendency to break up into unit charge vortices, although the physical mechanism that creates them may be different for different systems. The breaking up of optical vortices can be controlled by several external parameters [84]. A detailed theoretical description of breaking the degeneracy of an optical vortex core has been given by Freund [85]. The decay of a vortex due to perturbation and anisotropy produced by the nonlinear media has also been explored [86].

The break up of a high charge optical vortex leads to the formation of an array of unit charged vortices lying in the same host beam. However, such a composite structure of vortices has also been formed by the superposition of the two or more phase singular beams [87–91]. By a clever choice of different Laguerre Gaussian (LG) beams, one can generate a linear as well as a circular array of optical vortices. Franke-Arnold et al. [88] have generated a beautiful ring lattice of optical vortices, an optical ferris wheel, which is useful in the trapping of red and blue detuned cold atoms. The superposition of various phase singular beams was also utilized

by Berry and Dennis [89] to produce the knots and the links in optical dislocations. The theoretical results [89] were experimentally verified in separate experiments by Leach et al. [90] as well as Dennis et al. [91]. However, in their experiments instead of using two or more separate LG beams, they designed a phase hologram to produce such a superposition by a spatial light modulator (SLM) . In all of these experimental as well as theoretical studies [90,91], some kind of perturbation has been applied to cylindrically symmetric LG beams. Adding a perturbation breaks the symmetry of such beams and leads to the decay of the LG beams with a high topological strength [92, 93]. Dennis [92] has discussed different kinds of perturbations which may cause the breakup of high-order vortices. He differentiates between the elliptically perturbed LG beams and the LG beams perturbed by a small real constant.

We have studied the effect of introducing an asymmetry to a vortex [63]. The asymmetry was introduced through the CGH that produces the vortex. The introduced asymmetry destabilizes a high-order vortex that splits into a number of first order vortices, the number being same as the order of the vortex. We would like to point out that although a perfectly symmetric vortex is used in most of the discussions on vortices, no real system can exhibit a perfect symmetry. Therefore, an elliptically perturbed vortex provides a more realistic and widely applicable vortex model. It should be noted that optical vortices show a deep similarity with the quantized vortices in superfluids and Bose Einstein Condensates. Therefore, the results presented here may also be useful in fields other than optics.

4.2 Experiment

The experimental set up is shown in Fig. [4.1]. An intensity stabilized He-Ne laser (wavelength 632.8 nm and power 1 mW) is used as the light source. The light beam coming from the laser is reflected by a mirror M1 and is sent towards a beam splitter BS1 where it is divided into two parts. The reflected part goes towards the

SLM (Holoeye, LC-R 2500) and the transmitted part towards the mirror M2. The diffractive optical elements or the CGH with different fork patterns corresponding to different asymmetry parameters are introduced into the SLM via a computer PC1.

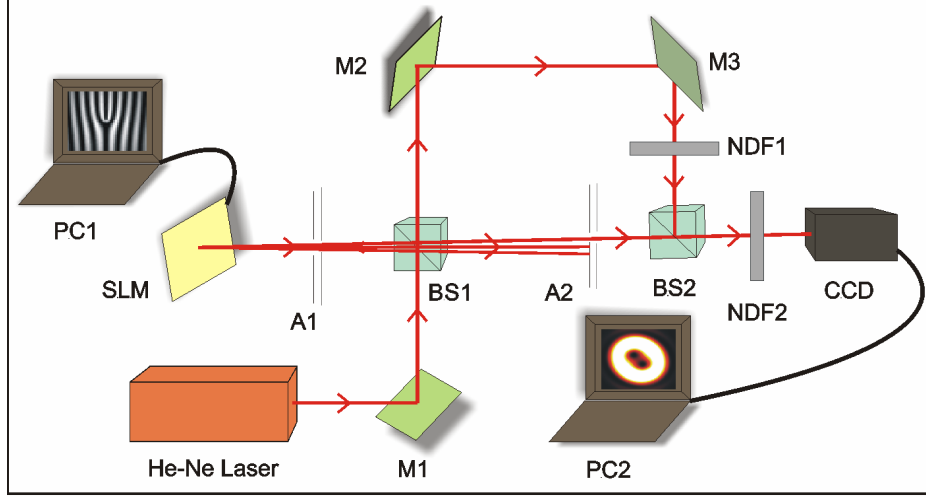


Figure 4.1: *Schematic of the experimental setup. M1, M2, M3 mirrors; BS1, BS2 beam splitters; A1, A2 apertures; PC1, PC2 computers; NDF1, NDF2 neutral density filters; SLM, spatial light modulator; CCD, charge coupled device camera.*

To generate a fork pattern for producing an optical vortex, we imprint an azimuthal phase dependence on a Gaussian beam by calculating the interferogram of the object beam $\exp(il\theta)\exp\{-(\xi^2 + \eta^2)/2\sigma^2\}$ and the reference beam $\exp(ik\xi)\exp\{-(\xi^2 + \eta^2)/2\sigma^2\}$. Here, l is the charge of the vortex, $\theta = \text{Arg}[a\xi + b\eta]$ is the azimuthal angle, σ is the beam radius and k is the component of the wave vector along the X-axis. The real parameters a and b define the asymmetry of the vortex core. The interference of these two beams gives the following intensity pattern,

$$U_i(\xi, \eta) = 2[1 + \cos(k\xi - l\theta)]\exp\left(-\frac{\xi^2 + \eta^2}{\sigma^2}\right) \quad (4.1)$$

This equation provides the required CGH for the production of an optical vortex. Here, the field amplitudes have been taken as unity. For a symmetrical vortex

the ratio a/b is unity, but in the case of an asymmetrical or an elliptical vortex, $a/b \neq 1$. In our experimental and numerical results we have chosen several values of the asymmetry parameter, $\alpha = a/b$ and recorded the images showing the splitting of the core of the vortices at a fixed distance in free space.

The ellipticity of an optical vortex can be controlled by the azimuthal angle α . The different values of α , yield different diffracting optical elements to produce asymmetric optical vortices (Eq. [4.1]). Since α contains a and b , the same can be achieved by varying the asymmetry parameter α . Therefore, to produce asymmetrical vortices, we have made a number of CGH by using different values of α . The diffracted light from the SLM contains optical vortices of increasing topological charge with increasing diffraction order. The zero or the central order remains a Gaussian, and vortices on either side of this central order acquire opposite topological charges. To check whether a given beam with a dark core is really a vortex, we use the interferometric method (the Mach-Zehnder Interferometer shown in Fig. [4.1]). If the interference of the beam with a reference beam produces a fork or a spiral pattern (depending on the wavefront curvatures of the interfering beams) then it proves the presence of a vortex.

In our experimental setup, aperture A1 is used to stop the higher diffracted orders. The selected first order diffracted beams along with the central Gaussian are sent to the beam splitter BS1. Therefore, the transmitted part from the BS1 contains the central Gaussian beam and vortices in the first order diffraction. We select one of these vortices by suitably adjusting the aperture A2 and send it to another beam splitter BS2. The Gaussian laser beam, coming from M1 and transmitted through BS1, is reflected by two mirrors M2 and M3. It is finally combined with the selected optical vortex at the beam splitter BS2. In our experiment, first we record the asymmetric vortex by blocking the reference beam. The image is recorded in a computer PC2 using a CCD camera, placed at 50 cm from the SLM. After recording the image of the vortex, we let the reference beam interfere with the vortex. To equalize the intensity of the interfering beams, for getting fringes

with a better contrast, we have used a neutral density filter NDF1 in the path of the reference beam. The interference fringes are recorded in PC2. Another neutral density filter NDF2, kept in front of the CCD camera, is used to avoid saturation of the CCD.

4.3 Theoretical Background

Elliptic vortices in an electromagnetic field are one of the solutions of linear as well as nonlinear wave equations [94,95]. Chávez-Cerda et al. [94] have shown the existence of elliptic vortices in scalar wave fields as a solution of Helmholtz and Schrödinger wave equations. The well known LG beams with cylindrical symmetry are also one of the solutions of the Helmholtz equation in the paraxial approximation. For mode indices l and $p = 0$ in the associated Laguerre polynomial (LG_p^l), the LG beam carries an optical vortex of order l . The effect of ellipticity in such a cylindrically symmetric beam has been discussed by Dennis [92] and also by Kotlyar et al. [93].

Like all wave fields, propagation of asymmetric vortices in free space can be dealt with using the Huygens-Fresnel principle [50]. We consider our observation plane at (x, y) , which is parallel to the initial vortex plane (ξ, η) and situated at a normal distance z from this plane. On illuminating a diffracting object by a Gaussian laser beam, the resulting expression for the field at (x, y) can be written as

$$U(x, y) = \frac{1}{i\lambda z} \int_{-\infty}^{\infty} \int_{-\infty}^{\infty} U_i(\xi, \eta) \exp \left[ikz \left\{ 1 + \frac{(x - \xi)^2 + (y - \eta)^2}{z^2} \right\}^{1/2} \right] d\xi d\eta \quad (4.2)$$

Under the Fresnel approximation [50], Eq. [4.2] reduces to

$$U(x, y) = \frac{\exp(ikz)}{i\lambda z} \int_{-\infty}^{\infty} \int_{-\infty}^{\infty} U_i(\xi, \eta) \exp \left[i \frac{k}{2z} \left\{ (x - \xi)^2 + (y - \eta)^2 \right\} \right] d\xi d\eta \quad (4.3)$$

where $U_i(\xi, \eta)$ is the aperture function used to produce optical vortices by a Gaus-

sian beam illumination as explained in Eq. [4.1]. Here, $k = 2\pi/\lambda$ and λ is the wavelength of light.

4.4 Effect of Asymmetry to High-Charge Optical Vortices

We have explored the splitting of high order optical vortices due to the asymmetry in a vortex core. It has been shown that the asymmetry introduced in the vortex beam during its generation is adequate for the splitting of the dark core. In Fig. [4.2], we show the experimental and simulated optical vortices of topological charge two with zero asymmetry and their interference with a reference beam.

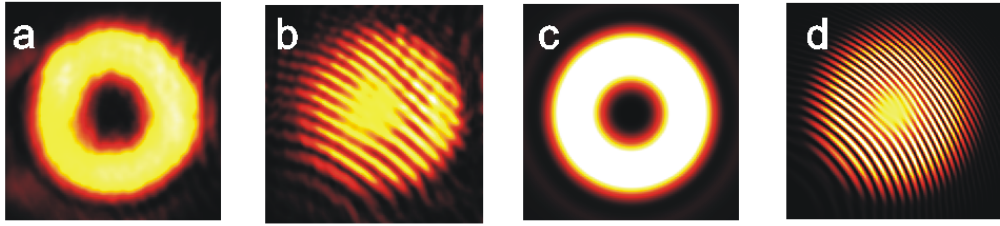


Figure 4.2: *Images of a second order vortex and the characteristic interferogram. (a, b) experimental; (c, d) simulated.*

It is clear from Fig. [4.2] that a vortex of charge two is located at the center of the beam, as the corresponding interference fringes show the branching of one line into three lines, the characteristic interferogram of a charge two vortex. However, if we introduce an asymmetry into this vortex beam, the dark core starts breaking (Fig. [4.3] and Fig. [4.4]).

4.4.1 Splitting of a Second Order Optical Vortex

In Fig. [4.3], we have shown the images of the optical vortices and their corresponding interferograms for different values of the asymmetry parameter.

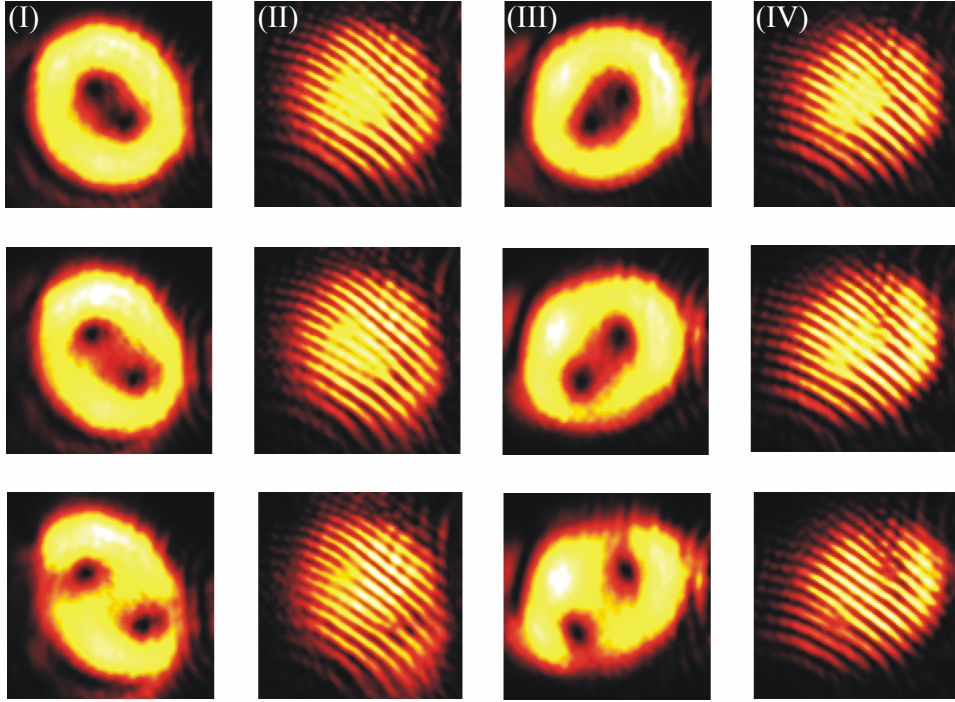


Figure 4.3: *Experimental results of the splitting of a second order optical vortex on increasing (top to bottom) the asymmetry i.e. asymmetry parameter α is moving away from the value 1.0. (I, II) optical vortices and interferograms with decreasing $\alpha = 0.7, 0.5$ and 0.3 ; (III, IV) optical vortices and interferograms with increasing $\alpha = 1.43, 2.0$ and 3.33 .*

Column (I) shows vortices generated through a hologram with different values of the asymmetry parameter $\alpha < 1$. The asymmetry to the core increases from top to bottom of any column. The asymmetry parameter α is defined in such a way that it is unity for a perfectly symmetric vortex and it goes away from unity with increasing asymmetry to the vortex core. It is clear from the images of the vortices and the corresponding interference fringes (column II) that with an increase in the asymmetry, the breaking of the core into vortices of unit charge becomes faster. The same is seen to be true for the values of $\alpha > 1$ (columns III and IV), with the only difference being that the singly charged vortices align themselves into a different orientation. The simulated results for the experimental observations are shown in Fig. [4.4] and found to be in good agreement. These results were obtained

by numerically solving the Fresnel integral (Eq. [4.3]) with the Simpsons' one third rule. The integral was solved by constructing a grid of 800×800 with a step size of $6.5 \mu\text{m}$ in (ξ, η) plane. The propagation distance z is taken to be 50 cm. The program written in C language was run on the PRL 3TFLOP HPC cluster.

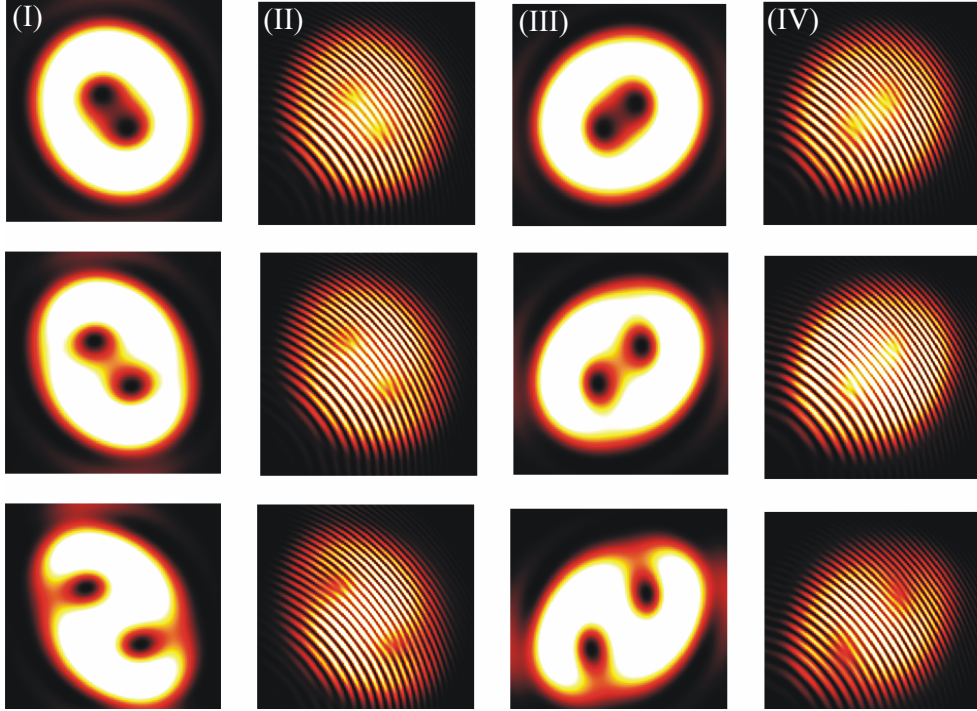


Figure 4.4: *Simulated results for the same asymmetry parameter values as in Fig. [4.3].*

4.4.2 Trajectories of Split Vortices

To investigate the path followed by singly charged vortices, produced from the splitting of a doubly charged core, we have plotted the trajectories of split vortices in Fig. [4.5a] and Fig. [4.5b] for $\alpha < 1$ and $\alpha > 1$. The center of a circularly symmetric vortex has been taken as the origin in these plots. In both graphs, the position of the vortices has been shown in normalized coordinates for different asymmetry parameters α indicated in the legend. It should be pointed out that the value of asymmetry increases along the trajectory on either side of the origin.

It is clear from the curves that the nature of the trajectories followed by the split vortices is similar in the two cases, $\alpha < 1$ and $\alpha > 1$, except their orientation. The trajectories followed by the simulated split vortices have been shown along with their experimental counterparts in Fig. [4.5a] and Fig. [4.5b]. Note that all these images have been recorded at $z=50$ cm.

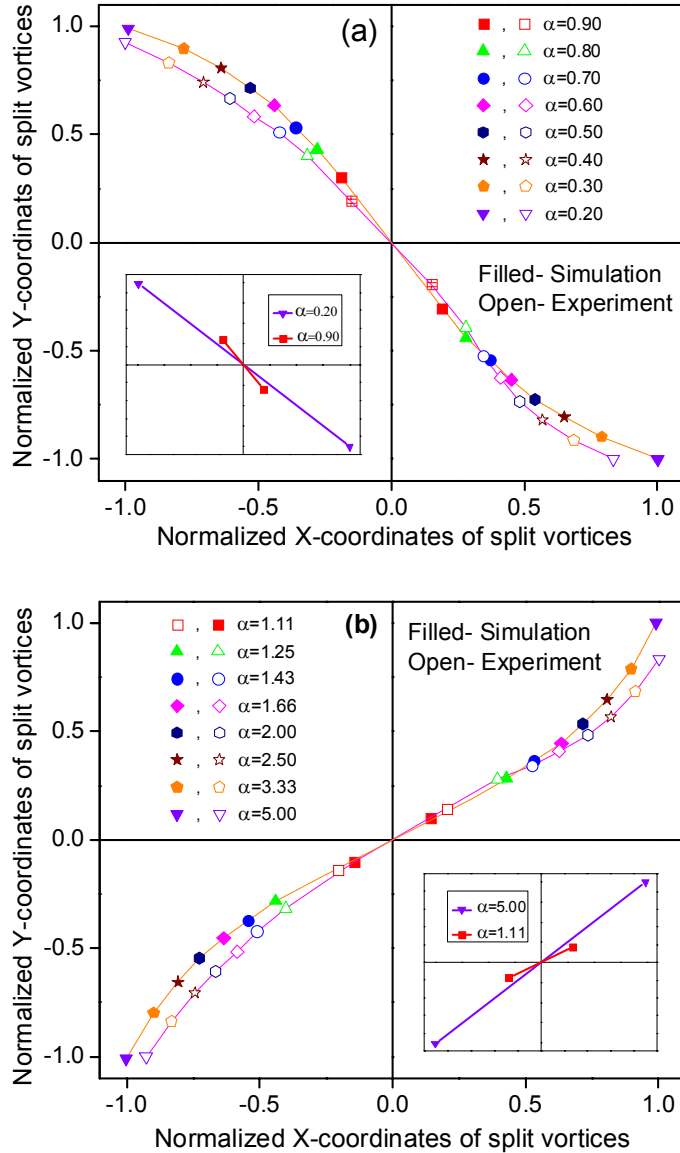


Figure 4.5: *Experimental (open symbols) and simulated (filled symbols) trajectories of the unit charge vortices after splitting from a doubly charge vortex as the asymmetry parameter (α) moves away from 1. (a) $\alpha < 1$; (b) $\alpha > 1$.*

It is understood that a perturbation breaks the rotational symmetry of a high-order vortex beam, thereby leading to its decay into single order vortices [92]. In the present case, an elliptic perturbation is given by the substitution $(\xi + i\eta) \rightarrow (a\xi + ib\eta)$ into the core of the wave function made on the input plane. It is known, when a beam carrying two or more single order vortices propagates in free space, vortices with similar charge rotate in the same direction around the center of the host beam [96]. Therefore, for $\alpha < 1$, a pair of vortices initially (at $z = 0$) located along the X-axis (Fig. [4.6(III)]) will rotate in the clockwise direction, giving rise to a negative slope as the beam propagates. However, for $\alpha > 1$, the vortices which are initially located along the Y-axis (Fig. [4.6(II)]) rotate clockwise, and give rise to a positive slope.

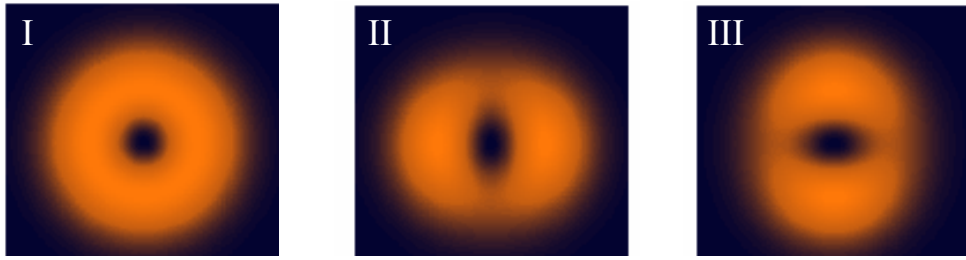


Figure 4.6: *Symmetric (I) $\alpha = 0$ and asymmetric (II) $\alpha > 1$, (III) $\alpha < 1$ vortices of order 2 at $z=0$.*

After propagation, the orientation of split vortices depends on their relative separation at $z = 0$. One finds that for $\alpha < 1$, contours of the amplitude are elliptical along the X-axis at $z = 0$, therefore, the initial split vortices are located along the X-axis only [92]. However, as the beam propagates, the split vortices start rotating in a clockwise direction [96]. The vortices with smaller separation (lesser asymmetry) rotate faster than vortices with larger separation (higher asymmetry). This fact is clear in Figs. [4.5a] and [4.5b]. The inset in Fig. [4.5a] shows that for a small value of asymmetry ($\alpha = 0.90$), the vortex separation is smaller than that for a large asymmetry ($\alpha = 0.20$). Also, it is clear from the lines joining the

split vortices that the slope for the vortices with smaller asymmetry (line joining rectangles) changes faster than that of larger asymmetries (line joining triangle) as the beam propagates. A similar kind of behavior for the asymmetry parameter values $\alpha > 1$ has been shown in the inset of Fig. [4.5b].

The effect of asymmetry on the separation between the split vortices has been quantified in Fig. [4.7]. Both, the experimental as well as the simulated results verify our earlier assertion that the distance between the split vortices increases with increasing the asymmetry. In the plot shown in Fig. [4.7], the distance between the split vortices is maximum (1, normalized unit) for $\alpha = 0.2$ and it is minimum (0.25, normalized unit) for $\alpha = 0.9$.

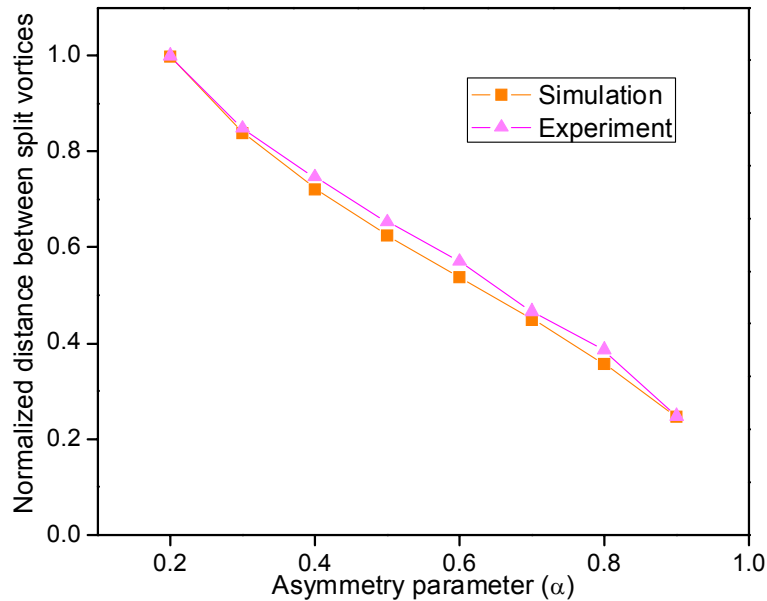


Figure 4.7: *Plot showing the increase of the distance between split vortices as the asymmetry parameter ($\alpha < 1$) moves away from the value 1.*

4.4.3 Splitting of Higher Order Optical Vortices

The splitting of vortices of the order higher than two has also been studied. It would be quite interesting to observe the alignment of split unit charge vortices

from a higher charge vortex. In order to demonstrate the effect of the asymmetry for high-order vortices, we have done the experiment with the third and the fourth order vortices. The experimental results are shown in Fig. [4.8], where column (I, II) show the splitting of a third order vortex with increasing asymmetry and the respective interferograms. Here, the asymmetry parameter α runs as 1.00, 0.70, 0.50 and 0.30 from top to bottom in each column.

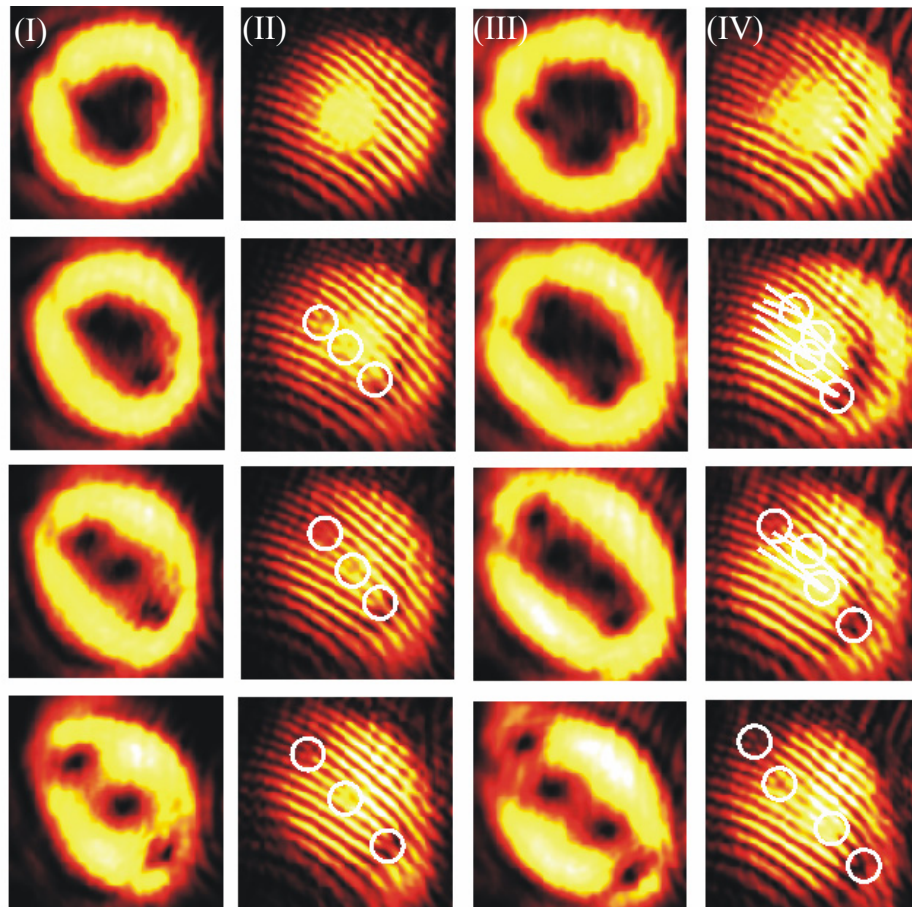


Figure 4.8: *Experimental results of the splitting of high-order optical vortex on increasing (top to bottom) the asymmetry, $\alpha = 1.00, 0.70, 0.50$ and 0.30 (I, II) optical vortices of third order and their characteristic interferograms; (III, IV) optical vortices of fourth order and their characteristic interferograms.*

In column (III, IV), an optical vortex of fourth order and its characteristic interferograms at the same α has been shown. The splitting of high charge vortices

into a linear array of unit charge vortices (separate isolated dark spots), and their separation with increasing asymmetry is clearly visible in the images as well as in the corresponding interferograms. Circles shown in the interferograms represent the positions of the single fork patterns which are the characteristic of the first order optical vortices. The simulated results for the experimental observation of splitting of the third and the fourth order vortices are shown in Fig. [4.9].

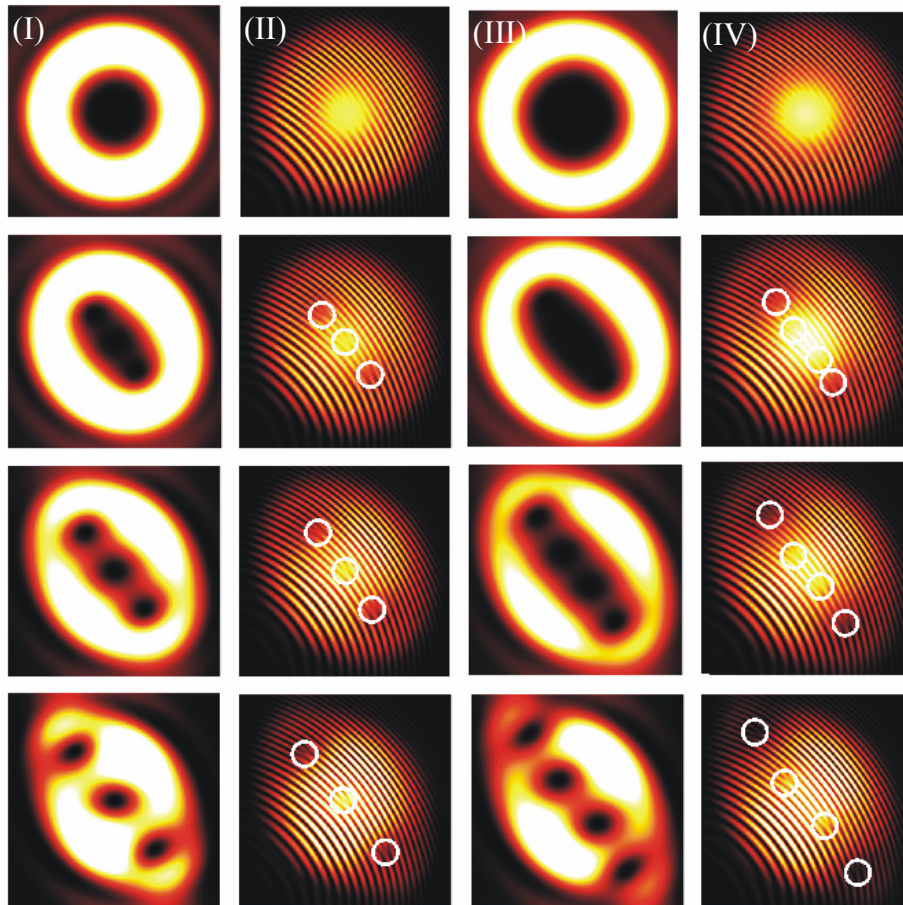


Figure 4.9: *Simulated results for the same asymmetry values as in Fig.[4.8].*

The simulated results for the decay of third and fourth order vortices are in very good agreement with the experimental results. The emergence of a linear array of single charge vortices could be seen after the splitting of a higher charge vortex.

4.5 Conclusion

In conclusion, we have shown the effect of asymmetry in experimentally produced high order optical vortices. It is observed that the splitting of high topological charge vortices into vortices of single charge becomes more pronounced with increase in the asymmetry. After the splitting, the single charge vortices align themselves in a straight row. In addition, we have verified our experimental observations with numerical simulations. The experimental and the numerical results presented here confirm results from earlier theoretical studies [92]. The results presented in this chapter show that the stability of high charge vortices breaks down with introduced asymmetry to the core. It is also to be noted that in earlier discussions on the stability of high charge vortices, the perturbation is applied externally after the formation of the vortex. However, in the present work, perturbation is applied to the vortex during their production itself. This perturbation is in the form of the asymmetry to the vortex core. We show that the inter-vortex spacing of single charge vortices, which break up from a high charge vortex, can be controlled by the asymmetry parameter. We anticipate that the control over the formation of a stable array of unit charge vortices will find use in a variety of optical trapping experiments. However, if one wishes to generate a stable high charge optical vortex he will have to be very careful on the perturbation in the system. As discussed, a very small perturbation may leads to the breaking of a high charge vortex.

Chapter 5

Spatial Coherence Properties of Optical Vortices

We study, experimentally as well as theoretically, the spatial coherence function and the Wigner distribution function for one-dimensional projections of optical vortices of different orders. The information entropy derived from the spatial coherence functions has been used to quantify the information content of the vortices and compared with those obtained for the Gaussian beam. The experimental results verify the earlier proposed theoretical results.

5.1 Introduction

Optical vortices, being points of darkness in a bright background, are easily recognizable light structures [4]. If one goes around the point of darkness and finds a phase change of $2\pi l$, it is called a vortex of topological charge l .

Coherence of an optical field plays a crucial role in almost all the issues pertaining to the fields. Therefore, study of the spatial coherence - a two-point correlation function (TPCF) $\Gamma_{nm}^{(2)}(x', y'; x, y) = \langle E^*(x', y')E(x, y) \rangle$ of optical vortices becomes quite important. Here $E(x, y)$ and $E^*(x', y')$ are the optical vortex field and its complex conjugate at points (x, y) and (x', y') and the angle brackets denote the ensemble average. However, unlike a Gaussian beam and other fields studied earlier [97, 98], the field associated with an optical vortex, $E(x, y)$, cannot be written in a separable form $f(x)g(y)$ [99]. A useful way to study fields of such two-dimensional (2D) beams is by means of their projections. Agarwal and Banerji (AB) [100] used this technique in the theoretical study of the vortex fields described by the Laguerre-Gaussian (LG) modes and derived the spatial coherence function and also the information entropy for one-dimensional (1D) projections of the LG beams.

To verify the theoretical results of AB, we produce vortices of different orders described by the LG modes with a spatial light modulator (SLM). To find the TPCF, the interference between vortices of the same order is scanned using a shearing Sagnac interferometer [97]. The TPCF for the 1D projections of the optical vortices is realized by summing over the contributions along one transverse direction. The experimentally observed TPCF is used to find the information entropy or the information content of optical vortices [101].

5.2 Theoretical Analysis

The field of an LG beam can be written as

$$u_{n,m}^{LG}(x,y) = \sqrt{\frac{2}{\pi w^2}} \frac{\min(n,m)!}{\sqrt{n!m!}} (-1)^{\min(n,m)} \exp[-i(n-m)\phi] \\ \times \exp\left[-\frac{r^2}{w^2}\right] \left(\frac{r\sqrt{2}}{w}\right)^{|n-m|} L_{\min(n,m)}^{|n-m|}\left(\frac{2r^2}{w^2}\right), \quad (5.1)$$

where $r^2 = x^2 + y^2$, $\phi = \arctan(y/x)$, w is the beam waist and $L_p^l(x)$ is the generalized Laguerre polynomial. For optical vortices, the mode indices, $l = m - n$ and $p = \min(n, m) = 0$. It is quite intuitive that when we project such a 2D field to 1D, we would not get all the information given by the 2D field, we lose some information in the 1D projection. We have compared the spatial coherence functions obtained for the 2D fields with their 1D projections. Also we have derived the information entropy, the degree of coherence and the Wigner distribution function (WDF) for the 1D projection of optical vortices and Gaussian laser beam.

The TPCF of the 1D projection of an LG beam is defined as

$$\Gamma_{nm}^{(1)}(x, x') = \int_{-\infty}^{\infty} u_{n,m}^{*LG}(x, y) u_{n,m}^{LG}(x', y) dy. \quad (5.2)$$

Since the LG and the Hermite-Gaussian (HG) modes form a complete basis set, either of the modes can be written as a superposition of the others. For example, the LG modes can be written as [9]

$$u_{n,m}^{LG}(x, y) = \sum_{k=0}^{m+n} i^k b(n, m, k) u_{m+n-k, k}^{HG}(x, y), \quad (5.3)$$

with

$$b(n, m, k) = \left[\frac{(n+m-k)!k!}{2^{n+m}n!m!} \right]^{1/2} \frac{1}{k!} \left. \frac{d^k}{dt^k} \left[(1-t)^n (1+t)^m \right] \right|_{t=0}. \quad (5.4)$$

Therefore, the TPCF of the 1D projection of an optical vortex field can be written

as

$$\Gamma_{nm}^{(1)}(x, x') = \sum_{j=0}^{m+n} b^2(n, m, m+n-j) \phi_j(x) \phi_j(x'). \quad (5.5)$$

which is known as Mercer's expansion. In Eq. [5.5],

$$\phi_n(x) = \left(\frac{\sqrt{2}}{\sqrt{\pi} 2^n w n!} \right)^{1/2} H_n(\sqrt{2}x/w) \exp(-x^2/w^2), \quad (5.6)$$

and

$$\int_{-\infty}^{\infty} \phi_n(x) \phi_m(x) dx = \delta_{mn}. \quad (5.7)$$

Using the coefficients of the Mercer's expansion (Eq. [5.5]), the information entropy is defined by

$$I_{nm} = \sum_{j=0}^{m+n} b^2(n, m, m+n-j) \log[b^2(n, m, m+n-j)]. \quad (5.8)$$

The degree of the coherence is given as

$$\mu_{nm} = \frac{\int \int dx dx' |\Gamma_{nm}^{(1)}(x, x')|^2}{[\int dx \Gamma_{mn}^{(1)}(x, x)]^2} = \frac{\sum_{j=0}^{m+n} b^4(n, m, m+n-j)}{\left[\sum_{j=0}^{m+n} b^2(n, m, m+n-j) \right]^2}. \quad (5.9)$$

The WDF that provides coherence information in terms of the joint position and momentum (direction) phase space distribution of the optical field is expressed in terms of the TPCF:

$$W_{nm}(x, p) = \frac{1}{2\pi\lambda} \int_{-\infty}^{\infty} d\xi \exp(-ip\xi/\lambda) \Gamma_{nm}^{(1)}(x - \xi/2, x + \xi/2). \quad (5.10)$$

5.3 Experiment

The experimental arrangement to find the spatial coherence function and the related quantities is shown in Fig. [5.1]. A Gaussian laser beam from an intensity

stabilized He-Ne laser (Spectra-Physics, 117A) is incident normally to the SLM (Holoeye, LC-R 2500) using the mirror M1 and the beam splitter BS1. Higher order vortices are produced in the first diffracted order by introducing different fork patterns onto the SLM via a computer (PC1). Apertures A1 and A2 are used to select an optical vortex of the desired order. A polarizer P is used to fix the polarization (here vertical) of the optical vortex. The vortex with a vertical polarization is coupled to the shearing Sagnac interferometer that comprises the beam splitter BS2 and two mirrors, M2 and M3. A quarter-wave plate QWP and a half-wave plate HWP are kept in common path for the quadrature selection. A glass block mounted upon a rotation stage is also kept in the common path to introduce the shear in the two transverse directions. The two counter-propagating beams are interfered and imaged by lens L onto a CCD camera and recorded in a computer PC2.

The same procedure is used to find the spatial coherence function of the Gaussian beam, except the forked grating is replaced with a normal grating.

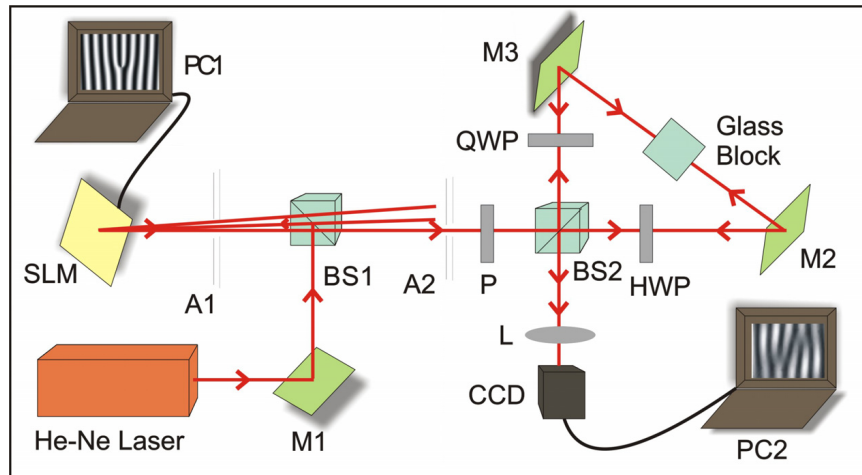


Figure 5.1: *Experimental setup of a shearing Sagnac interferometer for obtaining the TPCFs and the WDFs for the optical vortices. M1, M2, M3 mirrors; BS1, BS2 beam splitters; A1, A2 apertures; P, Polarizer; QWP, quarter wave plate; HWP, half wave plate; L, lens; SLM, spatial light modulator; CCD, charge coupled device camera; PC1, PC2 computers.*

5.4 Two Point Correlation Function of Optical Vortices

First, we have recorded the interferograms by keeping the fast axes of the QWP and the HWP parallel to the incident beam's polarization direction and rotating the glass block in both the transverse directions. The recorded interferograms with different lateral shifts contain the information of $\text{Re}[\Gamma_{nm}^{(2)}(x, y, x', y')]$. Keeping all of these lateral shift values the same, another set of interferograms is recorded by rotating the HWP through an angle of $\pi/4$. These interferograms contain the information of $\text{Im}[\Gamma_{nm}^{(2)}(x, y, x', y')]$.

The experimental results of the TPCF are derived from the recorded interferograms [8]. We take two sets of interferograms corresponding to $\text{Re}[\Gamma_{nm}^{(2)}(x, y, x', y')]$ and $\text{Im}[\Gamma_{nm}^{(2)}(x, y, x', y')]$ with two different shear values. The same types (real/imaginary) of interferograms are then subtracted to eliminate the contribution due to the individual beams. These results provide us with real and imaginary parts of the TPCF. The absolute square of the complex TPCF $|\Gamma_{nm}^{(2)}(x, y, x', y')|^2$ of a Gaussian beam and an optical vortex of order 1 are shown in Figs. [5.2a] and [5.2b], respectively. In Fig. [5.2b], the darkness seen at the center of the TPCF of an optical vortex is due to the presence of the phase singularity [102].

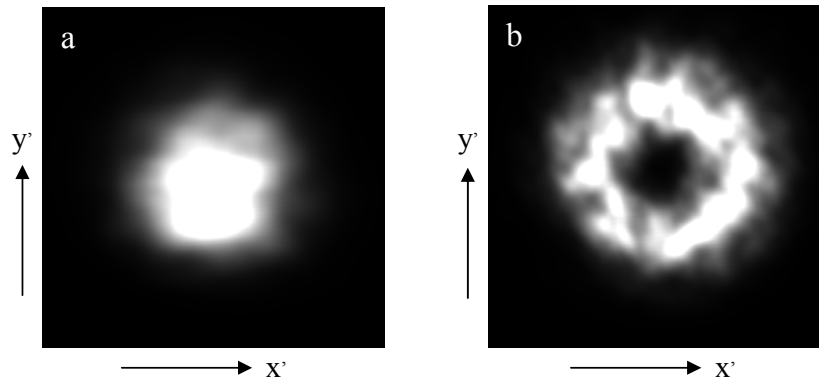


Figure 5.2: TPCF $|\Gamma_{nm}^{(2)}(x, y, x', y')|^2$ for (a) a Gaussian beam and (b) an optical vortex of order 1, for fixed x and y .

5.4.1 One Dimensional Projection of Two Point Correlation Function

Using Eq. [5.2], along with the experimental data for $\Gamma_{nm}^{(2)}(x, y, x', y')$, we obtained the TPCF for the 1D projections $\Gamma_{nm}^{(1)}(x, x')$ of optical vortices, with the results shown in Fig. [5.3]. Figures [5.3a-d] show the theoretical and Figs. [5.3e-h] show the experimental images of $|\Gamma_{nm}^{(1)}(x, x')|^2$ for a Gaussian beam ($l = 0$) and the optical vortices of orders 1, 2, and 3. On comparing the results shown in Figs. [5.2] and [5.3], one can easily see that the shape of the TPCF of a Gaussian beam remains unchanged for the TPCF of its 1D projection (Figs. [5.2a], [5.3a], and [5.3e]), while the TPCF of the 1D projection of an optical vortex changes (Fig. [5.2b], [5.3b], and [5.3f]). This change for an optical vortex can be attributed to the nonseparability of the vortex field.

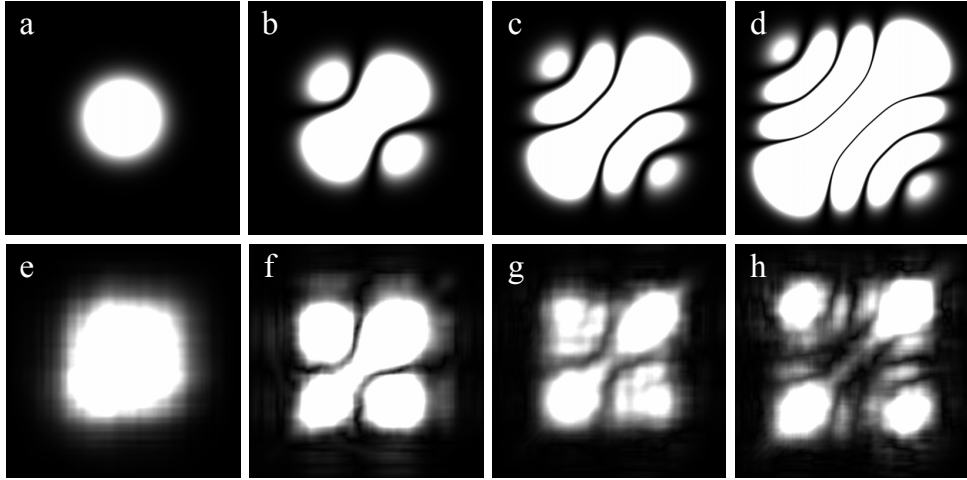


Figure 5.3: Plots of the TPCF $|\Gamma_{nm}^{(1)}(x, x')|^2$ for the 1D projections of beams with topological charges 0, 1, 2, and 3: (a-d) theoretical; (e-h) experimental.

A careful observation of the TPCF of the 1D projections of optical vortices (Fig. [5.3]) demonstrates that the number of side lobes is equal to the order of the vortex. Therefore, one can easily determine the vorticity of the unknown beam from the TPCF of its 1D projection.

5.4.2 Degree of Coherence

It is evident from the Eq. [5.9] that, for the estimation of the degree of coherence, we need the Mercer's coefficient $b^2(n, m, m + n - j)$. By using Eq. [5.5] and the images of $\Gamma_{nm}^{(1)}(x, x')$ (Fig. [5.3]), we have calculated $b^2(n, m, m + n - j)$ with help of the least square fitting method. Once the coefficients $b^2(n, m, m + n - j)$ for optical vortices of different orders are known, the degree of coherence is evaluated using Eq. [5.9] with the results shown in Fig. [5.4].

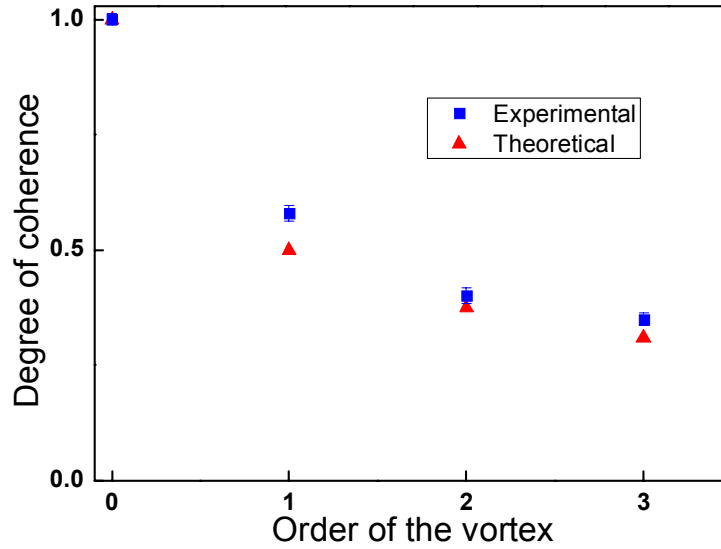


Figure 5.4: *Plot of degree of coherence of 1D projections of a Gaussian beam ($l = 0$) and optical vortices of different order ($l=1,2,3$).*

Figure [5.4] shows a plot of the degree of coherence for a Gaussian beam and the vortices of different orders. It is clear from the theoretical and the experimental results that the degree of coherence in 1D projections of optical vortices decrease with increase of the order. In a different context, it has been observed that the temporal coherence also decreases with increase in the order of the vortex [103].

5.4.3 Information Entropy

The information entropy given in Eq. [5.8] is calculated using the Mercer's coefficient $b^2(n, m, m + n - j)$. It is plotted in Fig. [5.5] with the order of the vortex. It is clear from the graph that the information entropy increases with the increase of the order of the vortex. Therefore, according to the information theory, we can conclude that higher order vortices will carry more information.

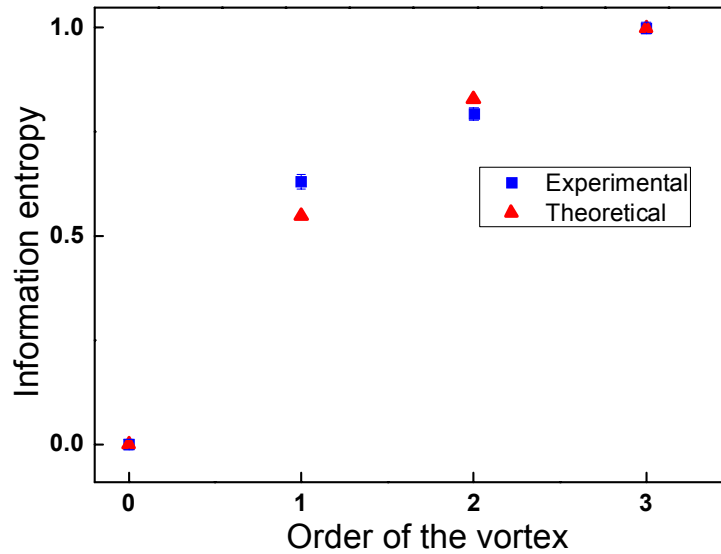


Figure 5.5: *Plot of information entropy of 1D projections of a Gaussian beam ($l = 0$) and optical vortices of different orders.*

Equation [5.8] describes the information entropy, a measure of the disorder, in terms of the distribution of TPCF for the 1D projections of optical vortex fields. Thus, the correlation properties of the field will dictate if the information entropy of the field is increasing or decreasing. It is natural that the correlation between two points across the field for a higher order vortex with more windings of the wavefront would be more complex. This increase in the complexity will result in higher information entropy for higher order vortices.

5.4.4 Wigner Distribution Function

The WDF for an optical vortex has already been studied by our group [99]. However, here we are reporting the WDF for the 1D projection of optical vortices and a Gaussian field. Figure [5.6] shows the theoretically calculated WDFs for the 1D projections of a Gaussian beam and the optical vortices of different orders, which have been normalized with their maximum values. The experimental counter-parts of these results are shown in Fig. [5.7]. The experimental results for the WDF are obtained by using the experimentally calculated values of the TPCF in Eq. [5.10]. It is clear from the theoretical as well as the experimental plots that the WDF for an optical vortex vanishes at the center, while for a Gaussian field, it is peaked at the center. Thus, an intensity minimum at the center of an optical vortex is manifested in its WDF also. The obtained results show good agreement between theory and experiment.

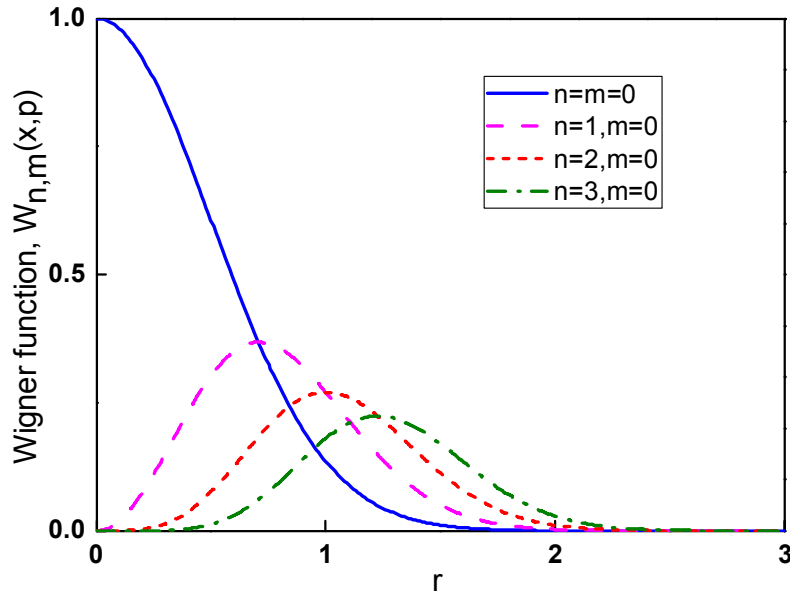


Figure 5.6: *Theoretical plots of the WDF of 1D projections of a Gaussian beam and optical vortices of order 1, 2 and 3 with $r = [(x/w)^2 + (wp/2\lambda)^2]^{1/2}$.*

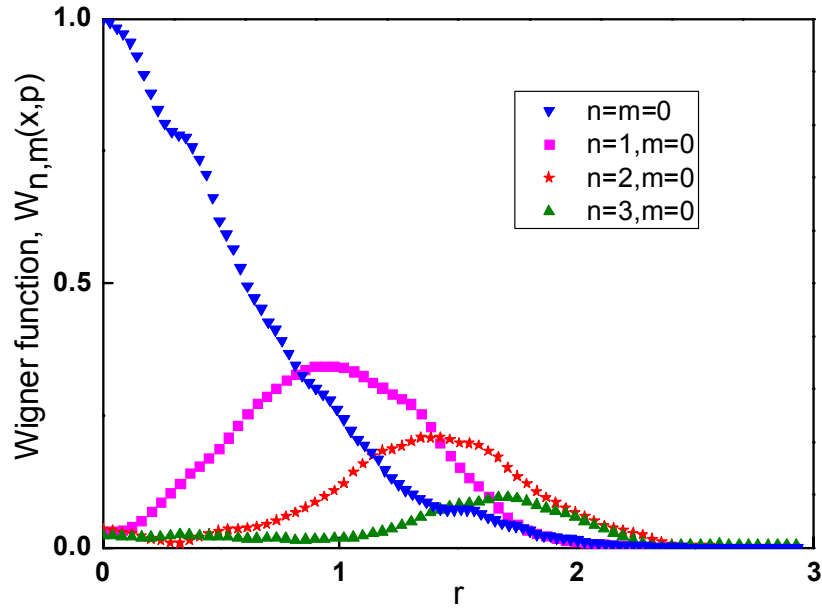


Figure 5.7: *Experimental plots of the WDF of 1D projections of a Gaussian beam and optical vortices of order 1, 2, and 3 with $r = [(x/w)^2 + (wp/2\lambda)^2]^{1/2}$.*

5.5 Conclusion

We have tested a fundamental property of vortices. In contrast to Gaussian fields, vortices are very unique in their 1D projections. This uniqueness is evident in the spatial coherence function or the TPCF of the 1D projections of a Gaussian and the optical vortex fields. It is of a Gaussian shape for a Gaussian field; however, for vortices, it has characteristic shapes that depend on the order of vortex (Fig. [5.3]).

In conclusion, we have found the spatial coherence function, the degree of coherence, and the information entropy of the 1D projections of beams with topological charges 0, 1, 2, and 3. We have also obtained the WDFs for all these beams, which show marked differences for different orders of vortices. Our results show that a higher order vortex may carry more information because of its higher information entropy.

Chapter 6

Intensity Correlation Properties of Optical Vortices

In this chapter we study the intensity correlation or the second order coherence properties of optical vortices vis-à-vis the TEM_{00} mode of a He-Ne laser beam. We also study the intensity correlation function for optical vortices passing through a rotating ground glass (RGG) plate and compare them with those of the TEM_{00} mode of a He-Ne laser beam passed through the same RGG. We have observed that the intensity correlation curves for the scattered optical vortices decrease much faster than the corresponding curve for a TEM_{00} mode of the He-Ne laser. The rate of decay of the correlation increases with the increase of the order of vortices. Our experimentally observed results are supported by exact analytical results.

6.1 Introduction

The properties of optical vortices discussed so far concern with the electric field correlation; Mach-Zehnder and shearing Sagnac interferometers are used to demonstrate the electric-field correlation with the result of interference fringes. However, in this chapter we would discuss the intensity correlation experiments with optical vortices. The experiments owe their origin to the landmark work of Hanbury-Brown and Twiss, dealing with the second order coherence or the measurement of the intensity correlation [29, 104]. In the 1950s, Robert Hanbury Brown and Richard Q. Twiss performed a series of intensity correlation experiments to measure the correlation between intensity fluctuations in the light beams coming from different sources. As discussed in the first chapter, results of HBT experiments heralded the birth of modern quantum optics [31].

The intensity correlation spectroscopy and the singular optics/optical vortices are the two completely different areas of research which are separately finding numerous applications in basic and applied sciences. However, to the best of our knowledge, nobody has tried to combine them. Therefore, it becomes imperative to explore the intensity correlation experiments with optical vortices. In this chapter, we present for the first time and to the best of our knowledge, the results of the intensity correlation function for optical vortices of different orders. In addition to the intensity correlation measurement of optical vortices, we have also scattered optical vortices through a rotating ground glass (RGG) plate and studied the intensity correlation functions for scattered vortices [103, 105]. These results have been compared with that of the TEM_{00} mode of He-Ne laser under the same experimental conditions.

6.2 Experiment

The experimental set-up is shown in Fig. [6.1]. An intensity-stabilized red He-Ne laser (Spectra-Physics, 117A) with a spatial light modulator (SLM, Holoeye LC-R 2500) is used to generate optical vortices. A fork like pattern is introduced into the SLM through the computer PC1. Mirror M is used to direct the laser beam onto the SLM and also used for the fine tuning to form a symmetrical vortex. To obtain vortices of different orders in the first diffracted order, we have introduced different fork patterns into the SLM via a desktop computer PC1. After introducing an appropriate fork pattern, the desired vortex is selected through apertures A1 and A2 (A1 is used for stopping higher diffracted orders from the SLM, and A2 is used for fine selection of a particular order of the vortex). In our first set of experiments, we don't use the lens L and the RGG plate shown in Fig. [6.1], instead we reduce the intensity of optical vortices with polarizer P and then send them directly to the photomultiplier tube PMT and the digital correlator installed in computer PC2.

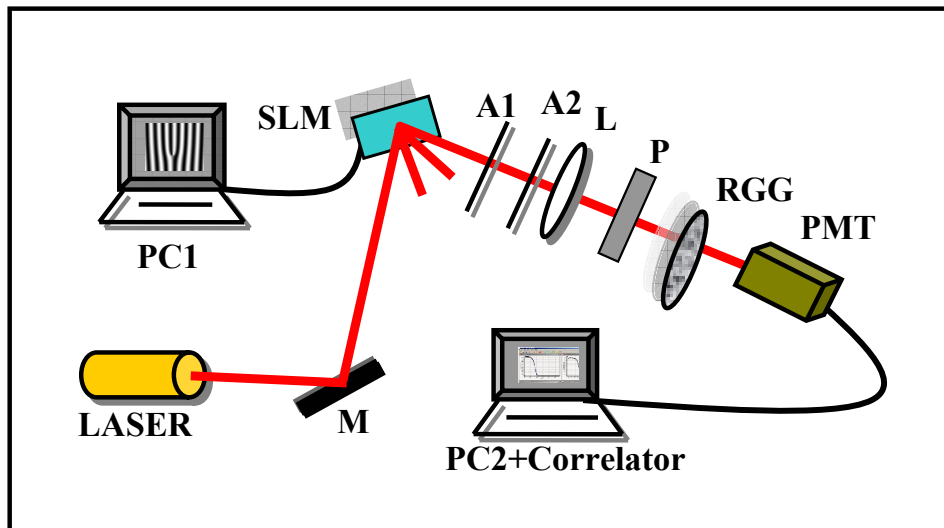


Figure 6.1: *Experimental arrangement to study the intensity correlation function. M, mirror; SLM, spatial light modulator; A1 and A2 Apertures; L, lens; P, polarizer; RGG, rotating ground glass plate; PMT, photomultiplier tube; PC1 and PC2, computers; the digital correlator card is installed in PC2.*

The photomultiplier tube (PMT-Hamamatsu R6358P) with dark count less than 50 counts/sec and shielded with an aperture (not shown in experimental figure) of size 0.20 mm, is used for the photon counting. A digital correlator (Photocor-FC) is used for acquiring the intensity correlation data. There are two types (linear and multi) of time binning modes in this correlator. We have set linear time binning mode, through which it stores intensity correlation data upto maximum 128 channels. The width of each channel is defined as the sample time, that can vary from 20 ns to 1.3 ms. The operating software (Photocor) for this correlator is also installed in computer PC2.

Once the data acquisition for the intensity correlation of optical vortices is over, we move to study the dynamic light scattering with optical vortices. For that purpose we passed optical vortices through a rotating ground glass plate (RGG). A lens L of focal length 240 mm is used to focus optical vortices towards the plane of the RGG plate. The normal distance between the lens plane and the RGG plane is 228 mm. The average inhomogeneity size in the RGG plate is $\sim 20 \mu\text{m}$. The size of the inhomogeneity is measured using an inverted microscope (NIKON ECLIPSE TE2000-U, MO 10X) and a CCD camera (Point Gray, pixel size $4.4 \mu\text{m}$). The RGG plate is mounted through a motor and can be rotated around its axis with different speeds. The speed of the RGG plate is calibrated using an optical method based on measuring a periodic signal obtained by blocking the laser spot with a sticker attached to the plate.

After completing data acquisition for vortices of different orders, the fork grating on the SLM is replaced with a usual grating so as to let the Gaussian beam traverse the same path as the vortices. Keeping all other experimental conditions unchanged, we recorded the intensity correlation values for a Gaussian (TEM_{00}) laser beam and for the same beam scattered through the RGG plate.

6.3 Intensity Correlation Function for Optical Vortices and TEM₀₀ Mode of He-Ne Laser

We have used an intensity stabilized He-Ne laser with intensity stability of $\pm 0.1\%$ over one hour operation. It is known that the intensity correlation function for such lasers remains constant with respect to the time delay. We have experimentally tested this fundamental result for the He-Ne laser being used and also obtained the intensity correlation values for the optical vortices of first and third order. It has been found that the intensity correlation for optical vortices follows similar trend as for the Gaussian laser beam. In Fig. [6.2], we show intensity correlation curves for a Gaussian beam as well as the first and the third order vortices.

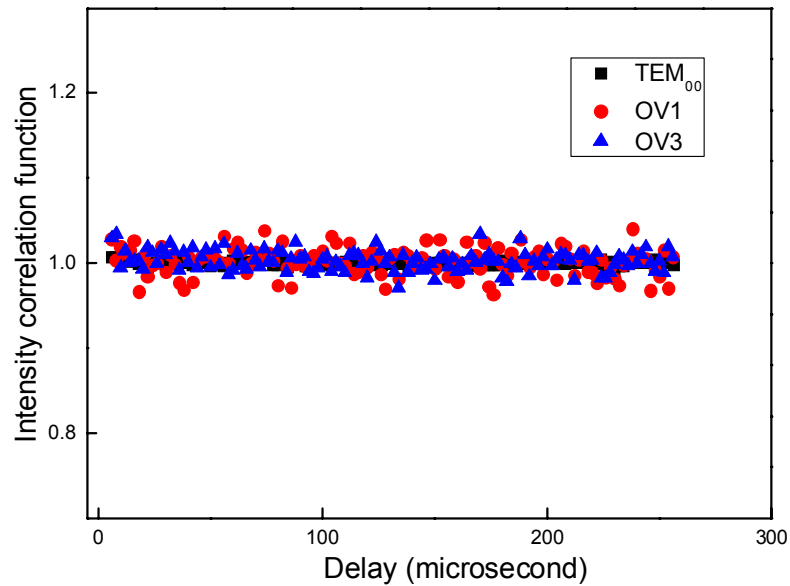


Figure 6.2: Intensity correlation curves for a Gaussian beam and optical vortices of first and the third order.

It could be noticed in Fig. [6.2] that the intensity correlation data for the TEM₀₀ mode of He-Ne laser are lying on a flat smooth line, however, for optical vortices, data points are a bit spreaded around the smooth line. The reason for this small deviation in case of vortices could be attributed to the change of the mode

of laser while forming vortices. Optical vortices are generated by the diffraction of TEM₀₀ mode of the He-Ne laser, therefore one could not expect them to be as stable as the initial mode of the laser.

6.4 Scattering of Optical Vortices through Rotating Ground Glass Plate

The light scattering by a plane wave has already been worked out theoretically as well as experimentally and finds a lot of applications, however, light scattering with helical wavefront has not yet been studied either theoretically or experimentally. Therefore it would be worthwhile to pursue the field that can supplement the knowledge gained by the plane wave scattering. Here, we have started the dynamic light scattering study with optical vortices. As a dynamic scattering medium, we have taken a rotating ground glass plate that has been considered the simplest device for such studies (details are given in Experiment section). A Gaussian laser beam and the optical vortices of orders 1, 4 and 7 are scattered through the RGG plate. Figure [6.3a] shows the experimental results obtained for the intensity correlation function of a Gaussian laser beam and for the optical vortices of different orders at a linear speed 645.1 ± 0.8 mm/sec of the RGG plate. It is clear from the curves that on passing optical vortices and a Gaussian laser beam through the same RGG plate, the intensity correlation function of optical vortices decreases faster than that of a Gaussian laser beam. The decay rate of the intensity correlation function is quantified in terms of the correlation time, which is the time at which the intensity correlation function falls to $1/e$ of its maximum value. The points in Fig. [6.3b] show the calculated correlation times obtained from the experimental intensity correlation curves for the optical vortices and a Gaussian beam. The point for the Gaussian beam lies much above the points for vortices.

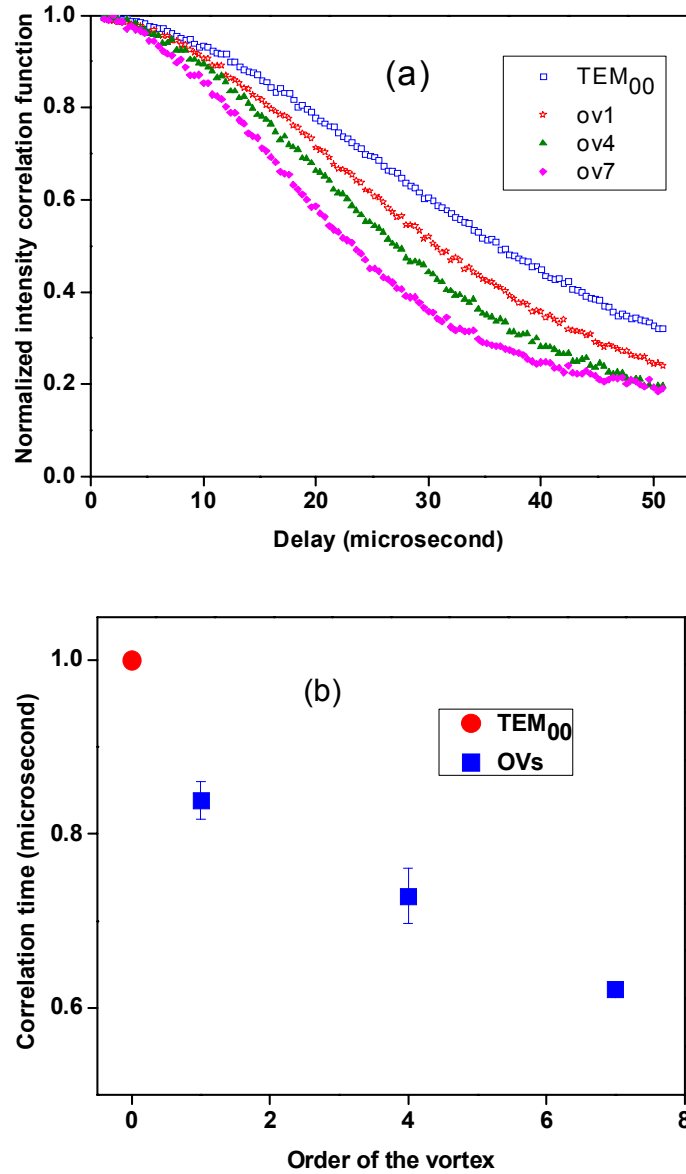


Figure 6.3: (a) Experimental results for the normalized intensity correlation function of the scattered TEM_{00} mode and scattered optical vortices of order 1, 4, and 7; speed of the RGG plate is 645.1 ± 0.8 mm/sec. (b) Correlation time vs. order of the optical vortex.

We have repeated the experiment with the different speeds of the RGG plate. In Fig. [6.4(a,b)], we show the intensity correlation curves with linear speed of the RGG as 879.4 ± 0.4 mm/sec, and corresponding correlation times.

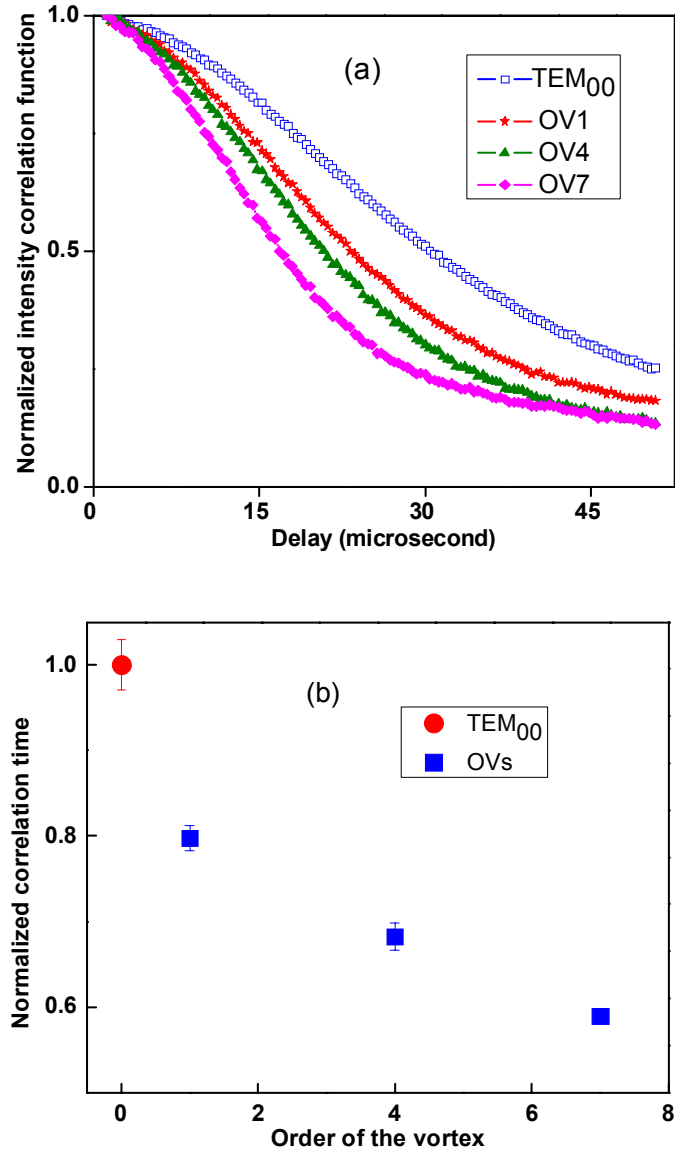


Figure 6.4: (a) Experimental results for the normalized intensity correlation function of the scattered TEM_{00} mode and scattered optical vortices of order 1, 4, and 7; speed of the RGG plate is 879.4 ± 0.4 mm/sec. (b) Correlation time vs. order of the optical vortex.

The results of the intensity correlation experiments are seen consistent at different speeds of the RGG. It could be seen that the slopes of the correlation curves are increasing with increasing speed of the RGG plate, which is the well known

observation in dynamic light scattering, it proves that the digital correlator we have used is working properly.

6.5 Theoretical Analysis

The electric field amplitude of an optical vortex of order l propagating along the z direction, at the plane (u, v) just after the spatial light modulator (SLM), is given as (we have ignored the overall phase factor owing to the optical path length throughout)

$$E_1(u, v) = E_0(u + iv)^l \exp \left[- \left\{ \frac{1}{w^2} + i \frac{k}{2R} \right\} (u^2 + v^2) \right] \quad (6.1)$$

where $w = w_0 \sqrt{1 + (z_1/z_0)^2}$ is the radius of the Gaussian beam containing the vortex, $w_0 = 0.3$ mm is the beam waist at the laser exit, $z_1 = 1000$ mm is the distance between the laser and the SLM, $z_0 = \pi w_0^2/\lambda$, $R = z_1 + z_0^2/z_1$ and $k = 2\pi/\lambda$ is the magnitude of the wave vector of light with the wavelength λ .

The field $E_2(x, y)$ at the receiving plane of the ground glass is calculated by using the Huygens-Fresnel diffraction formula. Thus

$$E_2(x, y) = \frac{ik}{2\pi B} \iint dudv E_1(u, v) \exp \left[- \frac{ik}{2B} \{ A(u^2 + v^2) - 2(xu + yv) + D(x^2 + y^2) \} \right] \quad (6.2)$$

where the $ABCD$ matrix for propagation of light beam from the SLM to the RGG plate have been calculated as $A = 1 - z_3/f$, $B = z_2 + z_3 - z_2 z_3/f$, $C = -1/f$ and $D = 1 - z_2/f$. Here, $f = 240$ mm is the focal length of the lens, $z_2 = 700$ mm is the distance from the lens to the SLM, and $z_3 = 228$ mm is the distance from the lens to the RGG plate.

Because the ground glass rotates with a constant angular velocity, the inhomogeneities in the RGG plate through which the laser/vortex scatters are repetitively changing. Figure [6.5a] shows a schematic of the focusing of laser towards the plane

of the RGG plate and Figs. [6.5(b,c)] show the geometry of RGG plate used in the experiment. The annular ring (Fig. [6.5b]) indicates a small section of the RGG plate from where the light is scattered, and the small circle within the annular ring shows the laser spot (not to scale) on the RGG. As a result of the rotation of ground glass, an inhomogeneity situated at a point $P(x, y)$ is moved to $P(x', y')$ in a certain amount of time τ . The linear velocity V of the RGG can be resolved into two components, $V_x = V \sin\phi$ and $V_y = V \cos\phi$, where ϕ is the angle subtended by the inhomogeneity at the x-axis in time τ . Hence, the new coordinates for the inhomogeneity become $x' = x + V\tau \sin\phi$, $y' = y - V\tau \cos\phi$.

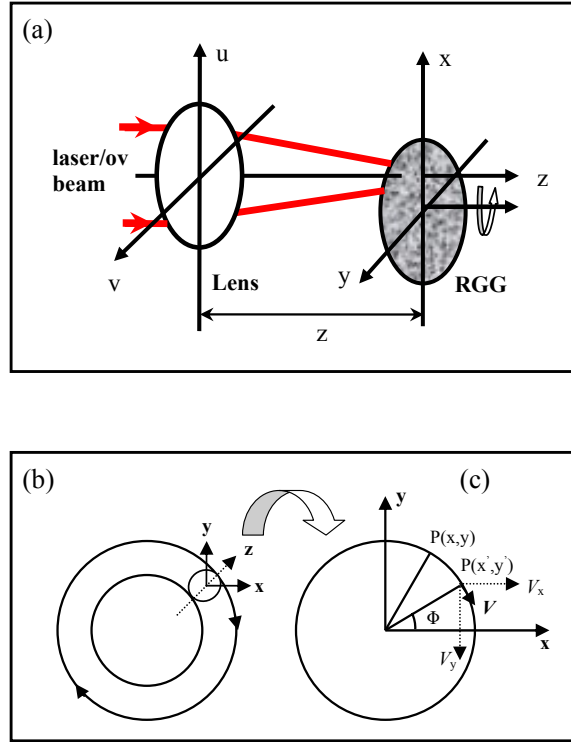


Figure 6.5: (a) *Focusing of laser/vortices towards the plane of rotating ground glass. The lens has been kept at (u, v) plane and the rotating ground glass is located at a distance z from the lens in (x, y) plane.* (b) *Annulus ring shows the portion of ground glass from where the light is being scattered.* (c) *Magnified laser/optical vortex spot. $P(x, y)$ was the position of a particular inhomogeneity which has been moved to $P(x', y')$ after a certain time interval τ .*

On using the new set of coordinates in Eq. [6.2], one can get the field amplitude $E_2(x, y)$ at the ground glass after a certain time τ .

The inhomogeneities of the RGG plate scatter the incident fields $E_2(x, y)$ and $E_2(x, y)$. Therefore, the resultant field at the detector can be calculated by taking the superposition of all the field amplitudes scattered by each inhomogeneity. The diffraction effects produced by each inhomogeneity can be summed up [106, 107] to account for the modification produced in the incident fields due to the RGG. The final form of the normalized field correlation function for the vortex scattered from the RGG is given by

$$g^{(1)}(\tau) = \alpha(\tau)/\alpha(0) = \exp\left[-\frac{ik}{2B}(D-1)V^2\tau^2 - \frac{1}{2}\left(\frac{V\tau|\zeta|}{w}\right)^2\right] \times \sum_{j=0}^l \frac{1}{j!} \left[-D\zeta\left(\frac{V\tau}{w}\right)^2\right]^j L_{l-j}^j\left[-\frac{\zeta^2}{2}\left(\frac{V\tau}{w}\right)^2\right] \quad (6.3)$$

where

$$\alpha(\tau) = \iiint dx dy d\phi E_2(x, y) E_2^*(x + V\tau \sin\phi, y - V\tau \cos\phi), \quad (6.4)$$

$$\zeta = 1 + \frac{ikw^2}{2B}(1 - A - B/R) \quad (6.5)$$

and $L_{l-j}^j(x)$ is an associated Laguerre polynomial.

For a large number of scatterers, i.e., in the Gaussian limit, the intensity correlation function $g^{(2)}(\tau) \propto |g^{(1)}(\tau)|^2$. The theoretical results of $|g^{(1)}(\tau)|^2$ obtained from Eq. [6.3] have been shown in Fig. [6.6a]. These results show a good similarity with the experimentally observed results for $g^{(2)}(\tau)$. The correlation times shown in Fig. [6.6b] are the calculated values from the theoretical plots of $|g^{(1)}(\tau)|^2$.

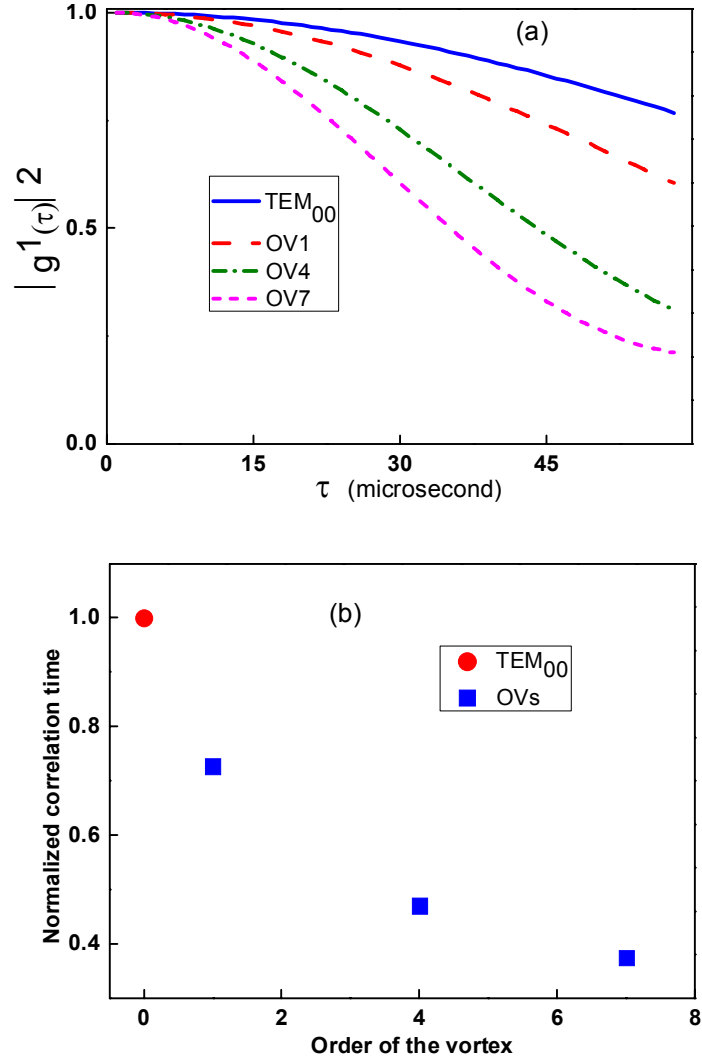


Figure 6.6: Plot showing analytical results for (a) $|g^{(1)}(\tau)|^2$ at the speed of RGG plate 879.4 mm/sec and (b) correlation time obtained from $|g^{(1)}(\tau)|^2$.

The results presented here bear a good similarity with the decoherence of optical vortices stored in atomic ensembles [108]. The theoretical results presented in [108] deal with diffusion-induced decoherence of the stored optical vortices in atomic ensembles. It shows that the coherence of optical vortices stored in such atomic ensembles decreases faster than a stored Gaussian beam, and also it decreases

with the order of vortex. We have observed a similar behavior in our intensity correlation experiments. We attribute this similarity to the topological structure of optical vortices.

6.6 Summary

In the work presented in this chapter, our motivation was to observe the results of the second order coherence function of optical vortices and the dynamic light scattering with optical vortices. Although, there is not any significant difference between the intensity correlation curves for optical vortices and the TEM₀₀ mode of a He-Ne laser. However, we see a clear difference in the correlation curves for scattered Gaussian beams and optical vortices; the intensity correlation of optical vortices decreases faster than that of a Gaussian laser beam. It means that for a given dynamical system the optical vortex is addressing the phenomenon on a different time scale than the Gaussian beam. We feel that the observed dependence of the correlation time on the order of the vortex can be effectively utilized to extract additional information about the system that might otherwise not be possible.

Chapter 7

Summary and Scope for Future Work

This thesis deals with the basic properties of optical vortices. The introductory chapter gives a broad overview of the singular optics, optical vortices and their coherence properties. We have observed that the resolution of the CGH introduced into the SLM is a key factor that determines the size of dark core of the vortex. The single charge vortex is found to be very robust and it is not destroyed even after the diffraction through an iris aperture. However, high-charge vortices are very sensitive to the perturbation or asymmetry, they break into equal number of unit charge vortices. The field of vortex beams can not be written as only the function of either x or the y coordinates. Such field distributions can be studied in one dimension by taking their projections. The degree of coherence of optical vortices in their one dimensional projection decreases with increase of the charge of the vortex. In intensity correlation experiment also, it has been observed that degree of temporal coherence of vortices scattered through a rotating ground glass plate decreases with increasing charge of the vortex.

The present study can be summarized as below :

Chapter 1 gives a brief introduction of the subject i.e. singular optics and optical vortices. We show that the Laguerre-Gaussian beam containing phase singularities or optical vortices is one of the solutions of scalar wave equation under the paraxial approximation. There could be other solutions also which contain vortices, one of them being the higher order Bessel beam. After the discussion on optical vortices, the first and the second order coherence properties of an optical field has been discussed in detail with their historical development.

In chapter 2, we discuss methods for the generation and the characterization of optical vortices. Vortex generation through the computer generated holography and the spatial light modulator are the most common methods which have been discussed in detail. A technique to design an optical vortex with a variable core size has been enumerated. It uses the resolution of the computer generated hologram as a parameter for controlling the core size. The other methods like astigmatic mode converter and spiral phase plates have also been discussed in brief. After providing methods for the generation of optical vortices, we highlight different characteristics like topological charge and orbital angular momentum of vortices. The last part of the chapter deals with the propagation properties of vortices.

In chapter 3, we have elaborated the diffraction characteristics of optical vortices. Although the phenomenon of diffraction is a very old concept in classical physics, nevertheless, it plays a role of utmost importance in many branches of physics and engineering that deal with the propagation of waves. The Fresnel and Fraunhofer diffraction of light through the circular aperture are well known with Airy pattern being one of the most ubiquitous diffraction patterns in optics. In the first section of the chapter, we have studied the diffraction effects produced by an iris diaphragm. It has been observed that the diffraction of an optical vortex and

a Gaussian beam through an iris aperture produces ball bearing sort of structure of darkness and brightness. The singularity of the vortex beam is found to be persistent even after diffraction through the aperture. The presence of singularity at the center of the diffraction pattern of an optical vortex has been confirmed by interferometry. In the second section, the diffraction through a two dimensional sinusoidal grating has been discussed. We find that the diffraction of optical vortex through a two dimensional sinusoidal grating produces four copies of vortex with the same topological charge, which may be useful in making copies of vortex with same orbital angular momentum in the context of optical communication.

Chapter 4 presents the stability and the propagation dynamics of high topological charge optical vortices. We introduce an asymmetry in the core of a high charge optical vortex by using an appropriate computer generated hologram. The splitting of a high charge optical vortex core into unit charge vortices has been found to depend on the extent of introduced asymmetry. For a second order vortex, trajectories of the split unit charged vortices and their separation have been recorded as a function of change in the asymmetry of the core. We also study the effect of core asymmetry to the third and the fourth order vortices which form an array of three and four unit charge vortices. We find a good agreement between the experimentally obtained and numerically calculated results.

In chapter 5, we examine the spatial coherence characteristics of optical vortices. Here, along with the spatial coherence, the information entropy and the Wigner distribution function have also been derived for the one dimensional projection of optical vortices. The spatial coherence functions of the one dimensional projection of optical vortices show characteristic features for different orders of the vortices. The degree of coherence is found to be decreasing with the increase of the order of the vortex. On the other hand, the information entropy increases with the increase of the order of the vortex. The experimental results verify the earlier

proposed theoretical results.

Chapter 6 describes the intensity correlation or the second order coherence properties of optical vortices vis-à-vis the TEM_{00} mode of a He-Ne laser beam. We also study the intensity correlation function for optical vortices passing through a rotating ground glass (RGG) plate and compare them with those of the TEM_{00} mode of a He-Ne laser beam passed through the same RGG plate. We have observed that the intensity correlation curves for the scattered optical vortices decrease much faster than the corresponding curve for a TEM_{00} mode of the He-Ne laser. The rate of decay of the correlation increases with the increase of the order of vortices. Our experimentally observed results are supported by exact analytical results.

Scope for Future Work

The intensity correlation properties of optical vortices need to be studied in more detail. In future, we would be studying intensity correlation properties of vortices scattered through different dynamical systems. Also, we would work on finding the exact relationship between first and second order coherence of optical vortices for these dynamical systems. Although, the intensity correlation properties of optical vortices scattered through a RGG plate has been discussed, the photon statistics of vortices needs to be explored. The photon correlation experiments with very less number of photons of optical vortices would be studied.

The spontaneous parametric downconversion experiments with a BBO crystal has also been planned out. Firstly we would generate the polarization entangled photons. As discussed, optical vortices carry one more degree of freedom i.e. the orbital angular momentum, we would also work on the entanglement between the orbital angular momentum states of vortices. We would perform the spontaneous

parametric downconversion experiments with optical vortices and use the coincidence technique to detect the entangled photons.

It has been observed that two vortices of the same charge, sitting in a same host beam (dipole vortex), rotate around their common center as the beam propagates. The rotation speed depends on their initial separation. We suggest a technique to measure the refractive index of a material based on the rotation of dipole vortices. We will take samples of different refractive indices and pass a dipole vortex through them and measure the angle rotated by dipole vortex. The measured value of rotation angle for different samples can be used to calculate the refractive index of the materials of samples. We would experimentally implement this technique in future.

Bibliography

- [1] T. Young, “Experiments and calculations relative to physical optics,” *Philosophical Transactions of the Royal Society (London)* **94**, 1–16 (1804).
- [2] J. F. Nye and M. V. Berry, “Dislocations in wave trains,” *Proceedings of the Royal Society A (London)* **336**, 165–190 (1974).
- [3] P. Couillet, L. Gil, and F. Rocca, “Optical vortices,” *Optics Communications* **73**, 403–408 (1989).
- [4] L. Allen, S. M. Barnett, and M. J. Padgett, *Optical Angular Momentum* (Institute of Physics Publishing, Bristol, 2003).
- [5] M. R. Dennis, K. O’Holleran, and M. J. Padgett, “Chapter 5 singular optics: Optical vortices and polarization singularities,” (Elsevier, 2009), pp. 293–363.
- [6] J. C. Maxwell, “On physical lines of force,” *Philosophical Magazine* **11**, pp. 161–175; 338–348 (1861).
- [7] J. C. Maxwell, “On physical lines of force,” *Philosophical Magazine* **12**, pp. 127–144; 85–95 (1862).
- [8] S. M. Barnett and L. Allen, “Orbital angular momentum and nonparaxial light beams,” *Optics Communications* **110**, 670–678 (1994).

- [9] M. Beijersbergen, L. Allen, H. van der Veen, and J. Woerdman, “Astigmatic laser mode converters and transfer of orbital angular momentum,” *Optics Communications* **96**, 123–132 (1993).
- [10] C. López-Mariscal, J. C. Gutiérrez-Vega, G. Milne, and K. Dholakia, “Orbital angular momentum transfer in helical mathieu beams,” *Optics Express* **14**, 4182–4187 (2006).
- [11] K. Volke-Sepulveda, V. Garcés-Chávez, S. Chávez-Cerda, J. Arlt, and K. Dholakia, “Orbital angular momentum of a high-order bessel light beam,” *Journal of Optics B: Quantum and Semiclassical Optics* **4**, S82 (2002).
- [12] F. Gori, G. Guattari, and C. Padovani, “Bessel-gauss beams,” *Optics Communications* **64**, 491–495 (1987).
- [13] M. A. Bandres and J. Gutiérrez-Vega, “Ince gaussian beams,” *Optics Letters* **29**, 144–146 (2004).
- [14] M. A. Bandres and J. C. Gutiérrez-Vega, “Circular beams,” *Optics Letters* **33**, 177–179 (2008).
- [15] V. V. Kotlyar, R. V. Skidanov, S. N. Khonina, and V. A. Soifer, “Hypergeometric modes,” *Optics Letters* **32**, 742–744 (2007).
- [16] E. Karimi, G. Zito, B. Piccirillo, L. Marrucci, and E. Santamato, “Hypergeometric-gaussian modes,” *Optics Letters* **32**, 3053–3055 (2007).
- [17] E. Karimi, B. Piccirillo, L. Marrucci, and E. Santamato, “Improved focusing with hypergeometric-gaussian type-II optical modes,” *Optics Express* **16**, 21069–21075 (2008).
- [18] J. F. Nye, *Natural Focusing and Fine Structure of Light* (Institute of Physics Publishing London, 1999).
- [19] M. Berry, “Making waves in physics,” *Nature* **403**, 21 (2000).

- [20] P. A. M. Dirac, “Quantised singularities in the electromagnetic field,” Proceedings of the Royal Society A (London) **133**, 60–72 (1931).
- [21] M. Berry and M. Dennis, “Polarization singularities in isotropic random vector waves,” Proceedings of the Royal Society A (London) **457**, 141–155 (2001).
- [22] R. J. Donnelly, *Quantized Vortices in Helium II* (Cambridge University Press, Cambridge, 1991).
- [23] M. S. Soskin and M. V. Vasnetsov, *Singular optics* (Elsevier Science, B. V., Amsterdam, 2001).
- [24] I. Basistiy, V. Bazhenov, M. Soskin, and M. Vasnetsov, “Optics of light beams with screw dislocations,” Optics Communications **103**, 422–428 (1993).
- [25] L. Allen, M. Beijersbergen, R. Spreeuw, and J. Woerdman, “Orbital angular momentum of light and the transformation of laguerre-gaussian laser modes,” Physical Review A **45**, 8185–8189 (1992).
- [26] M. V. Berry, “Disruption of wavefronts: statistics of dislocations in incoherent gaussian random waves,” Journal of Physics A: Mathematical and General **11**, 27–37 (1978).
- [27] R. P. Singh, A. Kumar, and J. Bhatt, *Vortices of Light: Generation, Characterization and Applications* (Nova Science Pub, NewYork, 2008).
- [28] J. Leach, M. R. Dennis, J. Courtial, and M. J. Padgett, “Laser beams: Knotted threads of darkness,” Nature **432**, 165 (2004).
- [29] R. Loudon, *The quantum theory of light* (Oxford Univeristy Press, Oxford, 2000).
- [30] R. Hanbury Brown and R. Q. Twiss, “A new type of interferometer for use in radio astronomy,” Philosophical Magazine **45**, 663–682 (1954).

- [31] L. Mandel and E. Wolf, *Optical Coherence and Quantum Optics* (Cambridge University Press, New York, 1995).
- [32] H. Z. Cummins and E. R. Pike, *Photon correlation and light beating spectroscopy* (Plenum Press, New York, 1974).
- [33] R. Hanbury Brown, R. Jennison, and M. Gupta, “Apparent angular sizes of discrete radio sources: Observations at jodrell bank, manchester,” *Nature* **170**, 1061–1063 (1952).
- [34] R. Hanbury Brown and R. Q. Twiss, “Correlation between photons in two coherent beams of light,” *Nature* **177**, 27–29 (1956).
- [35] R. Hanbury Brown and R. Q. Twiss, “Interferometry of the intensity fluctuations in light II. an experimental test of the theory for partially coherent light,” *Proceeding of the Royal Society A (London)* **243**, 291–319 (1957).
- [36] E. Brannen and H. I. S. Ferguson, “The question of correlation between photons in coherent light rays,” *Nature* **178**, 481–482 (1956).
- [37] E. M. Purcell, “The question of correlation between photons in coherent light rays,” *Nature* **178**, 1449–1450 (1956).
- [38] R. Hanbury Brown and R. Q. Twiss, “The question of correlation between photons in coherent light rays,” *Nature* **178**, 1447–1448 (1956).
- [39] R. Q. Twiss, A. G. Little, and R. Hanbury Brown, “Correlation between photons, in coherent beams of light, detected by a coincidence counting technique,” *Nature* **180**, 324–328 (1957).
- [40] R. Hanbury Brown and R. Twiss, “A test of a new type of stellar interferometer on sirius,” *Nature* **178**, 1046–1048 (1956).
- [41] R. Hanbury Brown and R. Q. Twiss, “Interferometry of the intensity fluctuations in light I. basic theory: the correlation between photons in coherent

- beams of radiation,” *Proceeding of the Royal Society A (London)* **242**, 300–324 (1957).
- [42] F. T. Arecchi, E. Gatti, and A. Sona, “Time distribution of photons from coherent and gaussian sources,” *Physics Letters* **20**, 27–29 (1966).
- [43] H. J. Kimble, M. Dagenais, and L. Mandel, “Photon antibunching in resonance fluorescence,” *Physics Review Letters* **39**, 691–695 (1977).
- [44] V. Y. Bazhenov, M. V. Vasnetsov, and M. S. Soskin, “Laser beams with screw dislocations in their wavefronts,” *Journal of Experimental and Theoretical Physics (JETP) Letters* **52**, 429–431 (1990).
- [45] N. R. Heckenberg, R. McDuff, C. P. Smith, and A. G. White, “Generation of optical phase singularities by computer generated holograms,” *Optics Letters* **17**, 221–223 (1992).
- [46] N. Heckenberg, R. McDuff, C. Smith, H. Rubinsztein-Dunlop, and M. Wegener, “Laser beams with phase singularities,” *Optical and Quantum Electronics* **24** (1992).
- [47] J. E. Curtis, B. A. Koss, and D. G. Grier, “Dynamic holographic optical tweezers,” *Optics Communications* **207**, 169–175 (2002).
- [48] J. Curtis and D. Grier, “Modulated optical vortices,” *Optics Letters* **28**, 872–874 (2003).
- [49] A. Kumar, P. Vaity, Y. Krishna, and R. Singh, “Engineering the size of dark core of an optical vortex,” *Optics and Lasers in Engineering* **48**, 276–281 (2010).
- [50] J. W. Goodman, *Introduction to Fourier Optics* (Roberts and Company, Greenwood Village, 2004).

- [51] M. Padgett, J. Arlt, N. Simpson, and L. Allen, “An experiment to observe the intensity and phase structure of laguerre-gaussian laser modes,” *American Journal of Physics* **64**, 77–82 (1996).
- [52] M. Beijersbergen, R. Coerwinkel, M. Kristensen, and J. Woerdman, “Helical-wavefront laser beams produced with a spiral phaseplate,” *Optics Communications* **112**, 321–327 (1994).
- [53] C. Rotschild, S. Zommer, S. Moed, O. Hershcovitz, and S. G. Lipson, “Adjustable spiral phase plate,” *Applied Optics* **43**, 2397–2399 (2004).
- [54] M. Padgett and L. Allen, “Light with a twist in its tail,” *Contemporary Physics* **41**, 275–285 (2000).
- [55] M. Soskin, V. Gorshkov, M. Vasnetsov, J. Malos, and N. Heckenberg, “Topological charge and angular momentum of light beams carrying optical vortices,” *Physical Review A - Atomic, Molecular, and Optical Physics* **56**, 4064–4075 (1997).
- [56] R. P. Singh and S. Roychowdhury, “Non-conservation of topological charge: Experiment with optical vortex,” *Journal of Modern Optics* **51**, 177–181 (2004).
- [57] D. P. Ghai, P. Senthilkumaran, and R. Sirohi, “Single-slit diffraction of an optical beam with phase singularity,” *Optics and Lasers in Engineering* **47**, 123–126 (2009).
- [58] J. M. Hickmann, E. J. S. Fonseca, W. C. Soares, and S. Chávez-Cerda, “Unveiling a truncated optical lattice associated with a triangular aperture using light’s orbital angular momentum,” *Physical Review Letters* **105**, 053904 (2010).
- [59] I. Basistiy, M. Soskin, and M. Vasnetsov, “Optical wavefront dislocations and their properties,” *Optics Communications* **119**, 604–612 (1995).

- [60] J. Vickers, M. Burch, R. Vyas, and S. Singh, “Phase and interference properties of optical vortex beams,” *Journal of the Optical Society of America A: Optics and Image Science, and Vision* **25**, 823–827 (2008).
- [61] G. Molina-Terriza, J. Recolons, J. Torres, and L. Torner, “Observation of the dynamical inversion of the topological charge of an optical vortex,” *Physical Review Letters* **87** (2001).
- [62] G. Molina-Terriza, J. Recolons, and L. Torner, “The curious arithmetic of optical vortices,” *Optics Letters* **25**, 1135–1137 (2000).
- [63] A. Kumar, P. Vaity, and R. P. Singh, “Crafting the core asymmetry to lift the degeneracy of optical vortices,” *Optics Express* **19**, 6182–6190 (2011).
- [64] A. T. O’Neil, I. MacVicar, L. Allen, and M. J. Padgett, “Intrinsic and extrinsic nature of the orbital angular momentum of a light beam,” *Physical Review Letters* **88**, 053601 (2002).
- [65] G. Molina-Terriza, J. Torres, and L. Torner, “Twisted photons,” *Nature Physics* **3**, 305–310 (2007).
- [66] J. Courtial, K. Dholakia, L. Allen, and M. Padgett, “Gaussian beams with very high orbital angular momentum,” *Optics Communications* **144**, 210–213 (1997).
- [67] H. He, M. Friese, N. Heckenberg, and H. Rubinsztein-Dunlop, “Direct observation of transfer of angular momentum to absorptive particles from a laser beam with a phase singularity,” *Physical Review Letters* **75**, 826–829 (1995).
- [68] J. Leach, M. Padgett, S. Barnett, S. Franke-Arnold, and J. Courtial, “Measuring the orbital angular momentum of a single photon,” *Physical Review Letters* **88**, 2579011–2579014 (2002).

- [69] J. Leach, J. Courtial, K. Skeldon, S. Barnett, S. Franke-Arnold, and M. Padgett, “Interferometric methods to measure orbital and spin, or the total angular momentum of a single photon,” *Physical Review Letters* **92**, 136011–136014 (2004).
- [70] S. Tao, X.-C. Yuan, J. Lin, X. Peng, and H. Niu, “Fractional optical vortex beam induced rotation of particles,” *Optics Express* **13**, 7726–7731 (2005).
- [71] I. Freund, “Optical vortex trajectories,” *Optics Communications* **181**, 19–33 (2000).
- [72] F. Roux, “Canonical vortex dipole dynamics,” *Journal of the Optical Society of America B: Optical Physics* **21**, 655–663 (2004).
- [73] F. Roux, “Coupling of noncanonical optical vortices,” *Journal of the Optical Society of America B: Optical Physics* **21**, 664–670 (2004).
- [74] R. P. Singh and S. R. Chowdhury, “Trajectory of an optical vortex: Canonical vs. non-canonical,” *Optics Communications* **215**, 231–237 (2003).
- [75] R. P. Singh and S. R. Chowdhury, “Noncanonical vortex transformation and propagation in a two-dimensional optical system,” *Journal of the Optical Society of America A: Optics and Image Science, and Vision* **20**, 573–576 (2003).
- [76] M. Born and E. Wolf, *Principle of Optics* (Cambridge University Press, Cambridge, 1997).
- [77] T. Brunet, J.-L. Thomas, and R. Marchiano, “Transverse shift of helical beams and subdiffraction imaging,” *Physical Review Letters* **105**, 034301 (2010).
- [78] A. Kumar, P. Vaity, J. Banerji, and R. P. Singh, “Making copies of optical vortices,” *Physics Letters A* (under review) .

- [79] I. S. Gradshteyn and I. M. Ruzhik, *Table of integrals, series and products* (Academic Press, San Diego, 2007).
- [80] D. Rozas, C. T. Law, and J. G. A. Swartzlander, “Propagation dynamics of optical vortices,” *Journal of the Optical Society of America B: Optical Physics* **14**, 3054–3065 (1997).
- [81] G. Molina-Terriza, E. Wright, and L. Torner, “Propagation and control of noncanonical optical vortices,” *Optics Letters* **26**, 163–165 (2001).
- [82] A. Mamaev, M. Saffman, and A. Zozulya, “Vortex evolution and bound pair formation in anisotropic nonlinear optical media,” *Physical Review Letters* **77**, 4544–4547 (1996).
- [83] V. L. Ginzburg and L. P. Pitaevskii, “On the theory of superfluidity,” *Soviet Physics JETP* **34**, 858-863 (1958).
- [84] X. Gan, P. Zhang, S. Liu, Y. Zheng, J. Zhao, and Z. Chen, “Stabilization and breakup of optical vortices in presence of hybrid nonlinearity,” *Optics Express* **17**, 23130–23136 (2009).
- [85] I. Freund, “Critical point explosions in two-dimensional wave fields,” *Optics Communications* **159**, 99–117 (1999).
- [86] A. V. Mamaev, M. Saffman, and A. A. Zozulya, “Decay of high order optical vortices in anisotropic nonlinear optical media,” *Physical Review Letters* **78**, 2108–2111 (1997).
- [87] I. Maleev and G. Swartzlander Jr., “Composite optical vortices,” *Journal of the Optical Society of America B: Optical Physics* **20**, 1169–1176 (2003).
- [88] S. Franke-Arnold, J. Leach, M. J. Padgett, V. E. Lembessis, D. Ellinas, A. J. Wright, J. M. Girkin, P. Ohberg, and A. S. Arnold, “Optical ferris wheel for ultracold atoms,” *Optics Express* **15**, 8619–8625 (2007).

- [89] M. Berry and M. Dennis, “knotted and linked phase singularities in monochromatic waves,” *Proceedings of the Royal Society A: Mathematical, Physical and Engineering Sciences* **457**, 2251–2263 (2001).
- [90] J. Leach, M. Dennis, J. Courtial, and M. Padgett, “Vortex knots in light,” *New Journal of Physics* **7**, 55(1–11) (2005).
- [91] M. R. Dennis, R. P. King, B. Jack, K. O’Holleran, and M. J. Padgett, “Isolated optical vortex knots,” *Nature Physics* **6**, 118–121 (2010).
- [92] M. Dennis, “Rows of optical vortices from elliptically perturbing a high-order beam,” *Optics Letters* **31**, 1325–1327 (2006).
- [93] V. Kotlyar, S. Khonina, A. Almazov, V. Soifer, K. Jefimovs, and J. Turunen, “Elliptic laguerre-gaussian beams,” *Journal of the Optical Society of America A: Optics and Image Science, and Vision* **23**, 43–56 (2006).
- [94] S. Chávez-Cerda, J. C. Gutiérrez-Vega, and G. H. C. New, “Elliptic vortices of electromagnetic wave fields,” *Optics Letters* **26**, 1803–1805 (2001).
- [95] Y. S. Kivshar and B. Luther-Davies, “Dark optical solitons: physics and applications,” *Physics Report* **298**, 81–197 (1998).
- [96] G. Indebetouw, “Optical vortices and their propagation,” *Journal of Modern Optics* **40**, 73–87 (1993).
- [97] C. Iaconis and I. A. Walmsley, “Direct measurement of the two-point field correlation function,” *Optics Letters* **21**, 1783–1785 (1996).
- [98] C. C. Cheng, M. G. Raymer, and H. Heier, “A variable lateral-shearing sagnac interferometer with high numerical aperture for measuring the complex spatial coherence of light,” *Journal of Modern Optics* **47**, 73–87 (2000).
- [99] R. P. Singh, S. Roychowdhury, and V. K. Jaiswal, “Wigner distribution of an optical vortex,” *Journal of Modern Optics* **53**, 1803–1808 (2006).

- [100] G. S. Agarwal and J. Banerji, “Spatial coherence and information entropy in optical vortex fields,” *Optics Letters* **27**, 800–802 (2002).
- [101] A. Kumar, S. Prabhakar, P. Vaity, and R. P. Singh, “Information content of optical vortex fields,” *Optics Letters* **36**, 1161–1163 (2011).
- [102] G. Indebetouw, “Coherence properties of doughnut modes with and without a vortex,” *Journal of Optics* **24**, 3–6 (1993).
- [103] A. Kumar, J. Banerji, and R. P. Singh, “Intensity correlation properties of high-order optical vortices passing through a rotating ground-glass plate,” *Optics Letters* **35**, 3841–3843 (2010).
- [104] R. J. Glauber, “The quantum theory of optical coherence,” *Physical Review* **130**, 2529–2539 (1963).
- [105] A. Kumar and R. Singh, “Experimental and theoretical investigation of loss of coherence on scattering of a beam with helical wavefront,” *Optics Communications* **284**, 1510–1516 (2011).
- [106] L. E. Estes, L. M. Narducci, and R. A. Tuft, “Scattering of light from a rotating ground glass,” *Journal of Optical Society of America* **61**, 1301–1306 (1971).
- [107] V. Harwalkar, H. Bohidar, and S. Chopra, “Theoretical and experimental investigations of light scattered from a rotating ground glass,” *Applied Physics B: Photophysics and Laser Chemistry* **31**, 215–220 (1983).
- [108] T. Wang, L. Zhao, L. Jiang, and S. Yelin, “Diffusion-induced decoherence of stored optical vortices,” *Physical Review A - Atomic, Molecular, and Optical Physics* **77**, 043815 (2008).

List of Publications

I. Publications in Journals

1. **Ashok Kumar**, Pravin Vaity, Yedhu Krishna, R. P. Singh. *Engineering the size of dark core of an optical vortex*, Optics and Lasers in Engineering 48, 276-281, 2010.
2. **Ashok Kumar**, Pravin Vaity, R. P. Singh. *Diffraction characteristics of an optical vortex passing through an aperture-Iris Diaphragm*, Optics Communication 72, 283, 4141-4145, 2010.
3. **Ashok Kumar**, J. Banerji, R. P. Singh. *Intensity correlation properties of high-order optical vortices passing through a rotating ground-glass plate*, Optics Letters 35, 3841-3843, 2010.
4. **Ashok Kumar**, R. P. Singh. *Experimental and theoretical investigation of loss of coherence on scattering of a beam with helical wavefront*, Optics Communication 284, 1510-1516, 2011.
5. **Ashok Kumar**, Pravin Vaity, R. P. Singh. *Crafting the core asymmetry to lift the degeneracy of optical vortices*, Optics Express 19, 6182-6190, 2011.
6. **Ashok Kumar**, Shashi Prabhakar, Pravin Vaity, R. P. Singh. *Information content of optical vortex field*, Optics Letters 36, 1161-1163, 2011.
7. **Ashok Kumar**, R. P. Singh. *Photon correlation spectroscopy: A comparative study of optical vortex and Gaussian beam*, Asian Journal of Physics (Invited article), accepted for publication.
8. **Ashok Kumar**, Pravin Vaity, J. Banerji, R. P. Singh. *Making copies of optical vortices*, Submitted to Physics Letters A.

9. Pravin Vaity, **Ashok Kumar**, R. P. Singh. *Optical vortex propagation through photorefractive materials: effect of the order of the vortex*, Submitted to Optics Letters.
10. Shashi Prabhakar, **Ashok Kumar**, J. Banerji, R. P. Singh. *Revealing the order of the vortex through its Intensity Record*, Submitted to Optics Letters.
11. Jitendra Bhatt, **Ashok Kumar**, R. P. Singh. *Directional motion of particles for microfluidics using an optical trap*, Submitted to Journal of Optical Society of America B.

II. Book Chapters

1. R.P. Singh, **Ashok Kumar**, Jitendra Bhatt., Vortices of Light: Generation, Characterization and Applications. Progress in Nonlinear Optics Research, eds. Takahashi, M., Gotô, H., Nova Science, New York, 359-381, 2008.

III. Full Length Conference Papers

1. **Ashok Kumar**, Pravin Vaity, R. P. Singh, Decay of high order elliptical optical vortices National Laser Symposium-19, 3153, Dec 1-4, 2010 at RRCAT Indore, India.
2. **Ashok Kumar**, Shashi Prabhakar, Pravin Vaity, R. P. Singh, Two point correlation function for optical vortices Photonics-2010, 556, Dec 12-15, 2010, at IIT Guwahati, India.
3. P. Vaity, **A. Kumar**, R. P. Singh, Experimental study of power decay of optical vortices in photorefractive material. National Laser Symposium-09, 75, Jan 13-16, 2010 at BARC Mumbai, India.
4. Pravin Vaity, **Ashok Kumar**, Shashi Prabhakar, R. P. Singh, 2-D Airy beam propagation through photorefractive materials Photonics-2010, 523, Dec 12-15, 2010, at IIT Guwahati, India.

5. **Ashok Kumar**, Pravin Vaity, R. P. Singh, Degeneracy of optical vortices and the core asymmetry XXXV OSI Symposium- International Conference on Contemporary Trends in Optics and Optoelectronics, 342, Jan 17-19, 2011 at IIST Thiruvananthapuram, India.
6. Pravin Vaity, **Ashok Kumar**, Shashi Prabhakar, R. P. Singh, Airy beams interaction through photorefractive material in presence of an applied electric field Accepted for SPIE Proceedings (Photonics 2010).
7. R. P. Singh. **Ashok Kumar**, Pravin Vaity, Shashi Prabhakar, Dynamic light scattering of optical vortices XXXV OSI Symposium- International Conference on Contemporary Trends in Optics and Optoelectronics, 37, Jan 17-19, 2011 at IIST Thiruvananthapuram, India.